UNIVERSITAT POLITÈCNICA DE CATALUNYA

Programa de Doctorat:

AUTOMÀTICA, ROBÒTICA I VISIÓ

Tesi Doctoral

PROGNOSTICS AND HEALTH AWARE MODEL PREDICTIVE CONTROL OF WIND TURBINES

Héctor Eloy Sánchez Sardi

Directors de tesi:
Dra. Teresa Escobet Canal
Dr. Vicenç Puig Cayuela

Maig de 2017

To my dad Hector, my mom Miriam and my brother Andrés.

Abstract

Wind turbines components are subject to considerable stresses and fatigue due to extreme environmental conditions to which they are exposed, especially those located offshore. Also, the most common faults present in wind turbine components have been investigated for years by the research community and that has led to propose a fault diagnosis and fault tolerant control wind turbine benchmark which include a set of faults that affect the sensors and actuators of several wind turbine components.

This thesis presents some contributions to the fields of fault diagnosis, fault-tolerant control, prognostics and its integration with wind turbine control which leads to proposing a control approach called health-aware model predictive control.

For wind turbine fault diagnosis, the work presented in this thesis proposes a model-based fault diagnosis approach for wind turbines and its application to a realistic wind turbine fault diagnosis benchmark proposed by the scientific community. The proposed approach combines the use of analytical redundancy relations (ARRs) and interval observers. Interval observers consider an unknown but bounded description of the model parametric uncertainty and noise using the so-called set-membership approach. This leads to formulate the fault detection test by means of checking if the measurements fall inside the estimated output interval, obtained from the mathematical model of the wind turbine and noise/parameter uncertainty bounds. Fault isolation is based on considering a set of ARRs obtained from structural analysis of the wind turbine model and a fault signature matrix that considers the relation of ARRs and faults. The obtained results are presented and compared with other approaches proposed in the literature.

In recent years, individual pitch control (IPC) has been developed for wind turbines, with the purpose of reducing blade and tower loads. Such algorithms depend on reliable sensor information. The azimuth angle sensor, which positions the wind turbine rotor in its rotation, is quite important. This sensor has to be correct as blade pitch actions should be different at different azimuth angle as the wind speed varies within the rotor field due to different phenomena. A scheme detecting faults within this sensor has previously been designed for the application of a high-end fault diagnosis and fault tolerant control of wind turbines benchmark model. In this thesis, the fault diagnosis scheme is improved and integrated with a fault accommodation scheme which enables and disables the individual pitch algorithm based on the fault detection. In this way, the blade and tower loads are not increased due to the individual pitch control algorithm operating with faulty azimuth angle inputs.

Wind turbine blades are under significant gravitational, inertial and aerodynamic loads which cause their fatigue and degradation during the wind turbine operational life. A fatigue problem is often present at the blade root due to the considerable bending moments applied to this zone. With the aim to investigate the damage loads and degradation in the blades, the present work explores two different approaches to fatigue damage estimation and remaining useful life predictions of wind turbine blades. The first approach uses the rainflow counting algorithm. The second approach comes from a stiffness degradation model that describes the propagation of damage at a microscopic scale due to matrix cracks which manifest in a macroscopic scale as stiffness loss.

Interest in the integration of control with fatigue damage minimization or RUL predictions maximization has increased in recent years. The integration of a fatigue-damage and RUL predictions based system health management module with model predictive control is proposed. This provides a mechanism for the wind turbine to operate safely and optimize the trade-off between blades life and energy production. In particular, this work proposes the control approach named health-aware model predictive control that integrates the fatigue damage and prognostics approaches to minimize the damage or increase RUL of wind turbine blades. Control oriented models based on the fatigue-damage using the rainflow counting algorithm and RUL predictions using a stiffness degradation model are proposed to obtain online information of the blades damage and RUL predictions that can be integrated with MPC. Then, the controller objective function is modified by adding an extra criterion that takes into account the damage and RUL predictions of the blade.

The proposed fault diagnosis, fault-tolerant control, prognostics and health-aware model predictive control approaches presented in this thesis have been validated on a wind turbine benchmark based on a 5MW reference utility-scale wind turbine implemented in the high fidelity wind turbine simulator FAST.

Resum

Els components dels aerogeneradors estan sotmesos a considerable estrès i fatiga, degut a les condicions ambientals extremes a les quals estan exposats, especialment els localitzats en alta mar. Per aquest motiu, al comunitat científica durant els últims anys ha investigat les averies més comunes presents en els aerogeneradors, fet que ha portat a proposar un cas d'estudi de diagnosi i control tolerant de fallades que inclou un conjunt de fallades que afecten a diversos components dels aerogeneradors.

Aquesta tesi presenta algunes contribucions en els camps de la diagnosi de fallades, el control tolerant de fallades i la prognosi, així com la seva integració amb el control d'aerogeneradors, fet que ha portat a proposar una tècnica de control anomenada control predictiu basada en models conscients de la salut del sistema (HAMPC).

En la diagnosi de fallades d'aerogeneradors, el treball presentat en aquesta tesi proposa una tècnica de diagnosi de fallades basada en models i s'aplica a un cas d'estudi realista de diagnosi de fallades d'aerogeneradors proposat per la comunitat científica. La tècnica proposada combina la utilització de relacions de redundància analítica (ARRs) i observadors intervalars. Els observadors intervalars parteixen d'una descripció desconeguda però acotada de la incertesa en els paràmetres del model i el soroll. La tècnica de pertinença a conjunts permet detectar avaries en els components de l'aerogenerador. L'aïllament de la fallada es fa en base el conjunt d'ARRs obtinguts de l'anàlisi estructural i de la matriu de signatures de fallades que relaciona les ARRs amb les fallades. En la tesis es mostren els resultats obtinguts i es comparen amb altres tècniques descrites a la literatura.

Recentment i amb la finalitat de disminuir les càrregues de les pales i la torre, s'han desenvolupat noves tècniques de control, una d'elles és el control individual de la inclinació de les pales (IPC). Aquest algorisme depèn de que la informació que arribi del sensor d'inclinació de l'angle de les pales (conegut com a azimuth) sigui correcte. En aquesta tesi es proposa un esquema de control tolerant a fallades que integra la detecció de fallades amb un algorisme d'acomodació de fallades, i té per objectiu evitar l'augment de càrregues en la pala i la torre quan es produeix una fallada en el sensor azimuth.

Les pales dels aerogeneradors estan sota importants càrregues gravitacionals, aerodinàmiques e inercials que causen fatiga i degradació durant la vida operacional de l'aerogenerador. La fatiga és un problema molt freqüent de l'arrel de la pala degut als moments de torsió als que està sotmesa. Amb la finalitat d'investigar la fatiga i la degradació de les pales, en aquesta tesis s'exploren dos mètodes diferents, un basat en l'estimació de la fatiga i l'altre en la predicció de la

vida útil restant (RUL). El primer mètode utilitza el algorisme denominat ”rainflow counting”. El segon mètode fa servir un model de degradació de la rigidesa del material que descriu la propagació del dany a escala microscòpica degut a les esquerdes del material, aquest dany es manifesta originant una pèrdua de rigidesa del material de la pala.

Durant els darrers anys ha crescut l'interès per dissenyar que controladors que tinguin en compte la minimització de la fatiga o la maximització de les prediccions de RUL dels components. En aquesta tesis es proposa integrar la gestió de la salut del sistema basat en danys per fatiga o prediccions de RUL amb control predictiu basat en models (MPC). Aquesta aportació proveeix a l'aerogenerador d'un mecanisme per operar amb seguretat i, al mateix temps, permet optimitzar el compromís que hi ha entre reduir el dany o incrementar les prediccions de RUL amb la producció d'energia. En particular, aquest treball proposa una tècnica de control HAMPC per minimitzar el dany o incrementar les prediccions de RUL en les pales dels aerogeneradors. Per a la seva implementació s'ha integrat els models de fatiga basats en l'algorisme del rainflow counting i els de prediccions de RUL basats en la degradació de la rigidesa que permeten obtenir informació en temps real sobre el dany i les prediccions de RUL de les pales amb el MPC. La integració s'ha realitzat incorporant en la funció objectiu un criteri addicional que té en compte el dany i les prediccions de RUL de la pala.

Les contribucions presentades en aquesta tesi per la diagnosi de fallades, el control tolerant de fallades, la prognosi i la tècnica de control HAMPC han sigut validades en un cas d'estudi d'aerogeneradors basat en un aerogenerador de referència de 5MW de potència implementat en el simulador d'aerogeneradors d'alta fidelitat conegut amb el nom de FAST.

Acknowledgements

First Thank God above all the things, it would not be enough pages to express gratitude for everything even during the most difficult times.

This thesis was carried out at the Research Center for Supervision, Safety and Automatic Control (CS2AC) at Universitat Politècnica de Catalunya (UPC) with the financial support of the Spanish MINECO through grant BES-2012-058489. This support is gratefully recognized.

Thanks to my advisors and Ph.D. supervisors: Prof. Teresa Escobet and Prof. Vicenç Puig for their dedication during all of these years to this work, without their advice and guidance this work would not have been possible. Thank you for the suggestions, encouragement words and your close insight to all the details of this work. Special thanks to Prof. Joseba Quevedo for playing a decisive role in my selection as a Ph.D. candidate at the CS2AC and also for his positive feedback and good moments shared during the last years. I would like to thank Prof. Silvio Simani and Prof. Horst Schulte for their valuable time spent in the revision of this thesis.

During these years I had the opportunity to perform three research stays abroad. I would like to thank Dr. Peter Fogh Odgaard, Prof. Rafael Wisniewski and Dr. José de Jesús Barradas for being excellent hosts and for all the interesting scientific discussions during my stay at the Control and Automation Section in Aalborg University, Denmark and the collaboration afterward.

From the Prognostics Center of Excellence (PCoE) at NASA Ames Research Center, United States of America, I would like to thank Dr. Shankar Sankararaman for his precise guidance in the field of prognostics and also, for encouraging and showing me a pragmatical point of view to the challenges that were faced in our research collaboration, Dr. Susan Frost for her expertise and for providing me advice with an authentic spirit of a teacher and Dr. Kai Goebel for his leadership, his valuable insight and time dedicated to my work, and also for giving me the opportunity to perform research stays with his group in two occasions. Special thanks to Dr. Abhinav Saxena for his expertise and guidance during the first stages of my research collaboration with the PCoE. My gratitude to all of the guys at the PCoE for their friendship, collaboration and making me feel like I was at home during both of my stays there.

I would like to thank the Universities Space Research Association (USRA) staff: Deanna, Susan, Saba and David for all their support in the logistics and practical aspects of both of my stays at NASA Ames and for making me feel welcomed and easily adapted to my experiences there.

Thanks to my colleagues at UPC for their companionship and good moments shared during these years. Thanks to Andreu Quesada and Judit Esteve for their administrative support and good disposition to help whenever was needed.

Special thanks to my family, which are a fundamental pillar of my life. To my dad Hector whose example of perseverance and sacrifice, teachings and love will always remain with me and to my mom Miriam for her spiritual support, good advice when I needed the most, and her love. Thanks also to the closest members of my family who have been there with their advice, support and affection all of the times, especially during the most difficult ones.

Contents

List of Figures

List of Tables

Acronyms

AI	Artificial Intelligence
AIS	Artificial Immune Systems
ANN	Artificial Neural Networks
ARRs	Analytical Redundant Relations
BRM	Blade Root Moment
CBD	Consistency Based Diagnosis
CI	Computational Intelligence
CMS	Condition Monitoring Systems
DOEs	Department of Energy's
DOWEC	Dutch Offshore Wind Energy Convertor
EAs	Evolutionary Algorithms
EC	Evolutionary Computation
EMA	Electro-Mechanical Actuator
EOL	End of Life
FAST	Fatigue Aerodynamics Structures Turbulence
FD	Fault Diagnosis
FDI	Fault Detection and Isolation
FDIF	Fault Detection and Isolation Filter
FFT	Fast Fourier Transform
FHOP	Finite Horizon Optimization Problem
FLC	Full Load Control
FNNs	Fuzzy Neural Networks
FS	Fuzzy Systems
FTC	Fault Tolerant Control
FSM	Fault Signature Matrix
GE	General Electric
HAC	Health Aware Control
HAMPC	Health Aware Model Predictive Control
IEA	International Energy Agency
IFAC	International Federation of Automatic Control
IBAO	Interval Based ARRs and Observers
IPC	Individual Pitch Control
ISET	Institut für Solare Energieversorgungs Technik
LPV	Linear Parameter Varying
LQR	Linear Quadratic Regulator

MPC	Model Predictive Control
NREL	National Renewable Energy Laboratories
OEMs	Original Equipment Manufacturers
OM	Operation and Maintenance
PHM	Prognostics and Health Management
PID	Proportional Integrative Derivative
RFC	Rainflow Counting
RBM	Residuals Based Method
RECOFF	Recommendations for Design of Offshore Wind Turbines
RUL	Remaining Useful Life
RMS	Root Mean Square
SHM	Structural Health Monitoring
SCADA	Supervisory Control and Data Acquisition
SI	Swarm Intelligence
SVM	Support Vector Machines
SVMO	Support Vector Machines and Observers
SVMR	Support Vector Machines and Residuals

Chapter 1

Introduction

1.1 Introduction and Motivation

Wind Turbines are one of the fastest growing sources of power production in the world today being a constant need to reduce the costs of maintenance and operation. System health monitoring is commonly employed for the early detection of faults/failures so as to minimize downtime and maximize productivity.

The arrival of new sensors/actuators in the complex technological systems and processes made possible the development of several sophisticated monitoring and control applications where a large amount of real-time data about the monitored environment is collected and processed to activate the appropriate control actions and to achieve the desired control objectives. However, the probability of failure of some of these components will increase exponentially with their number. Thus, the safe and reliable operation must take into account mechanisms for early fault detection avoiding performance degradation and damage to the machinery or human life.

Maintaining the health of a complex system is a difficult task that requires the in-depth analysis of the target system, principles involved and their applicability and implementation strategies. According to Ofsthun (2002), a System Health Monitoring (SHM) module once implemented in the target system will be able to: diagnose the root cause of a system failure, furnish data and recommend solutions in real time, provide prognostic capability to identify potential issues before they become critical and capture and retain knowledge for predictive maintenance and new designs.

To this aim, an SHM system consists of instrumentation components, a fault detection, isolation and response module, diagnostic and prognostic software, as well as processes and procedures responsible for information gathering about systems health and corresponding decision-making.

Fault diagnosis (FD) and fault tolerant control (FTC) of wind turbines are important issues in order to decrease the operation and maintenance costs and increase penetration into electrical grids because the enhanced reliability those techniques can provide. However, the complexity of large modern wind turbines makes difficult to transfer advanced FD and FTC methods from the theory to application.

Prognostics is another important aspect of the wind turbine system health monitoring. The prognostics system must have the ability to forecast the future conditions or failure risk of a component or system given the past operating environment and how the system is expected to be operated in the future.

As discussed in García et al. (2012), in the wind turbine industry, Condition Monitoring Systems (CMS) are commonly used for early detection of faults in order to minimize downtime and maximize productivity. CMS comprises a signal processing equipment/algorithms and a set of sensors that provide continuous indications of component (and, consequently wind turbine) condition. There have been a few literature reviews on wind turbine condition monitoring such as García et al. (2012).

As the wind energy has gained increasing attention from industries and academia since 2006, many new research works have been reported towards integrating advanced fault diagnosis algorithms in the CMS. Currently, most of the CMS in wind turbines are data-based and utilize e.g. vibration and acoustic emission measurements (Liu et al., 2012), frequency domain analysis (Yang et al., 2010), time domain analysis (Chen, 2010) and support vector machines (Zeng et al., 2013). Only recently, some work has been done on model-based fault diagnosis in wind turbines. For example, an observer based scheme to detect sensor faults in the pitch system was presented in Chen et al. (2011) and a parity equations based scheme for fault detection in wind turbines was proposed in Karimi et al. (2008).

Some of the wind turbine components are more likely to fail or have a higher cost than others, and because of this reason, many works found in the literature are focused in some of the components rather than others. Some works for the following components were found in the literature: gearbox (Chen, 2010) (Kia et al., 2009), bearings Gong et al. (2010), pitch system (Schulte et al., 2012) and electrical system (Karimi et al., 2008; Campos-Gaona et al., 2013; Parker et al., 2013; Bernal-Perez et al., 2013; Freire et al., 2013; Vedreño Santos et al., 2014).

Fatigue as a critical loading pattern has been identified by the scientific community as the cause of the majority of structural failures in both composite and conventional structures such as wind turbine blades (Vassilopoulos, 2013). Due to the high number of load cycles that occur during the life of the turbine, fatigue considerations are of particular importance in wind turbine control. Fatigue can be understood as the breakdown of the material subject to stress, especially when repeated series of stresses are applied. It is a phenomenon that occurs on a microscopic scale, manifesting itself as deterioration or damage. Consequently, it has been widely and exhaustively studied from different perspectives (Musallam and Johnson, 2012). The awareness of wind turbines as fatigue critical machines has led to a significant amount of research that covers several fatigue analysis techniques for different wind turbine components. A widely used damage rule to formulate fatigue analysis in wind turbines is the Palmgren-Miner linear damage rule (Miner, 1945). This rule commonly called the Miner's rule is being currently used throughout the industry and in the academia (Sutherland, 1999; Marín et al., 2008). In addition to Miner's rule based damage analysis, linear crack propagation models had been used for the fatigue analysis of wind turbines with successful applications (Lampman, 2009; Gray and Watson, 2010).

Fatigue and stiffness degradation for wind turbine rotor blades has been studied in depth in the work of Nijssen (2006), where the term ’damage’ is generally used for all kinds of physical deterioration of the material, despite its effects on material performance. In Miner’s sum, which is said to describe a linear accumulation of ’damage’ the nature of this damage is not specified, neither is its effect on material performance, such as stiffness or strength. In practice, ’damage’ should be application-related (Nijssen, 2006). In this work, both Miner’s rule and a stiffness degradation model for wind turbine rotor blades are considered as approaches to estimate damage and remaining useful life (RUL) predictions of wind turbine blades.

With the increasing size and complexity of wind turbines, the need for more sophisticated load control techniques has induced the interest for locally distributed aerodynamic control systems with build-in intelligence. Thus, there is a need for more advanced control systems emerging from the health condition of modern wind turbines and current load reduction control capabilities. Therefore there is an important motivation to diagnose the most common faults present in wind turbines as well to design advanced control systems that take into account these faults and the ’damage’ or degradation occurring in wind turbines for safe operation and to optimize the trade-off between power production, wind turbine system performance and degradation of the wind turbine components.

1.2 Thesis Objectives

The objectives of this Thesis are the following:

- To collect from the literature a wind turbine model suitable for fault diagnosis, prognostics and control.

- To propose a fault diagnosis scheme for a wind turbine benchmark proposed by the research community that is capable of diagnosing the proposed fault scenarios and improving the performance respect to other approaches.

- To design a fault tolerant control approach for the wind turbine that considers one of the fault scenarios proposed in the wind turbine benchmark.

- To investigate fatigue estimation techniques and degradation models that can be used to calculate remaining useful life (RUL) predictions of wind turbine blades and integrate these models and techniques with the information available on the high fidelity wind turbine simulator FAST.

- To propose and validate a control approach that integrates fatigue and RUL information considering the trade-off between power production and fatigue damage reduction or RUL extension on the wind turbine.

1.3 Outline of the Thesis

The Thesis manuscript is organized in seven chapters. **Chapter 2** presents the background theory and bibliography review. **Chapter 3** describes the wind turbine modeling which is used for diagnosis, prognostics and control purposes. **Chapter 4** proposes the fault diagnosis and fault tolerant control schemes applied to a wind turbine benchmark. **Chapter 5** explain two methods to estimate fatigue and calculate remaining useful life (RUL) predictions in wind turbine blades the application to the case study. **Chapter 6** proposes the health-aware model predictive control (MPC) approaches that integrate the methods described in the previous chapter. Finally, the conclusions are outlined in **Chapter 7**.

The outline of the thesis is detailed below:

- **Chapter 2:** This chapter presents the collected literature about the current health monitoring practice, fault diagnosis, prognostics and the integration of control and prognostics. The techniques that have been applied for fault diagnosis of wind turbines such as model-based, data-based and the ones that come from the artificial intelligence (AI) discipline are shown. It is also presented the prognostics approaches that have been found in wind turbine applications such as physical model-based, experience based, data-based and artificial intelligence (AI) approaches. Finally, previous efforts and works in the integration of control and prognostics approach are presented.

- **Chapter 3:** The wind turbine modeling is detailed in this chapter. The 5-MW reference wind turbine model and the high fidelity simulator FAST are used as the real plant system in this Thesis are described. Then, the nonlinear models for each of the subsystems that form the wind turbine are defined. In the last part of the chapter, a linear reduced order model is derived for control purposes.

- **Chapter 4:** A fault diagnosis (FD) and fault tolerant control (FTC) wind turbine benchmark presented by the research community (Odgaard and Johnson, 2013) is explained. Then, a model-based fault diagnosis approach that combines analytical redundant relations (ARRs) and interval observer is proposed for the set of ten fault scenarios introduced in the wind turbine benchmark and the results are compared to those obtained with other methodologies used by other authors. Also, a fault tolerant control scheme integrated with the fault diagnosis scheme which enables and disables the individual pitch control algorithm based on the fault detection of the fault in the rotor azimuth angle sensor is proposed.

- **Chapter 5:** Two approaches for fatigue estimation and calculation of remaining useful life (RUL) predictions with the respective application to the case study are investigated. The first approach is called Rainflow Counting which considers the fatigue cycles and amplitudes that together with Palmgren-Miner rule allow to calculate the accumulated fatigue damage in the blade. The second approach comes from the composites stiffness degradation theories, a stiffness degradation model from the literature is used to describe the damage growth in the blade and this model is later on embedded in a prognostics algorithm to calculate the remaining useful life (RUL) predictions of the blade. Both of the approaches are analyzed and compared using as inputs the flapwise blade root moment loads, which can be obtained as it is one of the sensors available in the wind turbine simulator FAST.

- **Chapter 6:** The health-aware model predictive control (HAMPC) approach is proposed. The proposed controller integrates the fatigue damage and RUL information from the approaches described in the previous chapter and considers the existing trade-off between power production and damage reduction or remaining useful life (RUL) increase. The controller is tested for realistic wind scenarios using the high fidelity wind simulator FAST.

- **Chapter 7:** The main contributions and conclusions of the Thesis are outlined as well some ideas for future work and research.

Chapter 2

Bibliography Review

This chapter presents a bibliography review of the areas of fault diagnosis, fault tolerant control and the integration of control with prognostics and fatigue applied to wind turbines where this thesis will contribute.

2.1 Current Health Monitoring Practice

Today wind turbines contribute to an important part of the world's power production, at the same time the size of the standard turbine is increasing.

An important part of system health management for wind turbines is to introduce advanced fault detection, isolation and accommodation systems. In the state-of-the-art industrial wind turbines, fault detection and accommodation schemes are simple and are often conservative. Consequently, the use of advanced fault detection, isolation and accommodation methods could improve the reliability of the turbine, even though it might result in production with limited power for some faults.

Wind turbines in the megawatt size as most often installed at present, are expensive. A major issue with wind turbines systems is the relatively high cost of operation and maintenance (OM), especially those located offshore. Wind turbines are hard-to-access structures, and they are often located in remote areas. These factors alone increase the OM cost for wind power systems.

According to General Electric (GE) Energy, a $5,000 bearing replacement can easily turn into a $250,000 project involving cranes, service crew, gearbox replacements, and generator rewinds, not to mention the downtime loss of power generation (Hatch, 2004). For a turbine with over 20 years of operating life, the OM and part costs are estimated to be 10-15% of the total income for a wind farm (Walford, 2006). Although larger turbines may reduce the OM cost per unit power, the cost per failure is increased. The OM cost for an offshore wind turbine is estimated to be 20-25% of the total income (Wilkinson et al., 2006; McMillan and Ault, 2007). Thus there is a growing research interest in developing automatic maintenance systems for offshore wind turbines which aim to reduce the costs detailed before, see for example (Pérez et al., 2011).

The ISET (Institut für Solare Energieversorgungs Technik, Germany) in (Ensslin et al., 2005) reported that electrical components have the highest failure rates, but drive-trains and blades cause the greatest down time and are the most expensive to repair. Thus, drivetrain and blade reliability is more important to monitor than the other components. Early knowledge of their impending failures allows maintenance planning and often can reduce repair costs dramatically.

Growing concern over failure rates of wind turbine gearboxes has caused many new megawatt-scale turbines to offer condition monitoring systems as standard equipment. In some cases, insurance companies require their installation. The condition monitoring systems usually include some type of vibration monitoring in multiple locations (Sheng et al., 2009). Some include lubrication particle counting. They potentially can provide the greatest insight and earliest detection of gear and bearing anomalies.

Other health monitoring techniques are not as mature. The next most important large component is the blade. Cracks can originate in a variety of locations such as the trailing edge and near structural transition regions (Butterfield et al., 2009).

Detecting such cracks is very difficult and is usually done by visual inspection. Fortunately, they usually grow rather slowly, which allows annual inspections to track and maintain them before they grow to catastrophic dimensions. However, they can occur in locations that are impossible to inspect visually. Furthermore, the blade has a tremendous surface area. So detection techniques that focus on one small region are likely to miss cracks in other areas of the blade, and it is impossible to know in advance where the cracks may originate. Finally, manual inspection is imperfect and can miss critical cracks in their incubation stage. Thus the need for a reliable, inexpensive, automated technique for detecting cracks over large areas of the blade. This is a major challenge that may require strategies that apply comprehensive techniques to one or two lead turbines in each wind plant (Butterfield et al., 2009).

2.2 Fault Diagnosis of Wind Turbines

Fault diagnosis covers several steps: fault detection (decide whether a fault has occurred and the time of occurrence), fault isolation (determining in which component a fault has occurred) and fault identification and estimation (identify the fault and estimate its magnitude). In general, fault detection is based on mathematical signal and process models and on methods of system theory and process modeling to generate fault indicators.

Fault-isolation methods use causal fault-symptom relationships by applying methods from a statistical decision, artificial intelligence and soft computing. Therefore, efficient supervision, fault detection and diagnosis is a challenging field encompassing physical-oriented system theory, experiments and computations (Isermann, 2011).

Condition monitoring has emerged as a tool for deciding the optimal interval between two maintenance inspections, which improves the system availability (Saranga, 2002). Condition monitoring is defined as the continuous or periodic measurement and interpretation of an item to determine the need for maintenance (British Standards, 1984).

Fault diagnosis is a sophisticated adaptation of condition monitoring systems (CMS) that incorporate intelligent algorithms suitable for early detection of incipient faults providing an insight into the corresponding level of criticality (Márquez et al., 2010).

Condition monitoring and fault diagnosis of wind turbines provide an important economic benefit since they allow the scheduled maintenance, reduces the downtime of the wind turbine and are capable of predicting a catastrophic failure of the wind turbine. In addition, wind turbine repair and maintenance that require extensive usage of cranes and lifting equipment create a highly capital-intensive operation as well as delayed services due to lack of crane availability and needs for optimal weather conditions. Also, the trend that has currently emerged to dampen prospects is a lack of personnel available to perform the consistent OM required to keep turbines functioning and efficient. Therefore, the reliability of these turbines is important. Their off time should be as little as possible.

Some literature reviews on wind turbine condition monitoring have been found, such as Hammeed et al. (2009); Amirat et al. (2007); Hyers et al. (2006); Wilkinson et al. (2007). However, as the renewable energies have gained dramatically increasing attention from industries and academia since 2006, many new research works have been reported in the condition monitoring and fault diagnosis areas.

Most condition monitoring and fault detection systems in wind turbines are signal-based and utilize e.g. vibration analysis to detect and isolate faults. This has enabled successful condition monitoring of bearings in the gearbox and the generator among others. Only a few model-based fault diagnosis approaches exist for wind turbines; among these are fault diagnosis systems for pitch sensors and actuators (Wei and Verhaegen, 2008; Donders, 2002). These diagnosis systems estimate some parameters in the pitch system and determine if a fault has occurred based on these estimates.

Side effects on other components such as the gearbox, bearings, blades pitch, rotor, generator, the braking system and several system sensors can be reduced significantly with online condition monitoring and diagnosis. Many faults can be detected while the defective component is still operational. Therefore, necessary repair actions can be planned in time and do not need to be taken immediately. This is important especially for offshore plants, where bad weather conditions (storms, high tides, etc) can prevent any repair actions for several weeks. Also, condition monitoring and fault diagnosis can detect extreme external conditions, such as icing or water induced tower oscillations of offshore plants, and can trigger appropriate control actions to prevent damage of wind turbine components.

Alternatively, autonomous online condition monitoring systems with integrated fault detection algorithms allow early warnings of mechanical and electrical faults to prevent major component failures.

Some work has been done recently on model-based fault detection, isolation and accommodation on wind turbines. In Wei et al. (2008), an observer based scheme to detect sensor faults in the pitch system were presented. A parity equations based scheme for fault detection on wind turbines was presented in Dobrila and Stefansen (2007), an unknown input observer was proposed for detection of sensor faults around the wind turbine drive train (Odgaard et al., 2009).

Fault detection of electrical conversion systems can be found in Poure et al. (2007). In Negre (2010), a fault diagnosis system for a wind turbine was designed using model-based fault diagnosis methods, real field data from a 3MW wind turbine was used to identify a nominal model and Linear Parameter Varying (LPV) models were used to do fault diagnosis in a wide range of operating points. Condition monitoring is used as well to monitor some mechanical components such as e.g. gearboxes, see Hammeed et al. (2009).

Modern wind turbine control systems are equipped with condition monitoring and fault detection systems. These systems detect and isolate faults and determine the current operating conditions of the wind turbine. The available information can then be utilized for predictive maintenance, which basically predicts when maintenance should be performed to avoid failures.

In Esbensen and Sloth (2009), a structural analysis of a wind turbine system was done and several analytical redundant relations were found to perform fault detection. The fault diagnosis system consists of fault detection and isolation algorithms that determine the current state of the system and reconfigure an extended Kalman filter, which is able to provide a fault-corrected state estimate at all times. This last work was taken as an important reference in the development of this master thesis.

Some recent research coming both from the academia and the industry motivated a benchmark model proposal of a wind turbine at a system level. This benchmark contained the most common faults present in sensors, actuators and system, and it was presented in Odgaard et al. (2013). This benchmark model was based on a realistic generic three blade horizontal variable speed wind turbine with a full converter coupling. In the spring of 2010, kk-electronic together with other partners (MathWorks and Aalborg University) launched an international competition on Fault Detection and Isolation of Wind Turbines based on this benchmark model of the wind turbine. The competition consisted on finding the best schemes to detect and handle the different faults proposed, and the results of the competition were presented in Odgaard and Stoustrup (2012). The competition drew enough high-quality papers to fill two sessions at the IFAC World Congress 2011 and also several proposals were published at the IFAC Safeprocess in 2012.

After the announcement of results of the first benchmark, a second challenge was presented in Odgaard and Johnson (2013), this new benchmark differed from the previous challenge in several ways. The second benchmark wind turbine model is modeled in FAST simulator (Manjock, 2005). In this case, there are no sensor models available and the whole wind turbine dynamics are implemented in the simulator differing from the first benchmark in which all the subsystem models were provided. Some solutions were presented for this second benchmark in Sheibat-Othman et al. (2013) where two methods were employed to isolate faults of different types at different locations: Support vector machines (SVM) and a Kalman-like observer. SVM could isolate most faults with the used data and characteristic vectors, except for high varying dynamics. In that case, the use of an observer, which is model-based, was found necessary.

Fault diagnosis methods can be model-based or model-free based depending upon the way process knowledge is incorporated within the signal processing unit (García et al., 2012).

2.2.1 Model based techniques

These techniques utilize a mathematical model of the monitored machine. Based on this explicit model, residual generation methods are used to obtain signals, called residuals, which are used to indicate fault presence in the system. Finally, the residuals are evaluated to provide fault detection, isolation and identification. Model-based approaches can be more effective than other model-free approaches if a correct and accurate model is built. However, explicit mathematical modeling may not be feasible for complex systems since it would be very difficult or even impossible to build mathematical models for such systems (Jardine et al., 2006).

Two different communities (FDI community in the Automatic Control area and DX community in the Artificial Intelligence area) have developed their own methodologies for model-based fault diagnosis, one independently from the other. The FDI community has its roots in the classical theory of systems and automatic control (Gertler, 1998). On the other hand, the DX community has its roots in consistency-based diagnosis developed by Reiter (1987). The type of models used to describe the dynamic process is mainly based on qualitative models described by qualitative differential equations. Recently, the BRIDGE community (Biswas et al., 2004), based on the work of Cordier et al. (2004) has provided to researchers of both fields with a common framework for sharing results and techniques.

Using different techniques both communities have developed several algorithms that combining the measurement model with the process model obtain a set of analytical redundancy relations (ARR) (Staroswiecki et al., 2000; Blanke et al., 2006; Krysander et al., 2008) or potential conflicts (Pulido and Alonso, 2004), which are defined as relations between known variables. Another important issue in fault diagnosis is the optimal sensor placement problem to guarantee fault detectability and isolability (Bagajewicz, 2000; Nejjari et al., 2007; Rosich et al., 2007; Sarrate et al., 2007). Fault diagnosis has been incorporated as a tool for System Health Management (SHM) (Singh and Ahmed, 2003; Fu et al., 2004; Garcia et al., 2006).

The use of the **Kalman filter** supports estimations of past, present and future states, even when the exact parameters of the modeled system are unknown (Entezami et al., 2012).

Another method of obtaining residuals is to compare the redundant information about the system if the system has some physical redundancy built on it (Ozdemir et al., 2011).

Table 2.1 shows a list of the model-based techniques that have been applied to wind turbines fault diagnosis.

In the aerospace and related control engineering literature, the input-output model-based residual generators are usually dynamic and are referred to as **parity equations**, since residuals are obtained from these parity equations and are widely used in FDI (Fault Detection and Isolation) systems (Gertler and Singer, 1990).

2.2.2 Data-based techniques

In data-based techniques no mathematical or physical models are used, they are based on data acquisition and data processing in which the analysis and handling of the data are performed in

Table 2.1: Model based approaches applied to wind turbines

Technique	Reference
Observers	(Schulte et al., 2012), (Odgaard et al., 2009), (Casau et al., 2012), (Chen et al., 2011)
Kalman Filters	(Donders, 2002), (Karami et al., 2010), (Sheibat-Othman et al., 2013)
Parity Equations	(Ozdemir et al., 2011), (Blesa et al., 2011)
Parameter estimation	(Rose and Hiskens, 2008)
Support Vector Machine	(Laouti et al., 2011), (Sheibat-Othman et al., 2013)

order the detect and diagnose faults in the system.

In García et al. (2012), different data-driven techniques used for fault diagnosis of wind turbines are explained: statistical methods, frequency analysis, time domain analysis, wavelet transformation.

In the **statistical methods**, the data signals from various sensors in wind turbines are analyzed. Common statistical measures such as root mean square (RMS), skewness, kurtosis, are widely used for fault diagnosis(García et al., 2012).

Time-domain analysis is directly based on the time waveform itself. The traditional time-domain analysis calculates characteristic features from time waveform signals as descriptive statistics such as mean, peak, peak-to-peak interval, standard deviation, crest factor, etc. These features are usually called time-domain features (Jardine et al., 2006).

Frequency-domain analysis is based on the transformed signal in frequency domain. The advantage of frequency-domain analysis over time-domain analysis is its ability to easily identify and isolate certain frequency components of interest. The most widely used conventional analysis is the spectrum analysis by means of fast Fourier transform (FFT) (Jardine et al., 2006).

One limitation of the frequency-domain analysis is its inability to handle non-stationary waveform signals, which are very common when machinery faults occur. Thus, time−frequency analysis, which investigates waveform signals in both time and frequency domain, has been developed for non-stationary waveform signals (Jardine et al., 2006).

Wavelet transformation is a time–frequency representation of a signal. The wavelet analysis of a waveform signal expresses the signal in a series of oscillatory functions with different frequencies at a different time by dilations via the scale parameter a and translations via the time parameter b as follows

$$W\left(a,b\right)=\frac{1}{\sqrt{a}}\int\limits_{-\infty}^{+\infty}x(t)\psi^{*}\left(\frac{t-b}{a}\right)dt \tag{2.1}$$

In the Table 2.2 the different techniques found in the literature are listed with their respective references.

Table 2.2: Data Driven Techniques applied to Wind Turbines

Technique	Reference
Statistical methods	(Zimroz et al., 2012), (Dong and Verhaegen, 2011), (Niknam et al., 2013), (Li and Frogley, 2013)
Time domain analysis	(Futter, 1995), (Miller, 1999), (Cheng et al., 2010)
Frequency analysis	(Wilkinson et al., 2007), (Yang et al., 2008a), (Liu et al., 2012), (Hatch, 2004), (Hammeed et al., 2009), (Caselitz and Giebhardt, 2005), (Zhang et al., 2011), (Shuting et al., 2006), (Liu et al., 2012), (Amirat et al., 2011), (Lei et al., 2010), (Ebersbach et al., 2006), (Qu et al., 2013), (Tamilselvan et al., 2013)
Wavelet transformation	(Huang et al., 2008), (Gong et al., 2010), (Yang et al., 2008b), (Lei et al., 2010), (Loutas et al., 2009), (Tsai et al., 2006), (Yang et al., 2009), (Tang et al., 2014), (Changzheng et al., 2005), (Chen, 2010), (Guo et al., 2010), (Yang et al., 2008a), (Miller, 1999), (Chase et al., 2013)

2.2.3 Artificial Intelligence techniques

Artificial intelligence (AI) is essentially employed to reproduce human reasoning as accurately as possible, the reasoning process is based on the behavior of the system, and written down in terms of rules (García et al., 2012).

In the review Jardine et al. (2006) are mentioned two popular AI techniques for machine diagnosis are artificial neural networks (ANNs) and expert systems. Other AI techniques used include fuzzy–logic systems, fuzzy–neural networks (FNNs), neural–fuzzy systems and evolutionary algorithms (EAs). Some works found in the literature where AI techniques are applied to wind turbines are listed in Table 2.3.

Table 2.3: Artificial Intelligence techniques applied to Wind Turbines

Technique	Reference
Neural Networks	(Zhe and Qingding, 2007), (Rafiee et al., 2007), (Kusiak and Verma, 2012)
Fuzzy Logic	(Simani et al., 2011), (Kamal et al., 2011), (Schlechtingen et al., 2013)
Evolutionary Algorithms	(Kusiak and Verma, 2011)
Expert Systems	(Zhi-Ling et al., 2012), (Godwin and Matthews, 2013)

2.3 Prognostics of Wind Turbines

Wind turbines are subject to considerable stresses due to unpredictable environmental conditions resulting from rapidly changing local dynamics. In that context, systems health management has the aim to assess the state-of-health of components within a wind turbine, to estimate remaining useful life, and to aid in autonomous decision-making to minimize turbine damage. As a consequence, recently the interest in prognostics and predictive maintenance has been emerged. The goal is to be able to predict the remaining useful life of a wind turbine and to schedule maintenance prior to the failure of a component. This will reduce downtime and even increase the lifetime of the wind turbine itself.

There is little disagreement in the published literature that prognostics is related and highly reliant upon diagnosis. However, although widely discussed, the exact demarcation between the two fields is not well defined. In the work of Sikorska et al. (2011), it is proposed a simple delineation: diagnosis involves identifying and quantifying the damage that has occurred (that is thus retrospective in nature), while prognostics is concerned with trying to predict the damage that is yet to occur. Although diagnosis may provide useful business outputs on its own, prognostics relies on diagnosis outputs (e.g. fault indicators, degradation rates, etc.).

One of the aspects that are desirable from operators and original equipment manufacturers (OEMs) perspective is to have information about the damage and remaining useful life predictions provided by condition or health monitoring systems (Frost et al., 2013). Structural health information is necessary for the wind turbine to continue operating and producing power without exceeding some damage thresholds resulting in unscheduled downtime.

The challenge is thus to decide maintenance actions on components on the way to continuously reduce and eliminate costly unscheduled downtime and unexpected breakdowns, see Iung et al. (2008).

For offshore wind turbines, the higher operation and maintenance costs represent a larger overall proportion of the cost of energy than for onshore turbines, even when the large initial investment required for the installation of offshore turbines is included. One of the reasons that these costs are likely to be higher offshore is that the offshore environment will bring increased work loading which is relatively uncharacterized (Myrent et al., 2013).

Fatigue can be understood as the breakdown of the material subject to stress, especially when repeated series of stresses are applied. It is a phenomenon that occurs on a microscopic scale, manifesting itself as deterioration or damage. Consequently, it has been widely and exhaustively studied from different perspectives (Musallam and Johnson, 2012). The awareness of wind turbines as fatigue critical machines has led to a significant amount of research that covers several fatigue analysis techniques for different wind turbine components. A damage rule used to formulate fatigue analysis in wind turbines is the Palmgren-Miner linear damage rule (Miner, 1945). This rule commonly called the Miner's rule is being currently used throughout the industry and in academia (Sutherland, 1999; Marín et al., 2008). In addition to Miner's rule based damage analysis, linear crack propagation models had been used for the fatigue analysis of wind turbines with successful applications (Lampman, 2009; Gray and Watson, 2010).

An understanding of the fatigue behavior of a wind turbine rotor blade is also valuable for the improvement of product development practices. Product development practice up to now has been based on an iterative process whereby a prototype rotor blade is built and tested against real, or realistic, loading patterns. However, this process is costly and time-consuming. The ability to simulate the fatigue behavior of the material, the blade structural component and/or the wind turbine rotor blade reduces the cost and allows the development of a wider range of products without the need for increasing the number of physical prototypes (Vassilopoulos, 2013).

In this thesis, fatigue in the blade root is analyzed. This component has been identified as a critical area for fatigue in several works such as Sutherland (1999) which shows, that the edgewise blade root bending moment frequency distribution from a small turbine contains two peaks; one originating from the wind loading, the other as a result of the blade being loaded by its own weight. In Caprile et al. (1995), histograms of mid-size wind turbine blade edgewise and flapwise blade root moments showing the same peak for the edgewise loading are presented. For larger rotor blades, the edgewise gravity fatigue loading becomes increasingly relevant for life prediction. In Kensche and Seifert (1990), typical root bending moments are estimated from measurements on wind turbine blades, both in flap and edgewise direction.

Experimental evidence (Nijssen, 2006) has shown that typical composite materials used in wind turbine rotor blades exhibit strength degradation trends. The degradation of those materials in fatigue conditions has been thoroughly studied in Vassilopoulos and Nijssen (2010).

Different methods have been proposed to characterize the degradation of composite materials used in the wind turbine blades. Some of them are based on phenomenological life predictions while others consider the actual mechanical damage modeling. In this work, one phenomenological method and one fatigue damage model are analyzed for the life prediction of wind turbine blades: the rainflow counting and a fatigue stiffness degradation model, respectively. Both methods are tested in a high fidelity wind turbine simulator.

Prognostics for SHM try to solve, mainly, two problems. First, to determine the time window over which maintenance must be performed without compromising the system's operational integrity. And, second estimating the time-to-failure and providing information to an operator whether it is possible to continue operating or an immediate shutdown for maintenance is required. The first shows if it is possible to reduce needed maintenance through optimized maintenance intervals and at the same time unplanned maintenance and associated costs as well as to improve safety and reduce environmental impacts. The second tries to provide advice on how to change operating conditions (speed, load, stress) to reduce damage as well to provide information about whether the equipment has high probability of safe operation for the planned mission.

Over recent years a significant amount of research has been undertaken to develop prognostic models that can be used to predict the remaining useful life of engineering assets over a prediction horizon. This horizon is selected, for example, according to the necessary time to plan maintenance actions.

Prognostics approaches have been classified by several authors in the paper of Sikorska et al. (2011).

Industrial implementations have only had limited success. By design, models are subject to specific assumptions and approximations, some of which are mathematical, while others relate to practical implementation issues such as the amount of data required to validate and verify a proposed model. Therefore, appropriate model selection for successful practical implementation requires not only a mathematical understanding of each model type but also an estimation of how a particular business intends to utilize a model and its outputs (Sikorska et al., 2011).

Prognostics and health management (PHM) is a method that allows the reliability of a system to be evaluated in its actual application conditions. Thus, by determining the advent of failure, procedures can be developed to mitigate, manage and maintain the system (Vichare, 2006).

Different approaches have been considered for prognostics and similar to diagnosis, the approaches to prognostics fall into three main categories: physical model-based techniques, stochastic/statistical approaches, data-based and artificial intelligent approaches (Welte and Wang, 2013).

Physical Model-Based Approaches

In the physical model based techniques, models based on physical laws are used to compute an estimated output for the remaining useful life of a component/machine from a mathematical representation of the physical behavior of the degradation processes (Sikorska et al., 2011).

Under this category the stress-based approaches which consider the environmental stresses (temperature, load, vibration, etc.) on the component can be found. These approaches are based on the estimation of the life of an average component under specific usage conditions.

On wind turbine applications, most applied physical models are the ones used for fatigue lifetime prediction. Two of the basic material fatigue models are Miner's rule and Paris law, where the former can be classified as a failure model, and the latter as a degradation model (Welte and Wang, 2013).

S-N-curves and the Palmgren-Miner rule (also simply called Miner's rule) are failure models for fatigue life assessment of many types of materials. If a material is subject to a sufficient number of stress cycles that are above the fatigue limit, a fatigue crack or damage will develop, leading finally to failure (Dowling, 1999).

Paris law is a physical degradation model that describes the growing of a fatigue crack. The model can be used to predict the further growing of a fatigue crack and estimate the remaining life until fracture of the material. More details about the approach can be found in Dowling (1999). Paris law, the S-N-curves approach and related approaches have frequently been applied to fatigue life analysis of wind turbine rotor blades (Welte and Wang, 2013).

Experience Based Approaches

These approaches determine the life expectancy of individual machine components with respect to the expected risk of deterioration under known operating conditions. In Sikorska et al. (2011), two types of models used for the RUL prediction, which can be put in this classification: stochastic models and statistical/reliability models, are established.

Stochastic models are based on probability theory and statistical methods. If a model is "purely" stochastic it does not represent a physical process or mechanism but is used to establish a relation between model inputs and outputs using any mathematical equation or expression that provides a good fit given the data (Loucks et al., 2005).

Parameter estimation in stochastic modeling is based on the observation of the model output. Thus, observations of the model output, such as observations of lifetime or degradation, are usually collected as a basis for parameter estimation. When possible, one should fit different stochastic models to the data and choose the model that gives the best prediction. Many techniques exist to choose the best model and to check the goodness of fit (e.g. p-value, confidence intervals, comparison of maximum likelihood values and various graphical methods such as probability plots).

Statistical/reliability models consider the historical time to failure data which are used to model the failure distribution. They estimate the life of an average component under average usage conditions as in Heng et al. (2009); Ramachandran et al. (2010). Forecasting of future deterioration is often undertaken by comparing the results of previous inspection results with models representing 'good' behavior. They typically utilize temporal data such as condition or process monitoring outputs and are also often categorized as 'data based' models (Sikorska et al., 2011).

According to Welte and Wang (2013), most of the statistical/reliability models are of general nature and can be applied to many different problems. An advantage of these models applied to lifetime prediction is that they provide an estimate of the mean lifetime and several measures of the associated uncertainty, such as the variance of the lifetime, confidence intervals for parameters and predictions, etc.

Fu2004

Data-based and Artificial Intelligent approaches

Data-based techniques utilize monitored operational data related to system health. They can be beneficial when understanding of first principles of system operation is not straightforward or when the system is so complex that developing an accurate alternative model is prohibitively expensive.

Many data-based models can be classified as black-box models because the relation of input and output variables and the model parameters is unclear in such types of models. Parameter estimation in black-box models is often based on learning and training. Thus, the models require data, and often data covering a time period where a failure was observed, in order to make a prediction of the lifetime (Welte and Wang, 2013).

Artificial intelligence includes subfields and groups such as machine learning, pattern recognition, computational intelligence (CI), expert systems, etc. Computational intelligent algorithms include artificial neural networks (ANN), evolutionary computation (EC), swarm intelligence (SI), artificial immune systems (AIS) and fuzzy systems (FS).

Since there are many models and methods in the field of AI, that in addition often are quite different, it is difficult to make general statements about models properties and the ways of parameter estimation. Many models can be considered as black-box models. Some others, as for example expert systems, are white-box models where the internal model logic is based on expert knowledge (Welte and Wang, 2013).

AI techniques applied to RUL estimation have been considered by some researchers. In Zhang and Ganesan (1997) self-organizing neural networks for multi–variable trending of the fault development are used to estimate the residual life of a bearing system. In the work of Wang and Vachtsevanos (2001), dynamic wavelet neural networks are applied to predict the fault propagation process and estimate the RUL as the time left before the fault reaches a given value. In Yam et al. (2001), a recurrent neural network for predicting the machine condition trend is applied. In Dong et al. (2004), a grey model and a BP neural network to predict machine condition is utilized. In Wang et al. (2004), the results of applying recurrent neural networks and neural-fuzzy inference systems to predict the fault damage propagation trend are compared. In Chinnam and Baruah (2004), a neural-fuzzy approach for estimating RUL is proposed for the situation where no failure data and no specific failure definition model are available, but domain experts with strong experience-based knowledge are available (Jardine et al., 2006).

Applications of AI models to wind turbine lifetime prediction are difficult to find. Case studies using real SCADA and condition monitoring data from wind turbines showed that the models presented are capable of providing warnings of potential failures several hours before they actually occur. Some of the models and methods that have been applied in these studies are ANNs, support vector machines, principle component analysis, auto-associative neural networks and self-organizing feature maps. In Table (2.4), the applications to wind turbines of the prognostics approaches explained in this section are summarized.

Table 2.4: Prognostics approaches applied to wind turbines

Approach	**Reference**
Model based	(Sutherland, 1999), (Nijssen, 2006), (Marín et al., 2008), (Ronold et al., 1999), (Sutherland and Mandell, 1996), (Andrawus et al., 2007)
Statistical/reliability	(Guo et al., 2009), (Spinato et al., 2009), (Coolen et al., 2010), (Tavner et al., 2005), (Tavner et al., 2007), (Hameedand and Vatn, 2011), (Byon and Ding, 2010), (Nielsen and Sørensen, 2010), (Zhu et al., 2013), (Nielsen and Sørensen, 2011)
Data-based and Artificial Intelligence (AI)	(Samanta and Nataraj, 2008), (Hussain and Gabbar, 2013)

2.4 Integration of Prognostics with Control Techniques

Two key technology drivers for turbine manufacturers are: increasing turbine up-time and reducing maintenance costs. What is desirable from operators and original equipment manufacturers (OEMs) perspective is to have a turbine controller that is capable of adapting to damage and remaining useful life predictions provided by condition or health monitoring systems.

Actuator systems are employed widely in aerospace, transportation and industrial processes, wind energy sector. There have been several efforts found in the literature to integrate prognostic information of components, i.e. Remaining Useful Life (RUL) predictions with control schemes that use prognostic information of the monitored component to reconfigure the control scheme in order to increase the RUL of the component by trading off system performance. In the work of Brown et al. (2009), a reconfigurable model predictive controller is proposed for an Electro-Mechanical Actuator (EMA) system that performs a trade-off between the RUL of the subsystem and the performance.

In the literature review, the integration of control strategies and load mitigation applied for two scenarios is found: one for a unique wind turbine and the second one where there are several wind turbines working at the same time (i.e. a wind farm). These two cases are rather similar. However, the case of wind farms has some other aspects to be considered such as the total wind farm power production demand, the different amount of loads suffered by the wind turbines, depending on their location in the wind farm, etc. Furthermore, by integrating the health of each turbine into the operation and control of the wind farm using a damage mitigating control strategy, the overall economic profit of the wind farm could be increased.

In Soleimanzadeh and Wisniewski (2011), the aim is to develop a wind farm controller which looks for the optimal distribution of power references among wind turbines controllers, while it lessens the fatigue-structural loads. Integrating the health of each turbine into the operation and control of the wind farm using a damage mitigating control strategy leads to an increase in the overall economic profit of the wind farm. Some other control strategies applied to wind turbine load mitigation can be found in (Parker and Johnson, 2009; Eide, 2011; Hand and Balas, 2007).

Predictions of the remaining useful life of the system may then be used to schedule maintenance actions (Banjevic, 2009). Eventually, it may be required to anticipate the maintenance action if PHM system indicates that the degradation level is approaching to the safe operation threshold. If such an anticipation is impractical or too costly, the operating conditions could be derated in order to mitigate degradation. For instance, if the degradation involves an actuator in a specific closed-loop system, the control effort could be re-distributed among the remaining actuators, so as to maintain the performance (Du et al., 2010). In Bento-Pereira et al. (2010), a model predictive control (MPC) approach is proposed being capable of distributing the control effort among actuators on the basis of PHM information and to exploit relations between control effort and actuator degradation. Another application of model predictive control in wind turbines load mitigation can be found in Spudic et al. (2012). According to Lio et al. (2014), in the recent years, many advanced control strategies have been proposed for the operational control of wind turbines. Unfortunately, they have not been adopted by the industry. However, the application of model predictive control (MPC) to wind turbines has started to attract the attention of academia and the industry (Odgaaard and Hovgaard, 2015a,b; Odgaard et al., 2016), because of the possibility of dealing with the conflicting power optimization and fatigue load reduction problem, as it has been shown in a number of publications. For example, the use of MPC for switching between partial and full load operation of the wind turbine while reducing tower fore-aft fatigue loads was reported in Adegas et al. (2013), which also addresses pole placement based objective functions, and a discussion of implementation structures for the MPC solution with the existing wind turbine controller as well.

A Full Load Control (FLC) with wind speed predictions based on light detection and ranging (LIDARS) have been proposed in Soltani et al. (2011). Control for floating and solid foundation wind turbines has been investigated in Henriksen (2007), where the application of MPC control for different wind speeds and modes of operation has been addressed. Feedback-Feedforward MPC control applied to the wind turbine collective pitch and torque control problem in full load operation is presented in Koerber and King (2013). This work concludes that the use of state constraints in the MPC formulation is useful to avoid unnecessary shutdowns of the wind turbine due to violations of the over the speed limit.

Switchless control considering tower fore-aft displacement by means of MPC is the focus of Evans et al. (2014) considering a data-driven prediction model. Nonlinear MPC has been used to tackle the non-linearities in the wind turbine (Dang et al., 2008) and also has been applied in Schlipf et al. (2013), where LIDAR systems are used to provide information of wind disturbances in various distances in front of the wind turbine. The performance of the proposed nonlinear MPC control is assessed in terms of fatigue loads reduction and power production. A data-based MPC strategy that incorporates fatigue estimation was presented in Barradas-Berglind et al. (2015). In Odgaard et al. (2015a), an approach including dynamic inflow into MPC control is proposed to reduce fatigue loads in wind turbine tower.

Following the idea of proposing control strategies for mitigating loads and damage in wind turbines, some authors propose strategies focused in different wind turbine components. In Griffith et al. (2012), the Miners rule is used to estimate the fatigue life of wind turbine blade, by using a model to determine the number of cycles to failure. This approach is based on that information in order to apply different prognostic control techniques to derate the wind turbine when the damage peaks are reached. If the structural loads in the blade can be reduced in the presence of damage, then the propagation of damage can be slowed. One means to reduce loads in the blade is to reduce the energy capture of the turbine, i.e. to derate the turbine. With derating, the turbine experiences lower aerodynamic and structural loads. The result is a decrease in production, but it may be more advantageous to sacrifice some production capacity in the near term in favor of greater benefits in the long term.

In Frost et al. (2013), the integration of condition monitoring of wind turbine blades with contingency control to balance the trade-offs between maintaining system health and energy capture is explored. The objective of the work presented in Frost et al. (2013) was to keep the wind turbine operating and producing power without exceeding some damage threshold resulting in unscheduled downtime. An observer was developed that predicts potentially damaging operating conditions. Using this information, the contingency controller is able to derate the turbine, that is, reducing the generator operating set-point which results in lower loads on the turbine blades. It is also provided information about blade health, operator goals, and operating conditions, which were linked in parametric form to determine when the contingency controller will derate the generator to mitigate further damage to turbine blades. The results presented in Frost et al. (2013) were demonstrated using FAST, which is a high fidelity simulator based on a utility-scale wind turbine (Jonkman and Buhl, 2005).

In Langeron et al. (2013), the actuator RUL based prognostics is used to online reconfigure an LQR control law. The main aim of the integration of PHM with the control law is to find a satisfactory trade-off between conflicting requirements i.e. system performance and system components health. This has become a topic of interest during the last years and researchers are exploring new paradigms and approaches, see for example Balaban et al. (2013); Farrar and Lieven (2007); Tang et al. (2008).

The main objective of operational control of wind turbines is to maximize the extracted wind power from the wind. However, wind turbines components are subject to considerable fatigue due to extreme environmental conditions to which are exposed, especially those located offshore. For this reason, interest in the integration of control with fatigue-based prognostics of components has increased in recent years. In the work of Frost et al. (2013), wind turbine blade state health information is integrated with contingency controls to mitigate damage in this component.

Chapter 3

Wind Turbine Modeling

The purpose of this chapter is to give the general description of the wind turbine and set up a mathematical model of the considered wind turbine. The model should be detailed enough in order to understand the system behavior.

3.1 System Description

This section briefly describes the components of the wind turbine considered in this work, and it was taken as a reference the work of Esbensen et al. (2008). The wind turbine components are showed in Figure 3.1.

The figure is taken as reference Layton (2006). The components and their purposes are described below in alphabetic order (Darling, ONLINE; Bianchi et al., 2007).

- **Anemometer** is used to measure the wind speed. The wind turbine is started when the wind speed reaches a lower limit, while operation is cut-out when wind speeds become too high.
- **Brakes** can be applied mechanically, electrically, or hydraulically and function as parking brakes.
- **Gearbox** connects the low-speed shaft to the high-speed shaft, thus increasing the rotational speed to a level required by the generator to produce electric energy.
- **Generator** converts rotational energy into electric energy.
- **High-speed shaft** drives the generator.
- **Hub and rotor blades** together make up the rotor of the wind turbine. The hub connects the rotor blades to the low-speed shaft. Pitching the blades is used to maximize the efficiency in low winds and reduce efficiency in high winds to protect the wind turbine from structural damage.
- **Low-speed shaft** connects the rotor to the gearbox.

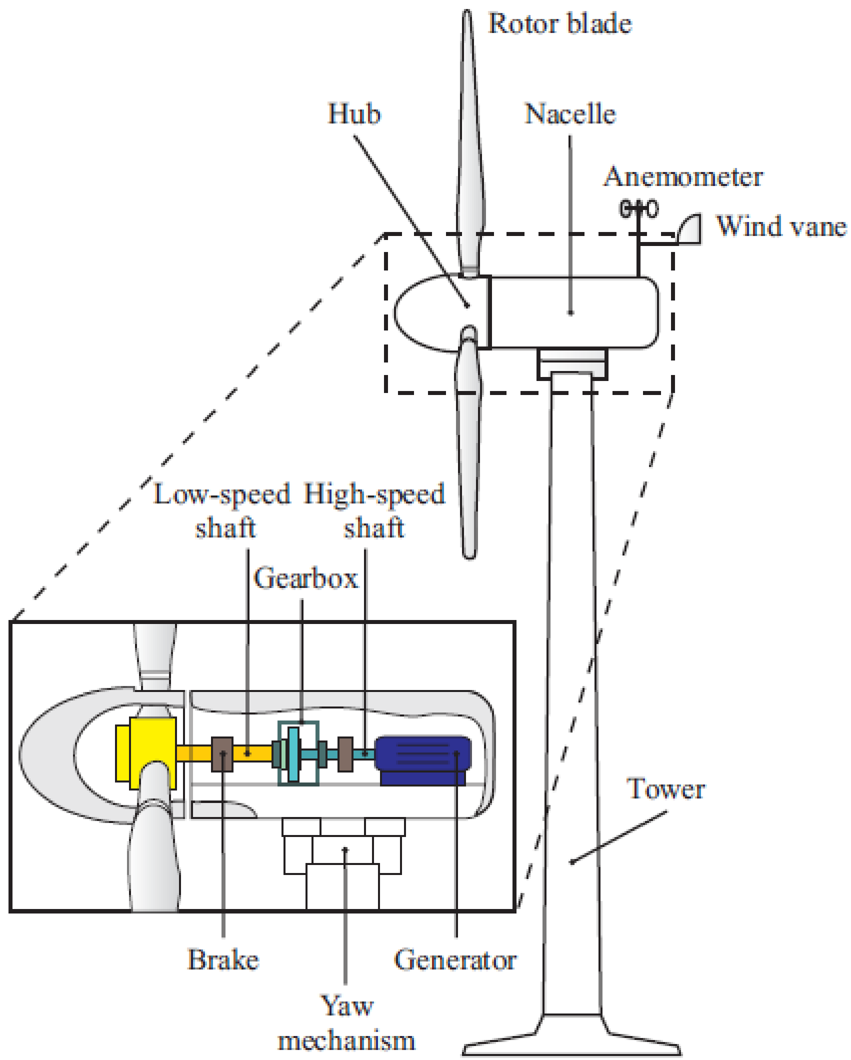

Figure 3.1: Main components of a horizontal-axis wind turbine.

- **Nacelle** is located at the top of the tower and contains the gearbox, low- and high-speed shafts, generator, and brakes.

- **Tower** carries the nacelle and the rotor. Since the wind speed increases with the height, a taller tower generally enables a wind turbine to generate more electric energy.

- **Wind vane** is used to measure the direction of the wind. The wind direction is used by the yaw mechanism to orient the wind turbine perpendicular to the wind.

- **Yaw mechanism** uses electrical motors to orient the wind turbine rotor perpendicular to the direction of the wind.

3.2 FAST 5MW Wind Turbine Simulation Model

FAST is an aeroelastic wind turbine simulator designed by the U.S. National Renewable Energy Laboratory (NREL) National Wind Technology Center and widely used for studying wind turbine control systems Jonkman and Buhl (2005). The code was verified by Germanischer Lloyd WindEnergie and found it suitable for "the calculation of onshore wind turbine loads for design and certification" (Manjock, 2005).

Several FAST models of real and composite wind turbines of varying sizes are available in the public domain. FAST can model a three bladed horizontal axis wind turbine with 24 degrees of freedom. This three-bladed, variable speed wind turbine with full span blade pitch control is available in both onshore and offshore versions, including four variations of off-shore structures.

The specifications of a representative utility-scale multimegawatt turbine now known as the NREL offshore 5-MW baseline wind turbine was developed by Jonkman et al. (2009). This wind turbine is a conventional three-bladed upwind variable blade-pitch-to-feather-controlled variable-speed turbine. To create the model, it was obtained some broad design information from the published documents of turbine manufacturers, with a heavy emphasis on the 5-MW power machine. However, because detailed data was unavailable, they also used the publicly available properties from the conceptual models in the WindPACT, RECOFF, and DOWEC projects. A composite from these data was created, extracting the best available and most representative specifications.

The report presented in Jonkman et al. (2009) documents the specifications of the NREL offshore 5-MW baseline wind turbineincluding the aerodynamic, structural, and control-system propertiesand the rationale behind its development. The model has been, and will likely continue to be, used as a reference by research teams throughout the world to standardize baseline offshore wind turbine specifications and to quantify the benefits of advanced land- and sea-based wind energy technologies. The parameters of the 5-MW reference wind turbine (Jonkman et al., 2009) used for characterizing the wind turbine subsystems in this thesis are shown below.

Table 3.1: Parameters NREL 5 MW Wind Turbine

Parameter	Description	Value	Units
J_g	Generator inertia about the high speed shaft	534.116	kg.m^2
B_{dt}	Drive train torsion damping coefficient	6.125×10^6	Nm$\times$(rad/s)$^{-1}$
N_g	Gear box ratio	97	-
J_r	Hub inertia about rotor axis	115.926×10^3	kg m^2
R	The distance from the rotor apex to the blade tip	63	m

FAST can utilize either uniform or full-field turbulent wind input files, with the turbulent files generated by the NREL software TurbSim (Jonkman, 2009). TurbSim generates turbulence using one of several atmospheric turbulence models and implements the wind field by creating the requested number of grids of 3-dimensional wind turbine velocity components, where the grids march forward toward the turbine in time based on the average wind speed. In the wind input files different wind speeds can be generated. Constant and variable wind inputs files with gusts can be generated as well by NREL software IECWind (Buhl and Jonkman, 2007).

As explained in Jonkman and Buhl (2005), Simulink has the ability to incorporate custom Fortran routines in a block called an S-Function. The FAST subroutines have been linked with a MATLAB standard gateway subroutine in order to use the FAST equations of motion in an S-Function that can be incorporated in a Simulink model. This introduces tremendous flexibility in wind turbine controls implementation during simulation. Generator torque control, nacelle yaw control, and pitch control modules can be designed in the Simulink environment and simulated while making use of the complete nonlinear aeroelastic wind turbine equations of motion available in FAST. The wind turbine block, as shown in Figure 3.2, contains the S-Function block with the FAST equations of motion. It also contains blocks that integrate the accelerations to get velocities and displacements. Thus the equations of motion are formulated in the FAST S-function but solved using one of the Simulink solvers.

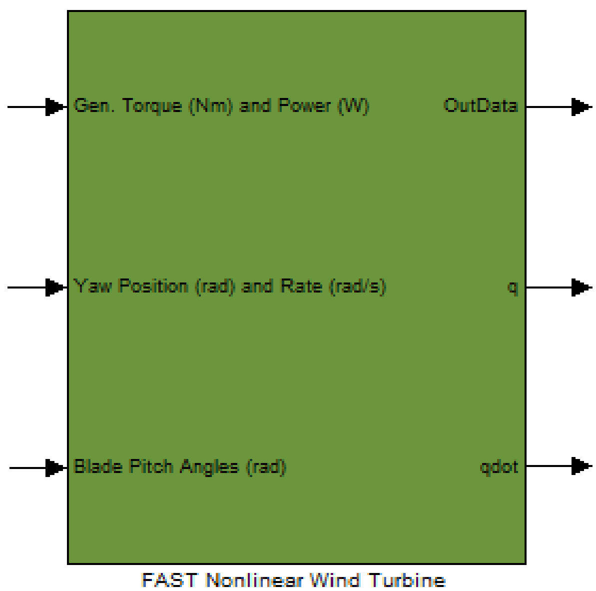

Figure 3.2: FAST Non Linear Wind Turbine

The inputs of the Simulink block are shown in Figure 3.2. These are the control signals applied to the system such as the applied generator torque, the pitch angle and the yaw position and rate in the case that this variable is controlled. The outputs can be any selection of the sensors that are available for the wind turbine, see Jonkman and Buhl (2005). The group of sensors that are used in this work is shown in Table 3.2. These sensors are the ones considered in a benchmark case study proposed by the scientific community for fault diagnosis and fault tolerant control of wind turbines (Odgaard and Johnson, 2013).

Table 3.2: Available sensors

Sensor Type	Symbol	Unit
Anemometer - Wind speed at hub height	$v_{\mathrm{w,m}}$	m/s
Rotor Speed	$\omega_{\mathrm{r,m}}$	rad/s
Generator Speed	$\omega_{\mathrm{g,m}}$	rad/s
Generator Torque	$\tau_{\mathrm{g,m}}$	Nm
Generated Electrical Power	$P_{\mathrm{g,m}}$	W
Pitch angle of ith Blade	$\beta_{i,\mathrm{m}}$	deg
Azimuth angle low speed side	$\theta_{\mathrm{r,m}}$	rad
Blade root moment ith blade	$M_{\mathrm{B},i,\mathrm{m}}$	Nm
Tower top acceleration (x and y directions) measurement	$\begin{bmatrix} \ddot{x}_{\mathrm{x,m}} \\ \ddot{x}_{\mathrm{y,m}} \end{bmatrix}$	m/s^2
Yaw error	$\Xi_{\mathrm{e,m}}$	deg

3.3 Non Linear Wind Turbine Model

In the following section the structure of the wind turbine model is presented in a block diagram. Afterwards, each sub-model of the wind turbine is presented and combined to obtain a complete model of the wind turbine. The overall wind turbine system model is divided into appropriate sub-models suitable of being modeled separately. The International System of Units (SI) is the the one used for the variables and magnitudes described by the models.

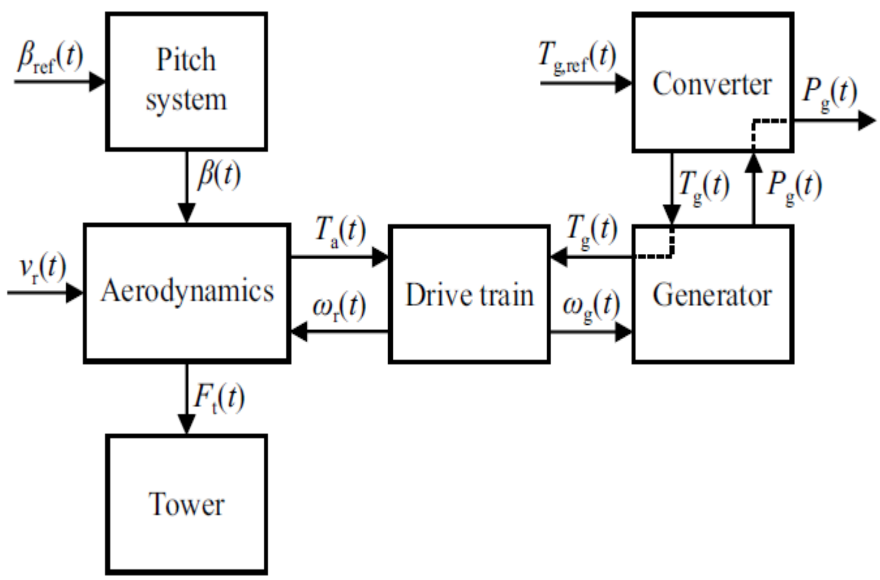

Figure 3.3: Subsystems models interaction of the wind turbine system model.

The wind speed $v_w(t)$ is the driving force of the system. As the wind blows over the turbine's blades they create "lift", much like an airplane wing, and begin to turn. Most turbines have three large blades that are aerodynamically designed to turn as easily as possible when the wind blows on them. These turning blades spin a shaft normally to some 30 to 60 times every minute (low-speed shaft). The gearbox connects the low-speed shaft with a high speed shaft that drives the generator. The gears also boost the rotation speed of the high-speed shaft to 1000 to 1800 rotations per minute. This rapidly spinning shaft drives the generator to produce electric power. The generator's electrical output is connected to a electrical grid.

The aerodynamic properties of the wind turbine are affected by the pitch angles of the blades, the speed of the rotor, and the wind speed. On this basis, an aerodynamic torque is transferred from the rotor to the generator through the drive train, and an aerodynamic thrust affects the rotor and thereby the tower. The output of the wind turbine is electric power which comes from the converter. To operate the wind turbine according to the set of operating requirements, the pitch angles of the blades and the generator torque are adjusted. A pitch system controls the pitch angles of the blades, while a converter controls the generator torque. In this section, the wind turbine model has been divided into six sub-models, in order to be individually modeled and combined afterwards.

3.3.1 Drive Train Subsystem

The function of the drive train is to step up the speed of the low-speed shaft (rotor) to a suitable value for the generator in order to produce electrical power.

As mentioned in Burton et al. (2011), in general, a drive train model consists of the following elements connected in series:

- A body with rotational inertia and damping (representing the turbine rotor).
- A torsional spring (representing the gearbox).
- A body with rotational inertia (representing the generator rotor).
- A torsional damper (modeling the resistance produced by slip on the induction generator).

Based on the physical laws, the authors from the consulted literature proposed different drive train models and three of them are analyzed in this section. These three models come from the main references encountered. The first one of them is developed in Bianchi et al. (2007), and consists in a single shaft drive train. The second one is proposed by Esbensen and Sloth (2009) and consists in two shafts linked together by a gearbox with its respective gear ratio. The third one is the drive train model proposed in the benchmark introduced in Odgaard et al. (2013). The drive train models can be obtained using Lagrange's energy equations or Newton's equations as will be showed in the next subsections.

Single Shaft Model

In Bianchi et al. (2007), the drive train subsystem is modeled as two rigid bodies linked by a flexible shaft, as shown in Figure 3.4.

The drive train is modeled as two rigid bodies linked by a flexible shaft. The rigid bodies encompass all the mechanical devices and parts of them located at each side of the effective shaft. Accordingly, the terms moment of inertia of the rotor (J_r), moment of inertia of the generator (J_g), torsion stiffness of the drive train (K_{dt}) and torsion damping coefficient of the drive train (B_{dt}) denote model parameters, rather than physical ones.

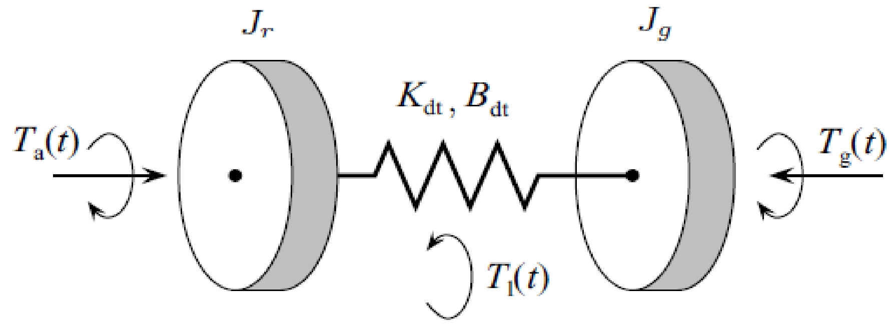

Figure 3.4: Drive-train

A mechanical system of arbitrary complexity can be described by the equation of motion

$$M\ddot{q} + C\dot{q} + Kq = Q(\dot{q}, q, t, u), \tag{3.1}$$

where M, C and K are the mass, damping and stiffness matrices and Q is the vector of forces acting on the system. For mechanical structures having few degrees of freedom, the Lagrange's equation

$$\frac{d}{dt}\left(\frac{\partial E_k}{\partial \dot{q}_i}\right) - \frac{\partial E_k}{\partial q_i} + \frac{\partial E_d}{\partial \dot{q}_i} + \frac{\partial E_p}{\partial q_i} = Q_i, \tag{3.2}$$

offers a systematic procedure to derive mathematical models. E_k, E_d and E_p denote the kinetic, dissipated and potential energy, respectively. Besides, q_i is the generalized coordinate and Q_i stands for the generalized force.

For the model of equation (3.2), the following generalized coordinates has been adopted:

$$q = [\theta_r \ \ \theta_g]^T, \tag{3.3}$$

where: $\theta_r = q_1$ and $\theta_g = q_2$ are the angles of the rotor and generator, respectively. After these definitions, the energy terms E_k, E_d and E_p can be written as:

$$E_k = \frac{J_r}{2}\omega_r^2 + \frac{J_g}{2}\omega_g^2, \tag{3.4}$$

$$E_d = \frac{B_{dt}}{2}(\omega_r - \omega_g)^2, \tag{3.5}$$

$$E_p = \frac{K_{dt}}{2}(\theta_r - \theta_g)^2, \tag{3.6}$$

where ω_r and ω_g are the rotational speeds of the rotor and generator, respectively, both of them referred to the low-speed side of the wind turbine.

The vector of generalized loads is:

$$Q = [T_a \quad -T_g]^T, \tag{3.7}$$

where $T_a(t)$ is the aerodynamic torque applied to the rotor and $T_g(t)$ is the generator torque.

Then, replacing the equations in the Lagrange's equation yields the motion equation(3.1) and applying the Lagrange's equation (3.2) to each of the the corresponding energy terms (3.4)-(3.7), the following equations are obtained.

For the first generalized coordinate ($\theta_r = q_1$), the derivative is denoted as $\dot{q}_1 = \omega_r$. The Lagrange terms for q_1 are developed below.

$$\frac{\partial E_k}{\partial \dot{q}_1} = J_r \omega_r, \tag{3.8}$$

$$\frac{\partial E_k}{\partial q_1} = 0, \tag{3.9}$$

$$\frac{\partial E_d}{\partial \dot{q}_1} = B_{dt} \left(\omega_r - \omega_g \right), \tag{3.10}$$

$$\frac{\partial E_p}{\partial q_1} = K_{dt} \left(\theta_r - \theta_g \right), \tag{3.11}$$

$$\frac{d}{dt} \left(\frac{\partial E_k}{\partial \omega_r} \right) = J_r \dot{\omega}_r, \tag{3.12}$$

$$Q_1 = T_a. \tag{3.13}$$

Substituting the equations (3.8)-(3.13) in the Lagrange equation (3.2), the dynamic of the rotor is obtained

$$J_r \dot{\omega}_r + B_{dt} \left(\omega_r - \omega_g \right) + K_{dt} \left(\theta_r - \theta_g \right) = T_a(t). \tag{3.14}$$

For the second generalized coordinate ($\theta_g = q_g$), the derivative is denoted as $\dot{q}_2 = \omega_g$. The Lagrange terms for q_2 are as follows

$$\frac{\partial E_k}{\partial \dot{q}_2} = J_g \omega_g, \tag{3.15}$$

$$\frac{d}{dt} \left(\frac{\partial E_k}{\partial \omega_g} \right) = J_g \dot{\omega}_g, \tag{3.16}$$

$$\frac{\partial E_k}{\partial \theta_g} = 0, \tag{3.17}$$

$$\frac{\partial E_d}{\partial \omega_g} = B_{dt}\left(\omega_g - \omega_r\right), \tag{3.18}$$

$$\frac{\partial E_p}{\partial q_2} = K_{dt}\left(\theta_g - \theta_r\right), \tag{3.19}$$

$$Q_2 = -T_g. \tag{3.20}$$

Substituting the equations (3.15)-(3.20) in the Lagrange's equation (3.2), the dynamic of the generator is obtained

$$J_g\dot{\omega}_g + B_{dt}\left(\omega_r - \omega_g\right) - K_{dt}\left(\theta_r - \theta_g\right) = -T_g(t). \tag{3.21}$$

In order to reduce the formulas complexity, the absolute angular positions of the shafts θ_r and θ_g were replaced with a single state variable shown in (3.22), denoting the torsion angle of the drive train

$$\theta_\Delta = \theta_r - \theta_g. \tag{3.22}$$

The rotor dynamics can be obtained using the Newton's equations as expressed follows

$$J_r\ddot{\theta}_r(t) = T_a(t) - T_1(t), \tag{3.23}$$

where the torsion of the drive train is modeled using a torsion spring and a friction coefficient model according to

$$T_1(t) = K_{dt}\theta_\Delta(t) + B_{dt}\dot{\theta}_\Delta(t). \tag{3.24}$$

Substituting (3.24) in (3.23), the following expressions are obtained

$$J_r\ddot{\theta}_r(t) = T_a(t) - K_{dt}\theta_\Delta(t) - B_{dt}\dot{\theta}_\Delta(t), \tag{3.25}$$

$$\ddot{\theta}_r(t) = \frac{1}{J_r}T_a(t) - \frac{1}{J_r}K_{dt}\theta_\Delta(t) - \frac{1}{J_r}B_{dt}\dot{\theta}_\Delta(t). \tag{3.26}$$

The following change to denote the angular speed of the rotor and generator is made

$$\begin{aligned} \dot{\theta}_r &= \omega_r, \\ \dot{\theta}_g &= \omega_g. \end{aligned} \tag{3.27}$$

Finally the dynamic of the rotor is defined as

$$\dot{\omega}_r(t) = \frac{1}{J_r}T_a(t) - \frac{1}{J_r}K_{dt}\theta_\Delta(t) - \frac{1}{J_r}B_{dt}\left(\omega_r - \omega_g\right). \tag{3.28}$$

The same method is used to obtain the dynamics of the generator

$$J_g\ddot{\theta}_g(t) = T_l(t) - T_g(t). \tag{3.29}$$

The torsion of the drive train is the same for the rotor and the generator, therefore

$$T_l(t) = K_{dt}\theta_\Delta(t) + B_{dt}\dot{\theta}_\Delta(t), \tag{3.30}$$

Then, substituting (3.30) in (3.29) the following equation is obtained

$$J_g\dot{\omega}_g(t) = K_{dt}\theta_\Delta(t) + B_{dt}\dot{\theta}_\Delta(t) \ - T_g(t). \tag{3.31}$$

The dynamics for the generator is the following

$$\dot{\omega}_g(t) = \frac{K_{dt}}{J_g}\theta_\Delta(t) + \frac{B_{dt}}{J_g}\left(\omega_r - \omega_g\right) - \frac{T_g(t)}{J_g}. \tag{3.32}$$

Two Shafts Model

A two shafts model consisting of a high speed shaft and a low speed shaft linked by a gearbox is proposed by Esbensen and Sloth (2009). The aerodynamic torque is transferred to the generator through the drive train in order to upscale the rotational speed of the rotor, to a higher speed required by the generator.

The drive train model includes a low-speed shaft and a high-speed shaft, each composed of a moment of inertia and a frictional coefficient as illustrated in Figure 3.5. The shafts are linked together by a gearbox modeled as a gear ratio without any loss. To describe the flexibility of the drive train, a torsion spring is included in the model.

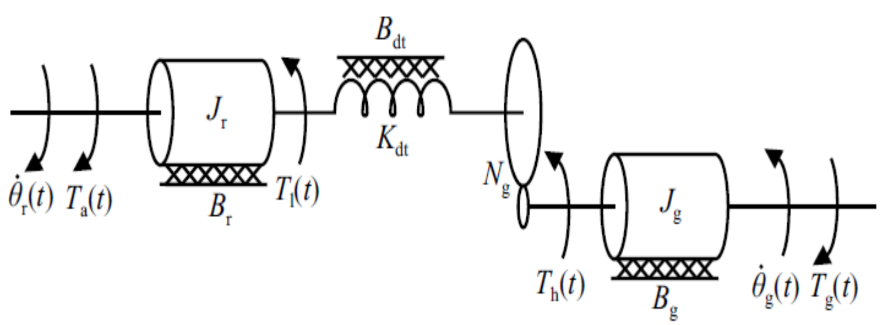

Figure 3.5: Drive-train model divided into four components

The inertia of the low-speed shaft also includes the inertia of the rotor, while the friction component includes bearing frictions. The dynamics of the low-speed shaft is

$$J_r\ddot{\theta}_r(t) = T_a(t) - T_l(t) - B_r\dot{\theta}_r(t), \tag{3.33}$$

where: B_r is the viscous friction of the low-speed shaft, J_r is the moment of inertia of the low-speed shaft, $T_l(t)$ is the torque acting on the low-speed shaft, $\theta_r(t)$ is the angle of the low-speed shaft [rad] and $T_a(t)$ is the aerodynamic torque applied to the rotor.
The inertia of the high-speed shaft also includes the inertia of the gearbox and the generator rotor. The friction coefficient covers bearing and gear frictions. The dynamics of the high-speed shaft is

$$J_g\ddot{\theta}_g(t) = T_h(t) - T_g(t) - B_g\dot{\theta}_g(t), \tag{3.34}$$

where: B_g is the viscous friction of the high-speed shaft, J_g is the moment of inertia of the high-speed shaft, $T_g(t)$ is the generator torque, $T_h(t)$ is the torque acting on the high-speed shaft and $\theta_g(t)$ is the angle of the high-speed shaft.
The remaining part of the gearbox modeling is to apply a gear ratio, as defined below

$$T_h(t) = \frac{T_l(t)}{N_g}, \tag{3.35}$$

where N_g is the drive train gear ratio.

The torsion of the drive train is modeled using a torsion spring and a friction coefficient model, described according to:

$$T_l(t) = K_{dt}\theta_\Delta(t) + B_{dt}\dot{\theta}_\Delta(t), \tag{3.36}$$

$$\theta_\Delta(t) = \theta_r(t) - \frac{\theta_g(t)}{N_g}, \tag{3.37}$$

where B_{dt} is the torsion damping coefficient of the drive train, K_{dt} is the torsion stiffness of the drive train, and $\theta_\Delta(t)$ is the torsion angle of the drive train.

With the exception of the torsion angle, $\theta_\Delta(t)$, absolute angles of the shafts are not of interest for modeling the drive train dynamics. Therefore, the replacement $\omega_r(t) = \dot{\theta}(t)$ is utilized in the following rewriting, where a state space model of the drive train is pursued. The states of the model are $\omega_r(t)$, $\omega_g(t)$, and $\theta_\Delta(t)$. First, Eq. (3.37) is substituted into Eq. (3.36) to obtain

$$T_l(t) = K_{dt}\theta_\Delta(t) + B_{dt}\left(\omega_r(t) - \frac{\omega_g(t)}{N_g}\right), \tag{3.38}$$

where $\omega_g(t)$ is the generator speed.

Substituting (3.38) into (3.33) results in (3.39). A similar approach is used to derive (3.40); however, in this case (3.38) first has to be substituted into (3.35) before inserting it in (3.34). Lastly, (3.37) is differentiated to obtain (3.41).

Three first order differential equations have been derived in this section in order to describe the behavior of the drive train

$$J_r\dot{\omega}_r(t) = T_a(t) - K_{dt}\theta_\Delta(t) - (B_{dt} + B_r)\,\omega_r(t) + \frac{B_{dt}}{N_g}\omega_g(t), \tag{3.39}$$

$$J_g\dot{\omega}_g(t) = \frac{K_{dt}}{N_g}\theta_\Delta(t) + \frac{B_{dt}}{N_g}\omega_r(t) - \left(\frac{B_{dt}}{N_g^2} + B_g\right)\omega_g(t) - T_g(t), \tag{3.40}$$

$$\dot{\theta}_\Delta(t) = \omega_r(t) - \frac{1}{N_g}\omega_g(t). \tag{3.41}$$

Benchmark Drive Train Model

The next drive train model proposed in the benchmark Odgaard et al. (2013) follows the same line of the previous one.

It is basically the same model proposed in Esbensen and Sloth (2009) with the addition of the drive-train's efficiency which gives a more realistic approach to the model

$$J_r\dot{\omega}_r(t) = T_a(t) - K_{dt}\theta_\Delta(t) - (B_{dt} + B_r)\,\omega_r(t) + \frac{B_{dt}}{N_g}\omega_g(t), \tag{3.42}$$

$$J_g\dot{\omega}_g(t) = \frac{\eta_{\mathrm{dt}}K_{dt}N_g}{\theta_\Delta}(t) + \frac{\eta_{\mathrm{dt}}B_{dt}}{N_g}\omega_r(t) - \left(\frac{\eta_{\mathrm{dt}}B_{dt}}{N_g^2} + B_g\right)\omega_g(t) - T_g(t), \tag{3.43}$$

$$\dot{\theta}_\Delta(t) = \omega_r(t) - \frac{1}{N_g}\omega_g(t), \tag{3.44}$$

where η_{dt} is the generator efficiency.

Simplified Drive Train Model

A simplification of drive train model can be obtained from equations (3.39)-(3.41) omitting the torsion angle and friction. In this case the simplified equations are

$$J_r\dot{\omega}_r(t) = T_a(t), \tag{3.45}$$

$$J_g\dot{\omega}_g(t) = -T_g(t), \tag{3.46}$$

$$\omega_r(t) = \frac{1}{N_g}\omega_g(t). \tag{3.47}$$

Combining these equations the simplified model is

$$J\dot{\omega}_r(t) = T_a(t) - N_gT_g, \tag{3.48}$$

with $J = J_r + N_g^2J_g$.

3.3.2 Pitch Subsystem

Following Odgaard and Johnson (2013), the hydraulic pitch system is modeled as a second order transfer function between the pitch angle β and the pitch reference angle β_{ref}

$$\frac{\beta(s)}{\beta_{ref}(s)} = \frac{\omega_n^2}{s^2 + 2\zeta\omega_n s + \omega_n^2}. \tag{3.49}$$

There is a transfer function associated to each of the three pitch systems. In normal operation, the system has the following parameters $\zeta = 0.6$ and $\omega_n = 11.11$ leading to an under-damped system.

Also, constraints on the values of pitch angles and rate are implemented. The pitch angle values are restricted to the interval [-2, 90] deg and pitch rate is restricted to the interval [-8, 8] deg/s.

Similarly to this approach, the pitch system is modeled by Esbensen and Sloth (2009) with a same transfer function to each of the three pitch systems in the wind turbine. However, in this model a time delay corresponding to the communication delay to the pitch actuator is added to the second order transfer function described as

$$\frac{\beta(s)}{\beta_{ref}(s)} = \frac{e^{(-t_d s)}\omega_n^2}{s^2 + 2\zeta\omega_n s + \omega_n^2}. \tag{3.50}$$

A different pitch actuator model is suggested in Bianchi et al. (2007). Here the model is a first-order dynamic system with saturation in the amplitude and derivative of the output signal

$$\dot{\beta} = -\frac{1}{\tau_p}\beta + \frac{1}{\tau_p}\beta_{ref}, \tag{3.51}$$

where τ_p is the time constant.

Applying the Laplace transform we obtain the corresponding first order transfer function

$$\frac{\beta(s)}{\beta_{ref}(s)} = \frac{{}^{1}\!/_{\tau_p}}{\left(s + {}^{1}\!/_{\tau_p}\right)}. \tag{3.52}$$

In this model, the pitch angle varies in the interval [-2,30] deg and the rate in the interval [-10,10] deg/s.

The first two models presented in Esbensen and Sloth (2009) and in Odgaard and Johnson (2013), considered an under-damped behavior of the pitch actuator. In the third model presented in Esbensen and Sloth (2009), an over-damped dynamic was modeled using a first order differential equation.

We consider that the time delay of the system is not very high in this case and can be neglected still obtaining a realistic representation of the system.

The first order system presented in Bianchi et al. (2007) is very simple and we consider that an over-damped dynamic does not represent in a realistic way the behavior of a pitch actuator.

3.3.3 Tower Subsystem

The tower of a wind turbine, as any flexible structure, exhibits many vibration modes. Some oscillatory movements inherent to these modes are illustrated in Figure 3.6. Particularly, simple models are very helpful for a comparative analysis of different control strategies and for the controller design, whereas the unmodeled dynamics can be treated as uncertainties. For this reason, the model presented here will include the first mode of tower bending and the first mode of flapping.

In this thesis, it is assumed that the thrust on the rotor acts in the direction of the wind speed. In reality this is not completely the situation since there is also the side-to-side mode of tower bending. This is produced by forces from the blades and a counter torque from the drive train and generator, which make the tower to swing sideways as well (Esbensen and Sloth, 2009).

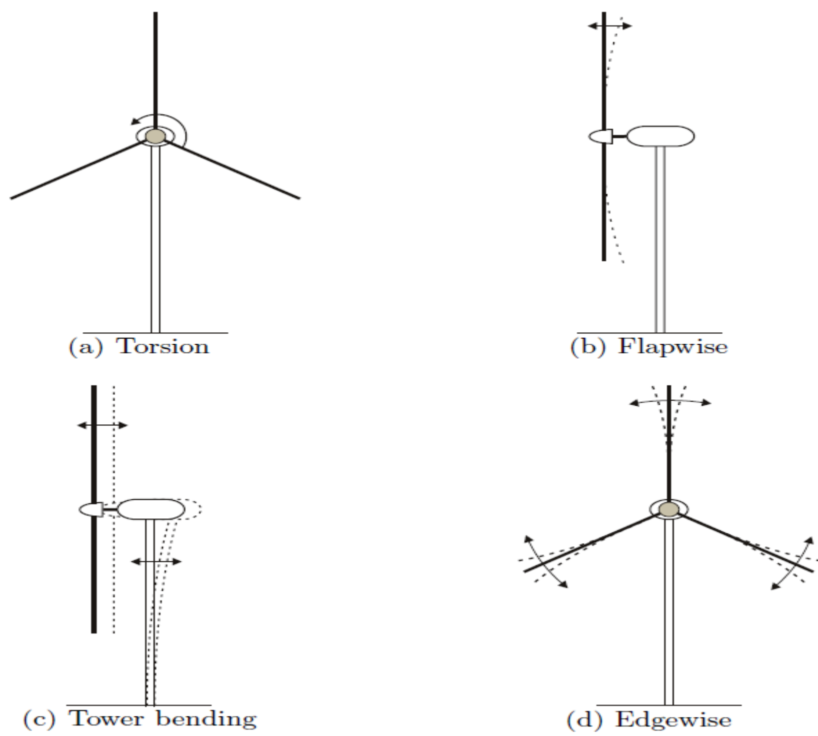

Figure 3.6: Mode shapes for horizontal-axis wind turbines.

The model presented in Figure 3.7 has two degrees of freedom, which are the axial tower bending and the flapping. For this model the following generalized coordinates are adopted

$$q = [d_t \;\; \zeta\,]^T, \tag{3.53}$$

where d_t is the axial displacement of the nacelle from the equilibrium position and ζ is the angular displacement out of the plane of rotation of the blades.

To obtain the model of the tower, the Lagrange energy method is used. The energy terms E_k,

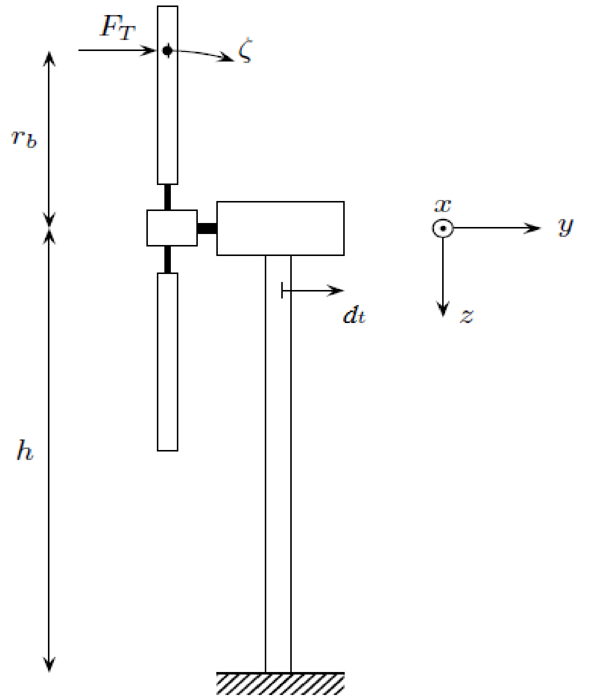

Figure 3.7: Schematic diagram of the tower.

E_d and E_p in (3.2) can be written as

$$E_k = \frac{m_t}{2}\dot{d}_t^2 + \frac{N}{2} m_b\left(\dot{d}_t + r_b\dot{\zeta}\right)^2, \tag{3.54}$$

$$E_d = \frac{B_t}{2}\dot{d}_t^2 + \frac{N}{2} B_b\left(r_b\dot{\zeta}\right)^2, \tag{3.55}$$

$$E_p = \frac{K_t}{2}{d_t}^2 + \frac{N}{2} K_b(r_b\zeta)^2, \tag{3.56}$$

and the vector of generalized loads is:

$$Q = [N F_T \;\; N F_T r_b]^T. \tag{3.57}$$

For the first generalized coordinate $q_1 = d_t$, the Lagrange terms are:

$$\frac{\partial E_k}{\partial \dot{q}_1} = m_t\dot{d}_t + N m_b\dot{d}_t + N m_b r_b\dot{\zeta}, \tag{3.58}$$

$$\frac{d}{dt}\left(\frac{\partial E_k}{\partial \dot{d}_t}\right) = \left(m_t + N m_b\right)\ddot{d}_t + N m_b r_b\ddot{\zeta}, \tag{3.59}$$

$$\frac{\partial E_k}{\partial d_t} = 0, \tag{3.60}$$

$$\frac{\partial E_d}{\partial \dot{q}_1} = B_t \dot{d}_t, \tag{3.61}$$

$$\frac{\partial E_p}{\partial q_1} = K_t d_t, \tag{3.62}$$

$$Q_1 = N F_T. \tag{3.63}$$

Substituting (3.58)-(3.63) in the Lagrange equation (3.2), the dynamic of the tower bending is

$$\left(m_t + N m_b\right) \ddot{d}_t + N m_b r_b \ddot{\zeta} + B_t \dot{d}_t + K_t d_t = N F_T. \tag{3.64}$$

For the second generalized coordinate $q_2 = \zeta$, the Lagrange terms are the following

$$\frac{\partial E_k}{\partial \dot{\zeta}} = \frac{N}{2} m_b \left(2 r_b \dot{d}_t + 2 r_b^2 \dot{\zeta}\right), \tag{3.65}$$

$$\frac{d}{dt}\left(\frac{\partial E_k}{\partial \dot{\zeta}}\right) = N m_b r_b \ddot{d}_t + N m_b r_b^2 \ddot{\zeta}, \tag{3.66}$$

$$\frac{\partial E_k}{\partial \zeta} = 0, \tag{3.67}$$

$$\frac{\partial E_d}{\partial \dot{\zeta}} = N B_b r_b^2 \dot{\zeta}, \tag{3.68}$$

$$\frac{\partial E_p}{\partial \zeta} = N K_b r_b^2 \zeta, \tag{3.69}$$

$$N m_b r_b \ddot{d}_t + N m_b r_b^2 \ddot{\zeta} + N B_b r_b^2 \dot{\zeta} + N K_b r_b^2 \zeta = N F_T r_b. \tag{3.70}$$

After simplifying (3.70), the dynamic of the blade flap-wise is

$$m_b r_b \ddot{d}_t + m_b r_b^2 \ddot{\zeta} + B_b r_b^2 \dot{\zeta} + K_b r_b^2 \zeta = F_T r_b. \tag{3.71}$$

Tower Model Simplification

In order to obtain a simplified model of the tower for further purposes, the blades are assumed to be stiff but in fact the blades are flexible as explained before. This simplification eliminates all the bending modes of the blades and transfers all forces acting on blades directly to the tower.

The tower top acceleration is typically the only measured variable in the tower model. Therefore, the movement of the tower is now described by a linear displacement of the tower top (Esbensen and Sloth, 2009). An illustration of this model is given in Figure 3.8.

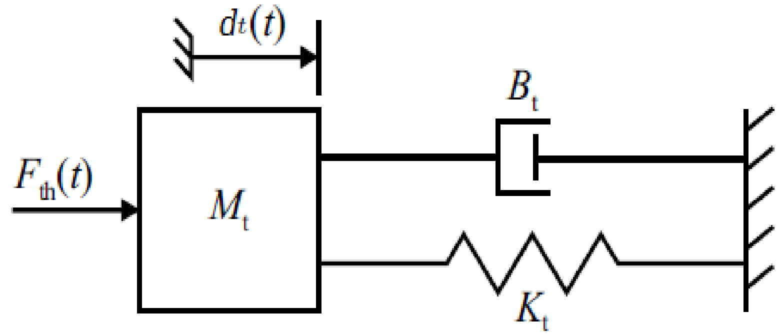

Figure 3.8: The movement of the flexible tower is modeled using a spring-damper system.

Using a spring-damper terminology, the tower model is rewritten as

$$M_t\ddot{d}_t(t) = F_t(t) - B_t\dot{d}_t(t) - K_t d_t(t), \tag{3.72}$$

where B_t is the tower damping coefficient, K_t is the tower torsion coefficient, M_t is the top mass of the tower and $d_t(t)$ is the displacement of the nacelle from its equilibrium position. The replacement $\dot{d}_t = v_t$ is utilized in the following notation, where a state space model of the wind turbine is pursued.

3.3.4 Blade Root Moment Dynamics

This section is based on the work of Van Engelen et al. (2007) from which the Blade Root Moment Dynamics can be obtained.

It is assumed that the wind speed signal, when it acts on the whole rotor blade, causes blade root loads that are similar to those that arise when a rotating rotor blade samples a turbulent wind field, affected by wind shear and tower shadow. This concept allows for describing the wind influence on the blade (root) loads via a single input signal while yet taking into account the properties of the rotationally sampled wind field.

The aerodynamic conversion in the simplified model taken from Burton et al. (2011); dynamic wake effects and unsteady aerodynamics are not taken into account. The aerodynamic conversion characteristics are translated into multipliers that map a variation in the flapwise relative wind speed v_{flap_i} to variations in the flap and leadwise blade root moments and forces (aerodynamic gains). Aerodynamic gains are also derived for the linearized influence of a variation in the pitch angle. The pitch angle variation β_i and relative wind speed variation v_{flap_i} for the i^{th} blade thus cause variations in the aerodynamic loads on the blade root described by:

$$M_{B,i}(t) = k_1\left(v_r(t) - v_t + \frac{9R_b}{8H}v_t\sin(\psi_i(t))\right) + k_2\beta_i(t), \tag{3.73}$$

where $M_{B,i}(t)$ is the blade root moment on blade i, $\psi_i(t)$ is the azimuth angle of blade i, $v_r(t)$ is the wind speed, v_t is the translation speed of the nacelle from its equilibrium position, R_b is the distance from the hub to where the thrust acts on the blade and H is the hub height.

The gains k_1 and k_2 are derived from the power and thrust coefficient data under the assumption of equal aerodynamic efficiency over the rotor radius in a chosen working point.

For azimuth angle ψ_i equal to 0, the i^{th} blade is in the horizontal position while it is rotating downward. The azimuth angle of the blade equals the rotor azimuth angle θ_r, which means

$$\theta_r = \psi_1(t). \tag{3.74}$$

The rest of the azimuth blade angles can be calculated as shown below:

$$\psi_2(t) = \theta_r + \frac{2}{3}\pi, \tag{3.75}$$

$$\psi_3(t) = \theta_r + \frac{4}{3}\pi. \tag{3.76}$$

3.3.5 Aerodynamic Model

In this section, basic aerodynamic principles exploited by wind turbines are described, and a model describing the transfer from wind energy to rotational motion of the rotor is presented.

The power available from the wind passing through the entire rotor swept area can be expressed as Bianchi et al. (2007):

$$P_w(t) = \frac{1}{2}\rho A v_r^3(t), \tag{3.77}$$

where $P_w(t)$ is the power available from the wind, A is the rotor swept area, $v_r(t)$ is the rotor effective wind speed, ρ is the air density, which is assumed to be constant.

From the available power in the wind, the power on the rotor is given based on the power coefficient, $C_p(\lambda(t), \beta(t))$, which depends on the tip-speed ratio and the pitch angle. The C_p-surface for the wind turbine used in the FDI benchmark (Odgaard and Johnson, 2013) is provided by kk-electronic a/s and is shown in the left subplot of Figure 3.9. Notice that the C_p-description implies that the aerodynamic model is static, which is a simplification.

The power captured by the rotor is:

$$P_a(t) = P_w(t) C_p\left(\lambda(t), \beta(t)\right), \tag{3.78}$$

where $P_a(t)$ is the power captured by the rotor, $C_p\left(\lambda(t), \beta(t)\right)$ is the power coefficient and $\lambda(t)$ is the tip-speed ratio.

The tip-speed ratio is defined as the ratio between the tip speed of the blades and the rotor effective wind speed

$$\lambda(t) = \frac{\omega_r(t) R}{v_r(t)}, \tag{3.79}$$

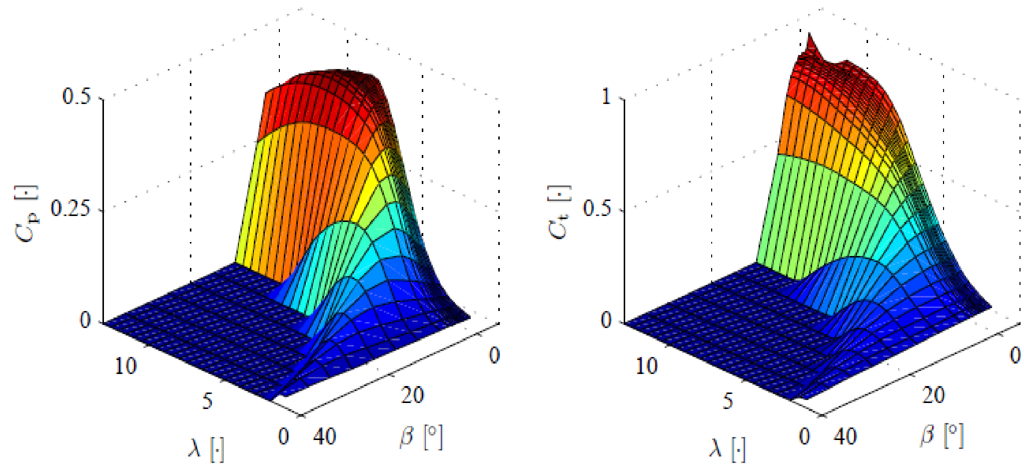

Figure 3.9: The C_p and C_t-coefficients as function of the pitch angle and the tip-speed ratio. Notice that negative values have been set to zero.

where $\omega_r(t)$ is the rotor speed and R is the rotor radius.

The aerodynamic torque applied to the rotor defined in Esbensen and Sloth (2009), can be expressed as:

$$T_a(t) = \frac{P_a(t)}{\omega_r(t)}. \tag{3.80}$$

Substituting the equations (3.77) and (3.78), in (3.80) the torque applied to the rotor is expressed as:

$$T_a(t) = \frac{1}{2\omega_r(t)} \rho A v_r^3(t) C_p\left(\lambda(t), \beta(t)\right), \tag{3.81}$$

where $T_a(t)$ is the aerodynamic torque applied to the rotor.

The wind acting on the rotor of the wind turbine also results in a thrust on the rotor. This thrust is calculated as shown below (Bianchi et al., 2007).

$$F_t(t) = \frac{1}{2} \rho A v_r^2(t) C_t(\lambda(t), \beta(t)), \tag{3.82}$$

where: $C_t(\lambda(t), \beta(t))$ is the thrust coefficient and $F_t(t)$ is the thrust exerted by the wind on the rotor.

To use the aerodynamic model when the wind speed is assumed to be non-identical on the three blades, the equations have to take into account different blade effective wind speeds. This is accomplished by averaging the thrust and torque introduced at each of the three blades, as illustrated below

$$F_{t,1}(t) = \frac{1}{2} \rho A v_r^2(t) C_t(\lambda(t), \beta_1(t)), \tag{3.83}$$

$$F_{t,2}(t) = \frac{1}{2}\rho A v_r^2(t) C_t(\lambda(t), \beta_2(t)), \tag{3.84}$$

$$F_{t,3}(t) = \frac{1}{2}\rho A v_r^2(t) C_t(\lambda(t), \beta_3(t)), \tag{3.85}$$

$$T_{a,1}(t) = \frac{1}{2\omega_r(t)}\rho A v_r^3(t) C_p\left(\lambda(t), \beta_1(t)\right), \tag{3.86}$$

$$T_{a,2}(t) = \frac{1}{2\omega_r(t)}\rho A v_r^3(t) C_p\left(\lambda(t), \beta_2(t)\right), \tag{3.87}$$

$$T_{a,3}(t) = \frac{1}{2\omega_r(t)}\rho A v_r^3(t) C_p\left(\lambda(t), \beta_3(t)\right), \tag{3.88}$$

$$T_a(t) = \frac{1}{3}\sum_{i=1}^{3} T_{a,i}(t). \tag{3.89}$$

Substituting (3.86), (3.87) and (3.88) in (3.89), the following equation for the aerodynamic torque is obtained

$$F_t(t) = \frac{1}{3}\sum_{i=1}^{3} F_{t,i}(t), \tag{3.90}$$

where $F_{t,i}(t)$ is the thrust exerted by the wind on blade i, $T_{a,i}(t)$ is the aerodynamic torque applied to the rotor by blade i.

It is assumed that the thrust $F_{t,i}(t)$ exerted on Blade i attacks where the thrust components towards the hub and towards the blade tip are equal. Since the thrust is dependent on R^2 the following equation can be set up to calculate the point where the thrust attacks

$$\begin{aligned} &\int_0^{r_b} r^2 dr = \int_{r_b}^{R} r^2 dr, \\ &r_b = 2^{-1/3} R, \end{aligned} \tag{3.91}$$

where r_b is the distance from the hub to where the thrust acts on the blade and R is the radius of the rotor.

Having determined where the thrust acts on the blades, it is possible to derive the torque which makes the tower move. This is a function of the azimuth angle of each blade and can be realized as a force acting on the tower at hub height

$$\begin{aligned} F_{th}(t) = {} & F_{t,1}(t)\left(1 + \tfrac{r_t}{h}\cos\left(\psi_1(t)\right)\right) + F_{t,2}(t)\left(1 + \tfrac{r_t}{h}\cos\left(\psi_2(t)\right)\right) \\ & + F_{t,3}(t)\left(1 + \tfrac{r_t}{h}\cos\left(\psi_3(t)\right)\right), \end{aligned} \tag{3.92}$$

where $F_{t,i}(t)$ is the thrust acting on blade i, $F_{th}(t)$ is the force acting on the tower at hub height and $F_{th,i}(t)$ is the force transferred to the tower from blade i at hub height.

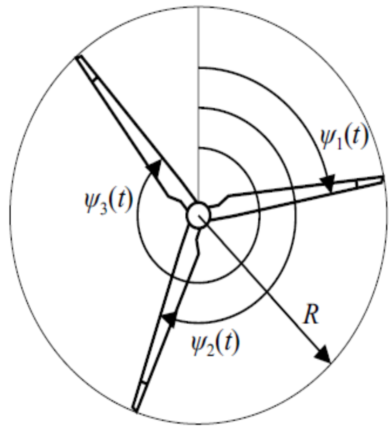

Figure 3.10: Sketch of a rotor and a wind turbine, showing parameters utilized in the wind model.

The basic aerodynamic principles of a wind turbine have been described, and models for the aerodynamic torque and the aerodynamic thrust acting on the rotor have been set up.

3.3.6 Power Subsystem Model

The power system as modeled in Odgaard and Johnson (2013) and Esbensen and Sloth (2009) is considered a standard first order system which is very similar in both cases.

Electric power is generated by the generator, and to enable variable-speed operation, currents in the generator are controlled using power electronics. Therefore, power electronic converters interface the wind turbine generator output with the utility grid. It is assumed that the converter consists of four similar units sketched in Figure 3.11, each having an internal controller. These units together load the generator with a certain torque, which depends on the currents drawn from the generator. Since torque and electric power are the only variables of interest in the simplified model of the energy conversion system, currents and voltages are not considered at all.

Since the converter consists of several converters having equal characteristics, this section describes only one of these.

On a system level of the wind turbine, the generator and converter dynamics can be modeled by a first order transfer function:

$$\frac{T_g(s)}{T_{\mathrm{g,ref}}(s)} = \frac{1}{\tau_{\mathrm{g}}\, s + 1}, \tag{3.93}$$

where $T_{\mathrm{g,ref}}(t)$ is the reference for the generator torque and τ_{g} is the time constant of the first order system.

The power produced by the generator depends on the rotational speed of the rotor and of the applied load, as described in the equation below. The following equation explains the mechanical

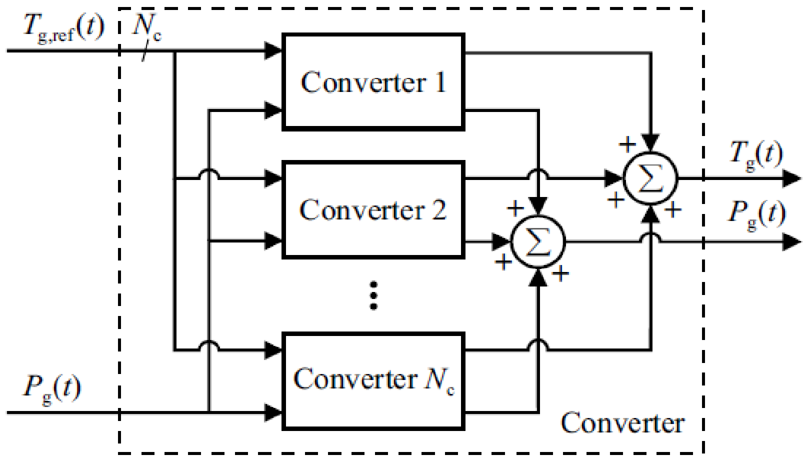

Figure 3.11: The converter consists of N_c units capable of loading the generator by a certain torque, specified by a torque reference.

power since the electronic system is not modeled:

$$P_{\mathrm{g}}(t) = \eta_{\mathrm{g}}\omega_{\mathrm{g}}(t)T_{\mathrm{g}}(t), \tag{3.94}$$

where $P_{\mathrm{g}}(t)$ is the power produced by the generator, η_{g} is the efficiency of the generator.

In the wind turbine FDI benchmark (Odgaard and Johnson, 2013), the parameter values for the efficiency and the time constant are $\eta_{\mathrm{g}} = 0.98$ and $\tau_{\mathrm{g}} = \frac{1}{50}$, respectively.

3.4 Control Oriented Model

The FAST-NREL 5 MW is a detailed and high fidelity wind turbine model with 24 degrees of freedom, this model is appropriate for testing control schemes and use the sensors information either for prognostics or fault diagnosis. However, a reduced-order dynamic model is more suitable for the purpose of control design, which is defined in this section.

To derive the control oriented model, the equations from the different sub-models described in section 3.3 are used, it is taken the reference model proposed by Knudsen and Bak (2013) and used as well for MPC control in Odgaard et al. (2015a). The drive-train simplified model (3.48), the tower (3.72), the pitch (3.51) and the generator/converter (3.93) can now be gathered into a nonlinear state space model, which is used later by the MPC after linearization

$$\begin{bmatrix} \dot{\omega}_r \\ \dot{d}_t \\ \dot{v}_t \\ \dot{\beta} \\ \dot{T}_g \end{bmatrix} = \begin{bmatrix} \frac{1}{J}\left(T_a - N_g T_g\right) \\ v_t \\ \frac{1}{M_t}\left(F_t - K_t d_t - B_t v_t\right) \\ \frac{1}{\tau_p}\left(\beta_{ref} - \beta\right) \\ \frac{1}{\tau_g}\left(T_{g,ref} - T_g\right) \end{bmatrix}, \tag{3.95}$$

while the output equations are given by:

$$\begin{bmatrix} P_{g,m} \\ v_{t,m} \\ \omega_{r,m} \end{bmatrix} = \begin{bmatrix} \eta_g N_g \omega_r T_g \\ v_t \\ \omega_r \end{bmatrix}. \tag{3.96}$$

Control of wind turbines deals with a number of objectives and tasks. Many of these are conflicting in nature, in this work a subset of these objectives is considered. The idea is to design an MPC which deals with the conflicting objectives of generating nominal power, while minimizing the blade root fatigue state and the tower fore-aft fatigue loads when operating the wind turbine at above-rated wind speed.

In order to have a model that can be used with an MPC controller, the nonlinear model needs to be linearized. The linearized model is derived from (3.95) and (3.96) applying the Jacobian linearization around a particular operating point.

Given the nonlinear system described by (3.95) and (3.96), an equilibrium point of the states, denoted as $\bar{x}$, obtained when the inputs $u = \bar{u}$ and disturbances $w = \bar{w}$, the linear discrete-time state space representation has the form

$$x(k+1) = Ax(k) + Bu(k) + Ew(k), \tag{3.97}$$

$$y(k) = Cx(k). \tag{3.98}$$

From the nonlinear model (A.1)-(A.2) the derivatives to obtain the linear model (3.97) are as follows

The model includes states representing the rotor speed ω_r, the tower fore-aft displacement d_t, the tower fore-aft velocity v_t, the generator torque T_g and the pitch angle β. The controlled inputs are generator torque and pitch references, respectively $T_{g,ref}$ and β_{ref}. The wind speed v_w is a measured non-controlled input. The model outputs are the generated power P_g, the tower fore-aft velocity v_t and the rotor speed ω_r. The new inputs u, disturbances w, states x, and outputs y represent the variation of u, y, w and x from the equilibrium value

$$u = \begin{bmatrix} T_{g,ref} - \bar{T}_{g,ref} & \beta_{ref} - \bar{\beta}_{ref} \end{bmatrix}^T, \tag{3.99}$$

$$w = \begin{bmatrix} v_w - \bar{v}_w \end{bmatrix}, \tag{3.100}$$

$$x = \begin{bmatrix} \omega_r - \bar{\omega}_r & d_t - \bar{d}_t & v_t - \bar{v}_t & \beta - \bar{\beta} & T_g - \bar{T}_g \end{bmatrix}^T, \tag{3.101}$$

$$y = \begin{bmatrix} P_{g,m} - \bar{P}_g & v_{t,m} - \bar{v}_t & \omega_{r,m} - \bar{\omega}_r \end{bmatrix}^T. \tag{3.102}$$

On the other hand, the state space matrix A, input matrix B, disturbance matrix E and output matrix C are

$$A = \begin{bmatrix} 1 + \frac{T_s}{J}\frac{\partial T_a}{\partial \omega_r} & 0 & -\frac{T_s}{J}\frac{\partial T_a}{\partial v_t} & \frac{T_s}{J}\frac{\partial T_a}{\partial \beta} & -\frac{T_s}{N_g}J \\ 0 & 1 + T_s & 0 & 0 & 0 \\ \frac{T_s}{M_t}\frac{\partial F_t}{\partial \omega_r} & -\frac{K_t T_s}{M_t} & 1 + \frac{T_s}{M_t}\left(-B_t - \frac{\partial F_t}{\partial v_t}\right) & \frac{T_s}{M_t}\frac{\partial F_t}{\partial \beta} & 0 \\ 0 & 0 & 0 & 1 - \frac{T_s}{\tau_p} & 0 \\ 0 & 0 & 0 & 0 & 1 - \frac{T_s}{\tau_g} \end{bmatrix}, \tag{3.103}$$

$$B = \begin{bmatrix} 0 & 0 \\ 0 & 0 \\ 0 & 0 \\ 0 & \frac{T_s}{\tau_p} \\ \frac{T_s}{\tau_g} & 0 \end{bmatrix}, \tag{3.104}$$

$$E = \begin{bmatrix} \frac{T_s}{J}\frac{\partial T_a}{\partial v_\omega} & 0 & \frac{T_s}{M_t}\frac{\partial F_t}{\partial v_\omega} & 0 & 0 \end{bmatrix}^T, \tag{3.105}$$

$$C = \begin{bmatrix} \frac{\partial P_g}{\partial \omega_r} & 0 & 0 & 0 & \frac{\partial P_g}{\partial T_g} \\ 0 & 0 & 1 & 0 & 0 \\ 1 & 0 & 0 & 0 & 0 \end{bmatrix}, \tag{3.106}$$

where T_s is the sampling time.

The control scheme is implemented to operate in region 3. Therefore, the following operating point is chosen:

$$\begin{aligned} \bar{v}_w &= 14\,\mathrm{m/s}, \\ \bar{\omega}_r &= 1.2671\,\mathrm{hz}, \\ \bar{T}_g &= 43093.5\,\mathrm{Nm}, \\ \bar{\beta} &= 4^\circ, \end{aligned} \tag{3.107}$$

where the matrices linearized on the operating point (3.107) and taking the system parameters from the work of Odgaard et al. (2015a) are the following

$$A = \begin{bmatrix} -0.0556 & 0 & -0.0263 & -0.008 & -2.300 \times 10^{-6} \\ 0 & 0 & 1 & 0 & 0 \\ 0.815 & -4.240 & -0.2094 & -0.1427 & 0 \\ 0 & 0 & 0 & -50 & 0 \\ 0 & 0 & 0 & 0 & -50 \end{bmatrix}, \tag{3.108}$$

$$B = \begin{bmatrix} 0 & 0 \\ 0 & 0 \\ 0 & 0 \\ 0 & 50 \\ 50 & 0 \end{bmatrix}, \tag{3.109}$$

$$E = \begin{bmatrix} 0.0263 & 0 & 0.1871 & 0 & 0 \end{bmatrix}^T, \tag{3.110}$$

$$C = \begin{bmatrix} 3.946 & 0 & 0 & 0 & 0.00012 \\ 0 & 0 & 1 & 0 & 0 \\ 1 & 0 & 0 & 0 & 0 \end{bmatrix}, \tag{3.111}$$

Chapter 4

Fault Diagnosis and Fault Tolerant Control of Wind Turbines

The content of this chapter is based on the following works:

- Sanchez et al. (2015a) Sanchez, H., Escobet, T., Puig, V., and Odgaard, P. (2015a). Fault diagnosis of advanced wind turbine benchmark using interval-based ARRs and observers. *IEEE Transactions on Industrial Electronics*, 62(6), 3783–3793.

- Odgaard et al. (2015b) Odgaard, P., Sanchez, H., Escobet, T., and Puig, V. (2015b). Fault diagnosis and fault tolerant control with application on a wind turbine low speed shaft encoder. In *9th IFAC Symposium on Fault Detection, Supervision and Safety for Technical Processes*, volume 48, 1357–1362. Paris, France.

Fault diagnosis (FD) and fault tolerant control (FTC) of wind turbines is an important issue in order to decrease the operation and maintenance costs and increase penetration into electrical grids because the enhanced reliability those techniques can provide. However, the complexity of large modern wind turbines makes difficult to transfer advanced FD and FTC methods from the theory to application. The approaches proposed are applied to the wind turbine benchmark defined in Odgaard and Johnson (2013) and described in Section 4.1. On of the contributions of this chapter is to propose a model-based fault diagnosis approach for wind turbines and its application to a realistic wind turbine FD and FTC benchmark proposed in Odgaard and Johnson (2013). The proposed fault diagnosis approach combines the use of analytical redundancy relations (ARRs) and interval observers. Interval observers consider an unknown but bounded description of the model parametric uncertainty and noise using the so-called set-membership approach (Puig, 2010). This approach leads to formulate the fault detection test by means of checking if the measurements fall inside the estimated output interval, obtained from the mathematical model of the wind turbine and noise/parameter uncertainty bounds. Fault isolation is based on considering a set of ARRs obtained from structural analysis of the wind turbine model and a fault signature matrix that considers the relation of ARRs and faults. Finally, the proposed fault diagnosis approach has been validated on a 5MW wind turbine using the NREL FAST simulator. The obtained results are presented and compared with other approaches proposed in the literature.

4.1 Overview of the FD-FTC Wind Turbine Benchmark

As discussed in the introduction of this thesis, the growing interest in wind turbines, coming from both the academia and the industry, motivated the proposal of a wind turbine benchmark for FD and FTC, containing the most common faults reported in practice (see (Odgaard et al., 2013)). This benchmark was based on a realistic generic three blade horizontal variable speed wind turbine with a full converter coupling. In the Spring of 2010, kk-electronic together with other partners (MathWorks and Aalborg University) released an international competition on Fault Detection and Isolation (FDI) in Wind Turbines based on this benchmark model of the wind turbine. The competition consisted on finding the best schemes to diagnose and handle the different faults proposed and the results were presented in (Odgaard et al., 2013).

After the announcement of results of the first benchmark, a second challenge was presented in (Odgaard and Johnson, 2013) that differs from the previous challenge in the wind turbine model that is modeled using the 5MW wind turbine reference model (Jonkman et al., 2009) on the high fidelity aeroelastic FAST simulator (Jonkman and Buhl, 2005), previously explained in Chapter 3. This simulator is able to consider the wind turbine flexible modes that are present in practice making FD more difficult when simple models neglecting these modes are used, as was the case in (Odgaard et al., 2013).

Figure 4.1 presents a block diagram of the wind turbine simulation model, provided with the benchmark, including the feedback loops corresponding to the pitch, yaw and torque variables. In this figure, it also appears the components which are affected by the set of faults and the fault diagnosis block that will be designed in this paper.

The wind turbine benchmark defines a set of ten fault scenarios mainly introduced in sensors and actuators (see Fault Generator in Figure 4.1). The types of faults are offsets, scaling, stuck, changes in the system dynamics and bit errors, as shown in Table 4.1. These faults are motivated by research in both public domain and proprietary sources (Odgaard and Johnson, 2013).

4.2 Fault Diagnosis Approach

The model based fault diagnosis methods are based in assessing the consistency between observations of a system and the outputs of a model. The behavior of the real process and the behavior of a model are compared, if the output of the system and the models output are different then a fault is detected. This idea is summarized in Figure 4.2.

A residual is a variable used for evaluating consistency and it is defined as:

$$r(t) = y(t) - \hat{y}(t), \tag{4.1}$$

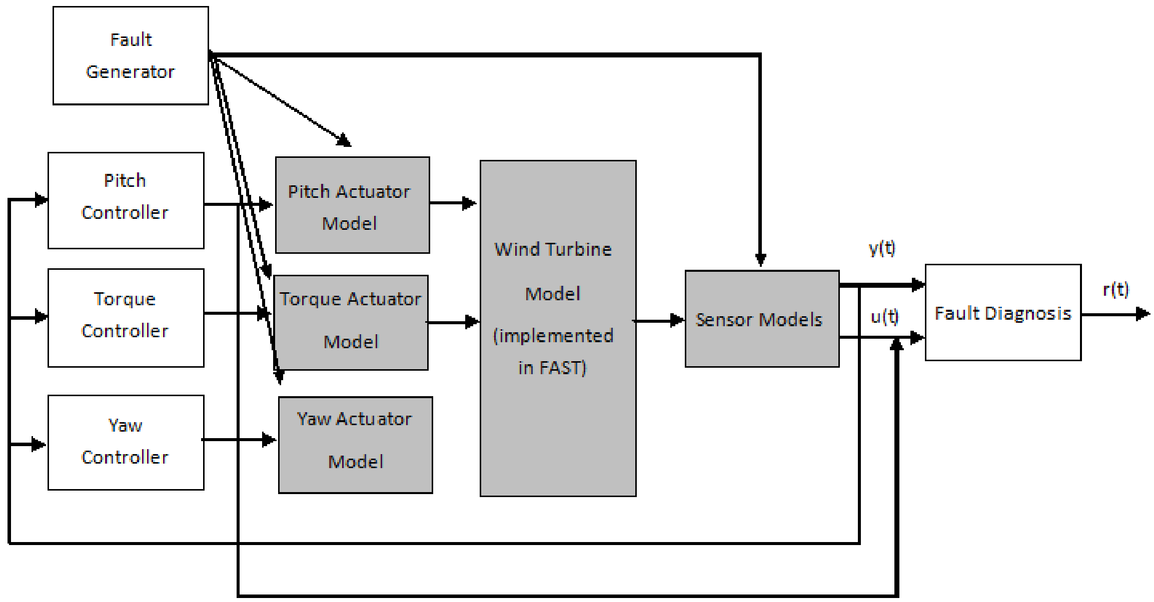

Figure 4.1: Block diagram of wind turbine simulation model

Table 4.1: Fault Scenarios

No.	**Faults**	**Type**
f_1	Blade root bending moment sensor	Scaling
f_2	Accelerometer	Offset
f_3	Generator speed sensor	Scaling
f_4	Pitch angle sensor	Stuck
f_5	Generator power sensor	Scaling
f_6	Low speed shaft position encoder	Bit error
f_7	Pitch actuator	Abrupt
f_8	Pitch actuator	Slow
f_9	Torque offset	Offset
f_{10}	Yaw drive	Stuck drive

where $y(t)$ is the real process output and $\hat{y}(t)$ is the predictor output.

Real and predicted outputs are always different due to the uncertainty. Uncertainty in industrial processes makes difficult the fault detection task.

Ideally residuals are 0 when there are no faults and not 0 when there are faults. But in many cases there are modeling errors, non-modeled dynamics, disturbances and noise which cause that residuals are not 0 even when there are no faults.

Model-based fault detection tests are based on the evaluation of a set of fault indication signals (residuals), obtained through analytical redundancy relations (ARRs). ARRs are defined as relations between known variables and can be derived combining the measurement model (known variables) with the system model (unknown variables). Also, each ARR is sensitive to a set of

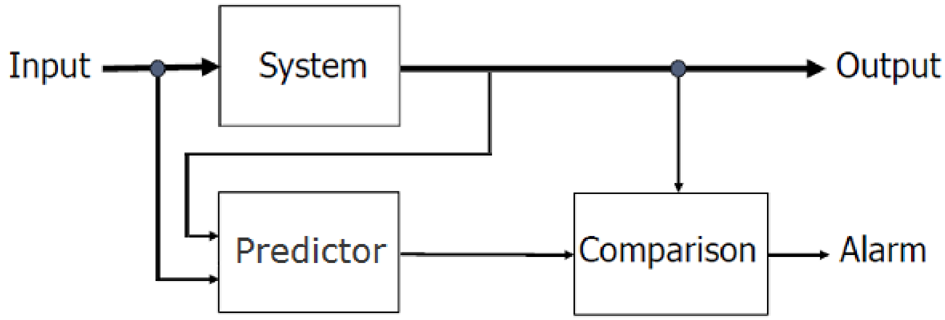

Figure 4.2: Model Based Fault Detection Scheme

faults.

A fault detection task decides if an ARR is violated at a given instant or not, generating a set of fault indicators, s_i according to:

$$s_i(k) = \begin{cases} 0, & if \quad \tau_{lower} < r_i(k) < \tau_{upper} \qquad\qquad (no\,fault), \\ 1, & if \quad r_i(k) \leq \tau_{lower} \; or \; r_i(k) \geq \tau_{upper} \; (fault), \end{cases} \tag{4.2}$$

where τ_{lower} and τ_{upper} are the limits of the threshold associated to the ARR r_i. The comparison of fault indicators patterns allows to diagnose the fault.

4.2.1 ARR Generation

The design of the fault diagnosis system is based on deriving a set of ARRs by combining the model equations (associated to the subsystems presented in Chapter 3) with the available sensors. This is the standard procedure to design a fault diagnosis system using model based approaches (for more details see Blanke et al. (2006)). Some of the model equations come directly from the benchmark model while the remaining are obtained using data-based techniques. In the case study used in this work, the set of available sensors to determine the ARRs are those presented in Table (3.2). Combining the model equations with the available sensors by means of the structural analysis approach and perfect matching algorithm (Blanke et al., 2006), the resulting set of ARRs is presented in the following.

ARR 1 is obtained directly from the power equation presented in (3.94)

$$P_{g,m}(t) = \eta_g \omega_{g,m}(t) T_{g,m}(t), \tag{4.3}$$

since the power generated $P_{g,m}(t)$, the generator speed $\omega_{g,m}(t)$ and the generator torque $T_{g,m}(t)$ are all measured variables.

ARR 2 is obtained from the generator/converter model described in (3.93) as follows

$$\tau_g \frac{dT_{g,m}(t)}{dt} + T_{g,m}(t) = T_{g,ref}(t). \tag{4.4}$$

During the simulation tests performed with the benchmark based on the FAST simulator, it was noticed that the blade root moment behavior observed in the simulations did not correspond to the one described by (3.73). After analyzing the blade root moment behavior and considering the influence of the wind speed and blades pitch angle on this variable, an experimental model was proposed to be used. This experimental model is based on the mean values of the blade root moment and pitch angle signals in steady state to filter the flexible modes. Several tests with different constant wind speeds ranging from 12 m/s to 30 m/s were performed obtaining different pitch angle values. Then, a relation between the different pitch angles and the mean value of the blade root moment in steady state was found. As it can be seen in Figure 4.3, first, second and third order polynomials were considered to represent the mean blade root moment as function of the pitch angle.

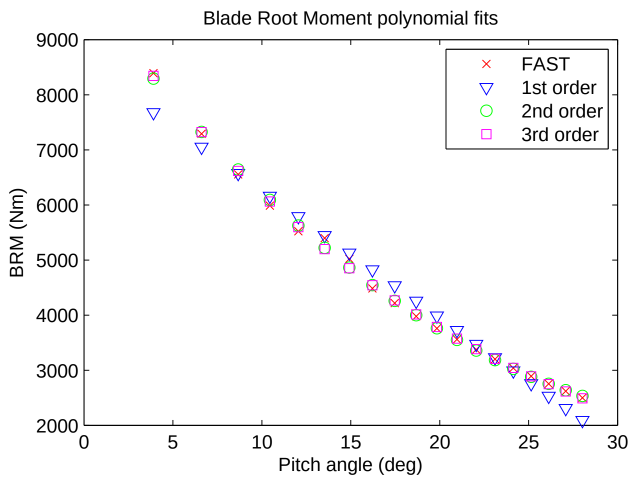

Figure 4.3: Estimated Blade Root Moments models

Finally, the proposed model for the blade root moment dynamics was the third order blade root moment mean model

$$\bar{M}_{B,j,m(t)} = a_{3,j}\beta_{j,m}(t)^3 + a_{2,j}\beta_{j,m}(t)^2 + a_{1,j}\beta_{j,m}(t) + a_{0,j}, \tag{4.5}$$

where $\bar{M}_{B,j}(t)$ is the mean blade root moment and β_j is the pitch angle on blade j. The values of the coefficients $a_{i,j}$ for blade root moment mean models for each blade, corresponding to experiments of winds higher than 12 m/s, are shown in Table 4.2.

Table 4.2: Blade Root Moment Mean Model Coefficients

Mean BRM model	a_3	a_2	a_1	a_0
$\bar{M}_{B,1(t)}$	-0.0778	9.3204	-469.4313	96482
$\bar{M}_{B,2(t)}$	-0.0777	9.3159	-469.3210	99720
$\bar{M}_{B,3(t)}$	-0.0776	9.3228	-469.6690	96495

Thus, *ARRs 3, 4* and *5* are obtained from the blade root moment model (4.5).

ARRs 6, 7 and *8* are obtained from the pitch subsystems derived directly from the model (3.49)

$$\frac{d^2\beta_{j,m}(t)}{dt^2} + 2\zeta\omega_n\frac{d\beta_{j,m}(t)}{dt} + \omega_n^2\beta_{j,m}(t) = \omega_n^2\beta_{ref}(t). \tag{4.6}$$

From the drive train model (3.39)-(3.40), the following relations can be established in steady state that filter the flexible modes. First, a relation between $\omega_g(t)$ and $T_g(t)$ can be established as explained below

$$B_g\omega_g(t) = -T_g(t) + K, \tag{4.7}$$

where the constant K is the torsion angle in steady state. In a similar way, a relation between $\omega_g(t)$ and $\omega_r(t)$ through N_g can also be derived

$$\omega_g(t) = N_g\omega_r(t). \tag{4.8}$$

Then *ARR 9* and *ARR 10* are derived from equations (4.8) and (4.7), as follows

$$B_g\omega_{g,m}(t) = -T_{g,m}(t) + K, \tag{4.9}$$

$$\omega_{r,m}(t) - \frac{1}{N_g}\omega_{g,m}(t) = 0. \tag{4.10}$$

Using the input/output equations of the drive train model presented in (3.39)-(3.40), with the dynamics of the torsion angle neglected because there is no sensor available for this variable in the benchmark, ARR 11 (eq. 4.11) and ARR 12 (eq. 4.12) are obtained as follows

$$f_1\left(\dot{\omega}_{r,m}(t), \omega_{r,m}(t), \hat{T}_a(t), T_{g,m}(t)\right) = 0, \tag{4.11}$$

$$f_2\left(\dot{\omega}_{g,m}(t), \omega_{g,m}(t), \hat{T}_a(t), T_{g,m}(t)\right) = 0, \tag{4.12}$$

where the aerodynamic torque $\hat{T}_a(t)$ can be computed by the following expression

$$\hat{T}_a(t) = f\left(\omega_{r,m}(t), v_m(t), \beta_m(t)\right). \tag{4.13}$$

The rotor speed $\omega_{r,m}(t)$ and the azimuth angle $\phi_{r,m}(t)$ of the low speed shaft are both known variables. Therefore, the *ARR 13* derived from (3.27) can be proposed as a relation between rotor speed and the derivative of the low speed shaft angle

$$\omega_{r,m}(t) = \frac{d\phi_{r,m}(t)}{dt}. \tag{4.14}$$

ARR 14 is derived from the yaw controller model proposed in Odgaard and Johnson (2013). The controller has the measured yaw error $\Xi_{e,m}(t)$ as an input and the yaw reference angular velocity $\omega_{y,r}$ as an output, which are both known variables. The yaw rate is modeled as in Odgaard and Johnson (2013) with a delay respect to the yaw reference angular velocity. Therefore, the following ARR can be obtained

$$f(\Xi_{e,m}(t), \omega_{y,r}(t)) = 0. \tag{4.15}$$

Wind tower deflects because of the loads and wind tower flexibility leading to the nacelle motion. This motion can be characterized by means of a deflection in wind direction (fore-aft) x_t and perpendicular to wind direction (sidewards) y_t. Some models in the literature were proposed such as the one proposed by Van Engelen et al. (2007). However, in order to perform fault diagnosis using this tower model, a tower bottom strain gauge is needed. This sensor is not an industrial standard in wind turbines, and therefore is not included in the FD benchmark. To overcome the lack of this sensor, an experimental model with the purpose of fault diagnosis is proposed for the tower system. From the simulation tests performed with the benchmark based on FAST simulator, a relation between the tower top accelerations and the blade root moments in steady state was observed. The proposed model establishes an ARR containing the signals of the blade root moment and tower top acceleration in the x direction (fore-aft), which are among the benchmark available sensors presented in Table 4.1.

The proposed model is the following

$$M_{B,j,m}(t) = a_{t_1}\ddot{x}_{x,m}(t) + b_{t_1}, \tag{4.16}$$

where $M_{B,j,m}(t)$ is the blade root moment on blade j, $\ddot{x}_{x,m}(t)$ is the accelerometer in the x direction, b_{t_1} is the mean value of $M_{B,j,m}(t)$ and a_{t_1} is a parameter used to scale the acceleration signal.

The *ARRs 15, 16* and *17* are obtained from the model (4.16).

As a summary of the derived ARRs related with the wind turbine components is shown in Table 4.3.

Table 4.3: ARRs with the respective wind turbine components

ARR	**Component**
ARRs 1,2	Generator/converter
ARRs 3,4,5	Blades
ARRs 6,7,8	Pitch systems
ARRs 9,10,11,12,13	Drivetrain
ARR 14	Yaw system
ARR 15,16,17	Tower,blades

4.2.2 Interval Models

The presence of flexible modes in the wind turbine (simulated with the aeroelastic FAST simulator) and the modeling errors inherent to the approximation of some model relations discussed in Section 4.2.1, lead to the necessity of using a robust fault detection algorithm able to handle uncertainty (Chen and Patton, 1999). One of the most developed families of approaches that deal with model uncertainty, called active, are based on generating residuals, which are insensitive to uncertainty (modeling errors and disturbances), while at the same time sensitive to faults using some decoupling method (Chen and Patton, 1999). On the other hand, there is a second family of approaches, called passive, which enhances the robustness of the fault detection system at the decision-making stage using an adaptive threshold (Puig et al., 2008). In this approach, the uncertainty will be located in the parameters bounding their values by intervals using the so-called interval models (Puig et al., 2008). The robustness in fault detection is achieved by means of the passive approach at the decision-making stage using an adaptive threshold generated by considering the set of model responses obtained by varying the uncertain parameters within their intervals.

Static and dynamic interval predicted models

ARRs introduced in Section 4.2.1 will be used to create residuals to detect and isolate faults. These residuals will be generated in order to check the consistency between the observed and the predicted process behavior. Looking at the obtained ARRs, they can be divided in two groups: static and dynamic. The static ARRs are: $ARR1$, $ARR3$, $ARR4$, $ARR5$, $ARR9$, $ARR10$, $ARR13$ and $ARR14$, while the remaining are dynamic. The generation of residuals is straightforward in case of static ARRs since they follow directly from the mathematical expressions. On the other hand, in case of dynamic ARRs several options for generating residuals are possible ranging from parity equations to observers. In this paper, interval observers are used because they handle in a natural way the effect of the uncertainty by generating adaptive thresholds used for fault detection. The model of each dynamic ARR is rewritten in observer canonical form as follows

$$x(k+1) = A(\tilde{\theta})x(k) + B(\tilde{\theta})u(k), \tag{4.17}$$
$$y(k) = C(\tilde{\theta})x(k) + \tilde{v}(k), \tag{4.18}$$

where $u(k) \in \mathbb{R}^{n_u}$ is the system input, $y(k) \in \mathbb{R}^{n_y}$ is the system output, with $x(k) \in \mathbb{R}^{n_x}$ is the state-space vector, $\tilde{v}(k) \in \mathbb{R}^{n_y}$ is the output noise that is assumed to be bounded $|\tilde{v}_i(k)| < \sigma_i$, with $i = 1, \ldots, n_y$, $A(\tilde{\theta})$, $B(\tilde{\theta})$, $C(\tilde{\theta})$, are matrices of appropriate dimensions where $\tilde{\theta} \in \mathbb{R}^{n_\theta}$ is the parameter vector. Uncertainty in the parameters is considered as follows

$$\theta \in \Theta = \left\{ \theta \in \mathbb{R}^{n_\theta} \mid \underline{\theta}_i \leq \theta_i \leq \bar{\theta}_i, i = 1, \ldots, n_\theta \right\}. \tag{4.19}$$

Then, from the dynamic ARR expressed in state space form (4.17)-(4.18), a interval linear observer with Luenberger structure can be derived as follows (Meseguer et al., 2010):

$$\begin{aligned}
\hat{x}(k+1,\theta) &= \left(A(\theta) - LC(\theta)\right)\hat{x}(k,\theta) + B(\theta)u(k) + Ly(k) \\
&= A_0(\theta)\hat{x}(k,\theta) + B(\theta)u(k) + Ly(k), \\
\hat{y}(k,\theta) &= C(\theta)\hat{x}(k,\theta),
\end{aligned} \tag{4.20}$$

where $\hat{x}(k,\theta)$ is the estimated system state vector, $\hat{y}(k,\theta)$ is the estimated system output vector and $A_0(\theta) = A(\theta) - LC(\theta)$ is the observer matrix. The observer gain matrix $L \in \mathbb{R}^{n_x \times n_y}$ is designed to stabilize the matrix $A_0(\theta)$ and to guarantee a desired performance regarding fault detection for all $\theta \in \Theta$ using the LMI pole placement approach (Chilali and Gahinet, 1996).

The input/output form of the observer (4.20) is expressed as follows

$$\hat{y}(k,\theta) = G(q^{-1},\theta)u(k) + H(q^{-1},\theta)y(k), \tag{4.21}$$

with:

$$\begin{aligned} G(q^{-1},\theta) &= C(\theta)(qI - A_0(\theta))^{-1}B(\theta), & (4.22)\\ H(q^{-1},\theta) &= C(\theta)(qI - A_0(\theta))^{-1}L. & (4.23) \end{aligned}$$

The effect of the uncertain parameters θ on the observer temporal response $\hat{y}(k,\theta)$ will be bounded using an interval satisfying

$$\hat{y}(k,\theta) \in \left[\underline{\hat{y}}(k), \overline{\hat{y}}(k)\right]. \tag{4.24}$$

Such interval can be computed independently for each output $i = 1, \ldots, n_y$, neglecting couplings among outputs, as follows

$$\underline{\hat{y}_i}(k) = \min_{\theta\in\Theta} \hat{y}_i(k,\theta) \quad \text{and} \quad \overline{\hat{y}}_i(k) = \max_{\theta\in\Theta} \hat{y}_i(k,\theta), \tag{4.25}$$

subject to the observer equations given by (4.21). The optimization problems (4.25) could be solved using numerical methods as in Puig et al. (2003) or, more efficiently by means of the zonotope approach presented in Alamo et al. (2005).

Finally, taking into account that the additive noise in the system (4.18) is bounded, the following condition should be satisfied

$$y_i(k) \in \left[\underline{\hat{y}_i}(k) - \sigma_i, \overline{\hat{y}_i}(k) + \sigma_i\right] i = 1, \ldots, n_y, \tag{4.26}$$

in a non-faulty scenario.

Parameter uncertainty estimation

One of the key points in passive robust model based fault detection is how models and their uncertainty bounds are obtained. Classical system identification methods are formulated under a statistical framework. Assuming that the measured variables are corrupted by additive noises with known statistical distributions and that the model structure is known, a parameter estimation algorithm will provide nominal values for the parameters together with descriptions of the associated uncertainty in terms of the covariance matrix or confidence regions for a given probability level (Kendall and Stuart, 1961), (Dalai et al., 2007). However, this type of approaches cannot be applied when measurement errors are described as unknown but bounded values and/or modeling errors exist. The problem of bounding the model uncertainty has been mainly stated in many references coming from the robust control field. Recently, some methodologies that provide a model with its uncertainty have been developed, but always thinking of its application to control (Reinelt et al., 2002). One of the methodologies assumes the bounded but unknown description of the noise and parametric uncertainty. This methodology is known as *bounded-error* or *set-membership estimation* (Milanese et al., 1996), which produces a set of parameters consistent with the selected model structure and the pre-specified noise bounds. Uncertainty in the parameters is considered as follows

$$\theta \in \Theta = \left\{ \theta \in \mathbb{R}^{n_\theta} \mid \underline{\theta}_i \leq \theta_i \leq \bar{\theta}_i, i = 1, \ldots, n_\theta \right\}, \tag{4.27}$$

where θ is a vector of uncertain parameters and n_θ is the number of uncertain parameters considered.

Given an input/output static equation expressed as

$$\hat{y}(k, \theta) = G(\theta)u(k) + H(\theta)y(k), \tag{4.28}$$

where $G(\theta)$ and $H(\theta)$ are uncertain parameters. The goal of the parameter estimation algorithm is to characterize the parameter set Θ (here a box) consistent with the data collected in a fault-free scenario and estimate the output $\hat{y}(k, \theta)$. Given N measurements of system inputs $u(k)$ and outputs $y(k)$ from a scenario free of faults and rich enough from the identifiability point of view, the parameters tolerance α, and a nominal model described by a vector of nominal parameters θ_n obtained using a standard least-square parameter estimation algorithm Ljung (1998), the uncertain parameter estimation algorithm proceeds by solving the following optimization problem

$$\begin{aligned}
&\min \ \alpha \\
&\text{subject to :} \\
&y_i(k) \in \left[\underline{\hat{y}}_i(k) - \sigma_i, \overline{\hat{y}}_i(k) + \sigma_i \right] \quad i = 1, ..., n_y \quad k = 1, ..., N \\
&\underline{\hat{y}}_i(k) = \min_{\theta \in \Theta} \hat{y}_i(k, \theta) \quad i = 1, ..., n_y \quad k = 1, ..., N \\
&\overline{\hat{y}}_i(k) = \max_{\theta \in \Theta} \hat{y}_i(k, \theta) \quad i = 1, ..., n_y \quad k = 1, ..., N \\
&\hat{y}(k, \theta) = G(q^{-1}, \theta)u(k) + H(q^{-1}, \theta)y(k) \quad k = 1, ..., N \\
&\Theta = \left[\theta_n(1 - \alpha), \theta_n(1 + \alpha) \right],
\end{aligned} \tag{4.29}$$

where $\underline{\hat{y}}_i(k)$ and $\overline{\hat{y}}_i(k)$ are the bounds of the system output estimation computed component-wise using the static input/output equation (4.28) and obtained according to (4.29), n_y are the number of measurements.

It is assumed that a priori theoretical or practical considerations allow to obtain useful intervals associated to measurement noises, leading to an estimation of the noise bound σ.

4.2.3 Fault Detection

Fault detection is based on generating a nominal residual comparing the measurements of physical system variables $y(k)$ with their estimation $\hat{y}(k)$ provided by the observer (4.20)

$$r(k) = y(k) - \hat{y}(k, \theta_n), \tag{4.30}$$

where $r(k) \in \mathbb{R}^{n_y}$ is the residual set and θ_n the nominal parameters. According to Gertler (1998), the form of the nominal residual generator, obtained using (4.21), is

$$r(k) = \left(I - H(q^{-1}, \theta_n)\right) y(k) - G(q^{-1}, \theta_n) u(k), \tag{4.31}$$

that has been derived taking into account the input/output form of the observer.

When considering model uncertainty located in parameters, the residual generated by (4.30) will not be zero, even in a non-faulty scenario. To cope with the parameter uncertainty effect, a passive robust approach based on adaptive thresholding can be used (Puig et al., 2006), as previously discussed. Thus, using this approach, the effect of parameter uncertainty in the components $r_i(k)$ of residual $r(k)$ (associated to each system output $y_i(k)$) is bounded by the interval (Puig et al., 2003):

$$r_i(k) \in [\underline{r}_i(k) - \sigma_i, \overline{r}_i(k) + \sigma_i], \quad i = 1, ..., n_y, \tag{4.32}$$

where

$$\underline{r}_i(k) = \underline{\hat{y}}_i(k) - \hat{y}_i(k, \theta_n) \text{ and } \overline{r}_i(k) = \overline{\hat{y}_i}(k) - \hat{y}_i(k, \theta_n). \tag{4.33}$$

The bounds $\underline{\hat{y}}_i(k)$ and $\overline{\hat{y}}_i(k)$ of the system output estimation are computed component-wise using the interval observer (4.21). Then, the fault detection test is based on checking if the residuals satisfy or not the condition given by (4.32). In case that this condition does not hold, a fault can be indicated. Notice that checking condition (4.32) is equivalent to check condition (4.24).

As discussed in Meseguer et al. (2010), fault detection based on interval observers presents non-detected faults (missed alarms) because of the uncertainty. This is due to the fact that there exists a minimum fault size that guarantees the activation of the fault detection test (4.32) despite the uncertainties. On the other hand, interval observers guarantee that there are no false alarms since uncertainty bounds are determined to explain all the data collected in non-faulty scenarios used for interval parameter estimation by means of (4.29).

4.2.4 Fault Isolation

Fault isolation consists in identifying the faults affecting the system. It is carried out on the basis of fault signatures, generated after the detection process, and their relation with all the considered faults. Robust residual evaluation presented in Section 4.2.3 allows obtaining a set of observed *fault signatures* $\phi(k) = [\phi_1(k), \phi_2(k), \ldots, \phi_{nr}(k)]$, where each fault indicator is given by

$$\phi_i(k) = \begin{cases} 0 & \text{if} \quad r_i(k) \in [\underline{r}_i(k) - \sigma_i, \overline{r}_i(k) + \sigma_i], \\ 1 & \text{if} \quad r_i(k) \notin [\underline{r}_i(k) - \sigma_i, \overline{r}_i(k) + \sigma_i]. \end{cases} \tag{4.34}$$

Standard fault isolation reasoning exploits the knowledge about the binary relation between the set of fault hypothesis and the set of residuals that is stored in the so called *Fault Signature Matrix* (FSM), denoted as M. An element m_{n_r,n_f} (n_r indicates rows, n_f indicates columns) of M is equal to 1 if the fault f_{n_f} affects the computation of the residual r_{n_r}; otherwise, the element m_{n_r,n_f} is zero-valued. A column of M is known as a *theoretical fault signature* and indicates which residuals are affected by a given fault. A set of faults is *isolable* if all the columns in M are different (two columns that are equal indicate two faults that can not be distinguished).

Based on the use of FSMs, different reasoning procedures have been proposed in the literature, see for instance (Cordier et al., 2004). The procedure accepted as standard by the FDI community involves finding a matching between the observed fault signature and one of the theoretical fault signatures. However, this reasoning is not appropriate in an unknown but bounded context. Due to the uncertainty, when a fault is present in the system, an undefined number of the residuals affected by the fault can be found inconsistent, mainly depending on the sensitivity of each residual with respect to the fault and on the fault magnitude. In this case, if the column-matching procedure is used, then the particular fault will not be identified. An appropriate reasoning which comes from the DX community only considers the residuals that are inconsistent when searching for the fault (that is, inconsistency is relevant, consistency is not). Based on the proposed framework by Cordier et al. (2004), the fault signature matrix is interpreted in DX CBD (Consistency-based Diagnosis) approach to fault isolation considering separately each line corresponding to a violated ARR, (i.e., a set of components that are to be considered abnormal in order to be consistent with the observed fault signature) before searching for a common explanation, i.e., follows a row view of the fault signature matrix.

Analyzing the effects of the faults presented in Odgaard and Johnson (2013), listed in Table 4.1, in the set of static and dynamic residuals obtained from the ARRs presented in Section 4.2.1, the fault signature matrix shown in Table 4.4 is obtained. This table shows the sensitivity of the obtained residuals in presence of the considered fault scenarios, where the sub-index j takes the following values $j = 1, 2, 3$.

Based on the information of FSM presented in Table 4.4, the logical test that allows isolating the faults has been generated. Tables 4.5 and 4.6 list the logical reasoning test in the case of applying column and row reasoning approaches respectively, where ΔNr_i indicates an abnormal behavior of i^{th} residual.

4.2.5 Fault Diagnosis Results

In the following section, some representative results considering the fault scenarios defined in the wind turbine benchmark (see Section 4.1) will be presented. The wind speed sequences used in

Table 4.4: Theoretical signature matrix

	$f_{1-M_{\mathrm{B},j,\mathrm{m}}}$	f_2	f_3	f_4	f_5	f_6	$f_{(7-8)}$	f_9	f_{10}
r_1			x		x			x	
r_2								x	
r_{j+2}	x	x		x			x		
r_{j+5}				x			x		
r_9			x					x	
r_{10}			x						
r_{11}								x	
r_{12}			x					x	
r_{13}						x			
r_{14}									x
r_{j+14}	x	x							

Table 4.5: Column reasoning approach

Logical Test	**Diagnostic**
ΔNr_{2+j}	$f_{1-M,B,j,m}$
$\Delta Nr_1 \wedge \Delta Nr_9 \wedge \Delta Nr_{10} \wedge \Delta Nr_{12}$	f_3
$\Delta Nr_{2+j} \wedge \Delta Nr_{5+j}$	$f_{4-\beta_j} \vee f_{(7-8)-PA_j}$
ΔNr_1	f_5
$\Delta Nr_1 \wedge \Delta Nr_2 \wedge \Delta Nr_9 \wedge \Delta Nr_{11} \wedge \Delta Nr_{12}$	f_3
ΔNr_{13}	f_6
ΔNr_{14}	f_{10}
$\Delta Nr_{15} \wedge \Delta Nr_{16} \wedge \Delta Nr_{17}$	f_2

Table 4.6: Row reasoning approach

Logical Test	**Diagnostic**
ΔNr_1	$f_3 \vee f_5 \vee f_9$
ΔNr_2	f_9
ΔNr_{2+j}	$f_{1-M,B,j,m} \vee f_{4-\beta_j} \vee f_{7-PA_j} \vee f_{8-PA_j}$
ΔNr_{5+j}	$f_{4-\beta j} \vee f_{7-PA_j} \vee f_{8-PA_j}$
ΔNr_9	$f_3 \vee f_9$
ΔNr_{10}	f_3
ΔNr_{11}	f_9
ΔNr_{12}	$f_3 \vee f_9$
ΔNr_{13}	f_6
ΔNr_{14}	f_{10}
ΔNr_{14+j}	$f_{1-M,B,j,m} \vee f_2$

the tests were some of the uniform mean wind speeds of 11 m/s, 14 m/s and 17 m/s, which are provided with the benchmark (Odgaard and Johnson, 2013). Additionally, a mean wind speed of 14 m/s with direction changes to test the detection of fault f_{10} in the yaw actuator was used.

Using the algorithm 4.29 to determine the uncertainty parameter α for each ARR, where the obtained values are shown in Table 4.7. The sub-index j takes the following values $j = 1, 2, 3$.

Table 4.7: Residuals with the uncertainty parameter value

ARR	Value of α
r_1	8.34×10^{-4}
r_2	3.4×10^{-4}
r_3	0.0343
r_4	0.0351
r_5	0.0353
r_{j+5}	1×10^{-4}
r_9	3.8×10^{-4}
r_{10}	8.3×10^{-5}
r_{11}	1.5×10^{-4}
r_{12}	2×10^{-4}
r_{13}	1.46×10^{-2}
r_{14}	1×10^{-9}
r_{j+14}	1×10^{-6}

In Figure 4.4, fault scenarios f_5 and f_2 are shown. Fault f_5 occurs in the generator power sensor scaled by a factor of 1.1 and it is present in the time interval from 240s to 265s. Fault scenario f_2 occurs in tower top accelerometer sensor in the x direction corresponding to an offset of -0.5m/s^2 present in the time period from 75s to 100s. In Figure 4.5, fault scenarios f_3 and f_4 are shown. Fault 3 causes the generator speed to be scaled by a factor of 0.95 and it is present between 130s and 155s. Fault 4 results in blade 1 having a stuck pitch angle sensor, which holds a constant value of 1 degree. Fault 4 is active from 185s to 210s. All of the faults defined in the benchmark (Odgaard and Johnson, 2013) are only present during a determined period of time.

In the fault scenarios shown in Figures (4.4)-(4.5), it can be observed that the measurement goes out of the detection thresholds and that the fault indicator activates during the interval of time in which the fault is present, either permanently or intermittently.

In Table 4.8, it is shown which residuals were activated for each one of the considered fault scenarios during the simulation tests. From this table, it can be observed that during the tests not all of the residuals are activated according to the FSM shown in Table 4.4.

The fault detection results are resumed in Table 4.9. The values for the required detection time (t_D) are those specified in the benchmark. The real time detection (t_D real) is the one obtained for the first residual activated in presence of the fault, where T_s is the sampling period. The performance of the FDI scheme (summarized in Table 4.9) is assessed with wind realizations which are inside the zone 3 (constant power production) of the wind turbine benchmark control scheme, i.e. wind speed in the range 12 m/s - 25 m/s, (see Odgaard et al. (2013) for more details). The results obtained show that the FDI performance presented in this paper are not highly affected when wind velocity change within this range of wind velocities. For the control zone 2 (power optimization or partial load), i.e. wind speed in the range 3 m/s - 12 m/s, the pitch actuators are not active meaning that the faults regarding to this subsystem are not detectable. Moreover, a complete dif-

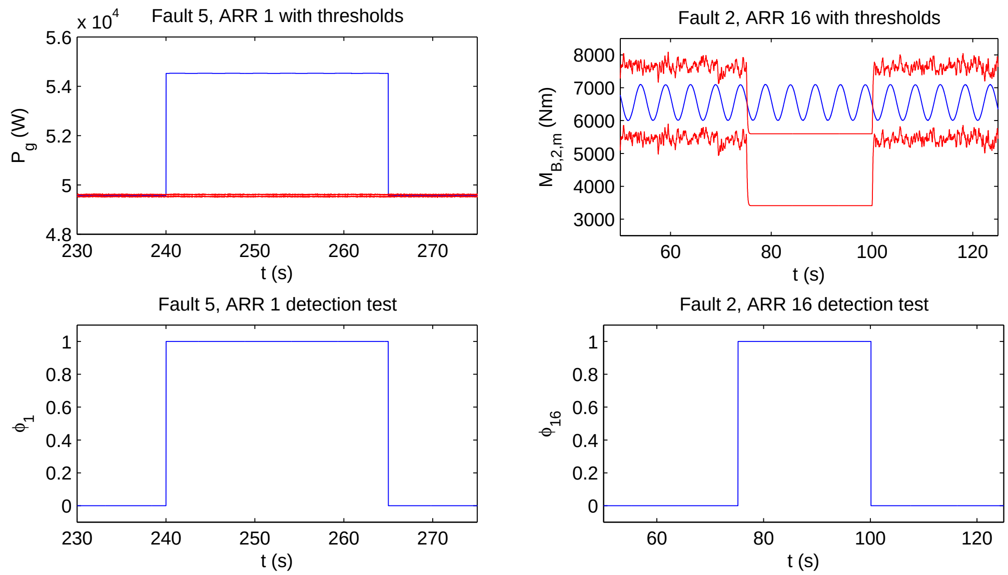

Figure 4.4: Fault scenarios f_5 and f_2: (up) measurement and detection thresholds and (down) fault indicator

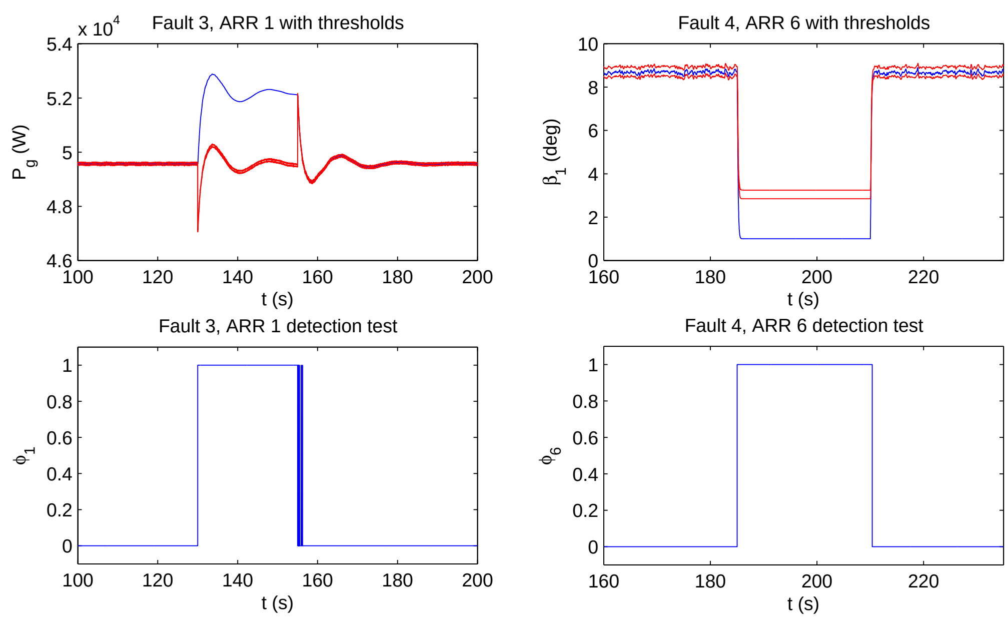

Figure 4.5: Fault scenarios f_3 and f_4: (up) measurement and detection thresholds and (down) fault indicator

ferent set of models would be needed in order to perform FDI for the rest of the faults neglecting the pitch subsystem model. In Table 4.9, the results of performing tests with smaller fault sizes with scaling and offset types of faults are shown. It is observed that the approach presented here

Table 4.8: Activated residuals for each fault

Fault No.	Activated Residuals
f_1	r_3, r_4, r_5
f_2	r_{15}, r_{16} and r_{17}
f_3	r_1, r_9 and r_{10}
f_4	r_3, r_4, r_5, r_6, r_7 and r_8
f_5	r_1
f_6	r_{13}
f_7, f_8	r_3, r_4 and r_5
f_9	r_2 and r_9
f_{10}	r_{14}

is capable of detecting smaller faults than the nominal ones proposed in the benchmark (Odgaard and Johnson, 2013), showing a good resolution of the proposed approach.

Table 4.9: Fault Detection Results

Fault No.	t_D required	t_D real	Nominal Value	Minimum Fault
f_1	<10 T_s	3 T_s	0.95	0.997
f_2	<10 T_s	18 T_s	-0.5	-0.145
f_3	<10 T_s	3 T_s	0.95	0.9999
f_4	<10 T_s	3 T_s	-	-
f_5	<10 T_s	3 T_s	1.1	1.00035
f_6	<10 T_s	6 T_s	-	-
f_7	<8 T_s	375 T_s	-	-
f_8	<100 T_s	33 T_s	-	-
f_9	<3 T_s	3 T_s	1000	25
f_{10}	<50 T_s	3 T_s	-	-

Isolation based on Column Reasoning

Comparing the activated residuals in Table 4.8 with the logic conditions described in Table 4.5, it is noticed that faults f_5, f_6 and f_{10} can be isolated.

Faults f_4, f_7 and f_8 correspond to faults that occur in the sensors and actuators of the pitch subsystems, presenting the same fault signature. Consequently, they cannot be isolated between each other. The same occurs with faults f_1 and f_2. Faults f_3 and f_9 signatures do not match exactly with its theoretical ones because not all its residuals were activated, see Table 4.8. Therefore in a strict reasoning, these faults scenarios are not isolable because do not match with any of the signatures in the theoretical signature matrix. However, in the case these fault scenarios occur, it is possible to calculate which of the fault signatures is the one that adjust the best to the current observation.

Isolation based on Row Reasoning

Comparing the activated residuals in Table 4.8 with the logic conditions described in Table 4.6, the following diagnosis results could be obtained. In the case of activation of r_1, the possible faults would be f_3, f_5 or f_9. In the case of r_3 or r_6 activation, the fault would be $f_{4-\beta_1} \vee f_{7-PA_1} \vee f_{8-PA_1}$, detecting a fault in pitch subsystem 1 but not being able to isolate whether the faulty is the sensor or the actuator. The same diagnosis is obtained in case that r_4 or r_7 and r_5 or r_8 activates, the fault would be in pitch subsystem 2 or 3 either in the sensor or in the actuator. If r_2 activates, f_9 would be isolated. In the case of r_9 activation, the possible faults would be f_3 or f_9. If r_{15}, r_{16} or r_{17} activates, a fault $f_{1-M_{B,j,m}}$ with $j = 1, 2, 3$ or the fault f_2 could be indicated. The case of r_{11} activation would result in f_9 isolation. If r_{10} activates, the isolated fault would be f_3. In the case of r_{13} or r_{14} activation, the isolated faults would be f_6 and f_{10}, respectively.

Comparison with other approaches

Reviewing the literature, the advanced wind turbine benchmark case study used in this paper has been considered for model-based FDI in Sheibat-Othman et al. (2013), Zeng et al. (2013) and Svetozarevic et al. (2013). The different approaches and results are briefly presented and discussed next:

- *Support Vector Machines and Observers (SVMO)*: In Sheibat-Othman et al. (2013), two methods were employed to isolate faults of different types at different locations: Support vector machines (SVM) and a Kalman-like observer. SVM could isolate most faults with the used data and characteristic vectors, except for high varying dynamics. In that case, the use of an observer, which is model-based, was found necessary. The results obtained in Sheibat-Othman et al. (2013) are compared with those obtained with the approach proposed in this paper. From this comparison, it can be seen that the approach introduced here outperforms results obtained in Sheibat-Othman et al. (2013).

- *Support Vector Machines and Residuals Based Method (SVMR)*: In Zeng et al. (2013), support vector machines (SVM) and residual-based methods (RBM) are used to detect and isolate faults proposed in the benchmark. From the total set of ten faults, nine are treated in Zeng et al. (2013). For the detection and isolation of four of the faults, SVM is employed. On the other hand, for the remaining five faults, RBM is used. The thresholds in the RBM methods proposed in Zeng et al. (2013) are generated by means of a time-variant variable function of the residuals and their mean values while the ones introduced here are adaptive thresholds determined by the effect of the uncertainty in the residuals parameters.

- *Fault Detection and Isolation Filter (FDIF)*: the fault detection and isolation filter presented in Svetozarevic et al. (2013) based on an optimization-based approach is proposed to deal with measurement noises in the residual generator. There are two approaches considered in Svetozarevic et al. (2013) for the FDI filter design. The first approach does not take into account measurement noise while the second approach considers the effect of the noise in the residual, determining the transfer function and then formulating an optimization problem with the objective of minimization of the H_2 norm of the calculated transfer function. The way of dealing with measurement noise in the work presented here can be related to the second approach proposed in Svetozarevic et al. (2013) because an optimization algorithm is used to consider the variance of the noise and the approach introduced in this work uses an optimization algorithm considering the standard deviation of noise measurements. In Svetozarevic et al. (2013), only four faults (f_3, f_4, f_7 and f_8) of the total set of ten faults were considered. The fault detection times for the considered faults were not provided in Svetozarevic et al. (2013), therefore the comparison with FDIF approach is not included in Table 4.10.

Table 4.10: Comparison of Fault Detection Results

Fault No.	t_D **required**	t_D **real**		
		IBAO	SVMO	SVMR
f_1	<10 T_s	3 T_s	NC	NC
f_2	<10 T_s	18 T_s	3 T_s	6 T_s
f_3	<10 T_s	3 T_s	22 T_s	1 T_s
f_4	<10 T_s	3 T_s	44 T_s	6 T_s
f_5	<10 T_s	3 T_s	11 T_s	2 T_s
f_6	<10 T_s	6 T_s	34 T_s	6 T_s
f_7	<8 T_s	375 T_s	-	2 T_s
f_8	<100 T_s	33 T_s	12 T_s	2 T_s
f_9	<3 T_s	3 T_s	35 T_s	3 T_s
f_{10}	<50 T_s	3 T_s	NC	36 T_s

In the Table 4.10, a comparison in terms of fault detection times and the benchmark specifications is carried out for the different approaches analyzed above, where NC means not considered. The approach proposed in the present work is denoted in this table as IBAO from Interval Based ARRs and Observers. It can be seen that the IBAO approach improves the detection times for the faults f_4 and f_{10}. Moreover, it is the only approach from the analyzed works which considers and detects fault f_1 within the time detection requirements. Fault f_1 corresponds to a fault in the blade root moment sensor. From this result, it can be concluded that the model proposed for the blade root moment dynamics used for fault detection provided a good performance. The IBAO approach proposed in this work can detect all the fault scenarios presented in the benchmark challenge (Odgaard and Johnson, 2013). It obtains a good detection performance in the majority of them except for the fault f_7 that corresponds to an abrupt change in the pitch actuator dynamics. This is due to the fact that the observer adapts very fast to the dynamics that is tracking and consequently a considerable period of time is needed to detect fault f_7.

4.3 FTC applied to Wind Turbine Low Speed Shaft Encoder

In recent years, individual pitch control has been developed for wind turbines, with the purpose of reducing blade and tower loads. Such algorithms depend on reliable sensor and the azimuth angle sensor, which positions the wind turbine rotor in its rotation, is quite important. This sensor has to be correct as blade pitch actions should be different at different azimuth angle as the wind speed varies within the rotor field due to different phenomena. A scheme detecting faults in this sensor has previously been designed for the application of a high end fault diagnosis and fault tolerant control of wind turbines benchmark model.

Here, the fault diagnosis scheme is improved and integrated with a fault accommodation scheme which enables and disables the individual pitch algorithm based on the fault detection. In this way, the blade and tower loads are not increased to due and individual pitch control algorithm operating with faulty azimuth angle inputs. The proposed approach is evaluated on a wind turbine benchmark model, which is based on the FAST aero-elastic code provided by NREL (Jonkman and Buhl, 2005).

The problem of fault tolerant control (FTC) and fault detection (FD) in wind turbines is still an open issue. A number of benchmark models have been developed to facilitate research in this problem, see Odgaard et al. (2013) and Odgaard and Johnson (2013), the later is based on FAST wind turbine simulator from NREL, USA. One of the faults in the second benchmark model is a fault in the azimuth angle sensor, which is the interest of this paper. An scheme detecting faults within this sensor has previously been designed (Odgaard et al., 2015b) and integrated on the previously mentioned benchmark model.

The fault diagnosis scheme proposed in Odgaard et al. (2015b) was extended and integrated with a fault accommodation scheme which enables and disables the individual pitch algorithm based on the fault detection, such that blade and tower loads are not increased to due and individual pitch control algorithm operating with faulty azimuth angle inputs.

4.3.1 Individual Pitch Control

The standard baseline industrial wind turbine controller operates in two modes:

- power optimization, in which the blades are kept at their optimal position, and the generator torque is set to keep the wind turbine at the optimal rotational speed, and

- constant power in which the generator torque is kept at its nominal value, and the blade are pitch to regulate the rotor speed at the nominal value, see Johnson et al. (2006).

The constant power mode, results in a collective pitch reference to all blade pitch actuators. The wind speeds in the rotor fields are non uniform, due to a number of reasons, like turbulence, wind shear, etc. Therefore, it is relevant to adjust the blade pitch angles to mitigate the structural loads induced by these differences in the rotor field to due to the different wind speeds.

The Individual Pitch Controller (IPC) is a scheme proposed to deal with this problem. It is based on computing a component on the pitch reference signals which are non collective, meaning that the each pitch actuator are feed with a pitch reference signals consisting of a sum of the collective pitch reference and the specific reference to the specific pitch actuator computed by the IPC scheme. A conceptual scheme can be seen in Fig. 4.6 The generator torque controller uses the generator speed and power ω_g and P as inputs, and determines a power reference as output, P_r. The collective pitch controller takes ω_g as input and gives the collective pitch reference β as output. The IPC scheme utilizes the three blade root bending moments τ_{b1}, τ_{b2} and τ_{b3} and the azimuth angle ϕ as inputs, it computes the IPC pitch references β_{b1}, β_{b2} and β_{b3} as output.

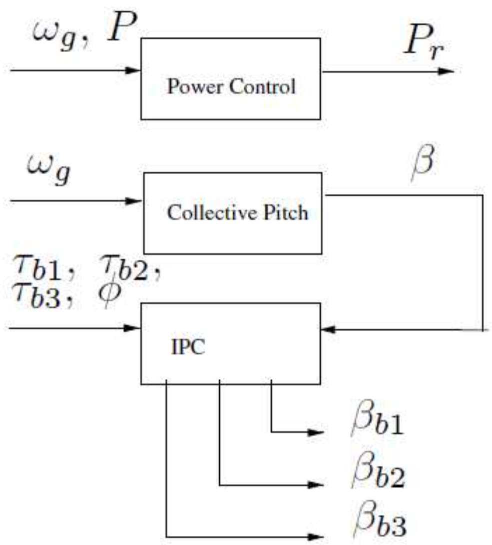

Figure 4.6: Conceptual representation of the IPC scheme.

The IPC scheme has developed for controlling loadings on the wind turbine structures. It can be developed for different oscillation modes of the wind turbine. Typically, it is designed for dealing with the so-called 1P frequency which corresponds to the rotational frequency of the wind turbine, and therefore it is not constant. It uses sensor inputs from the blade root bending moments. The control scheme uses Coleman transformation to transfer these moments from a 3 dimensional rotating coordinate system to a 2 dimensional fixed coordinate system describing the tower moments. In this dimension, PID controllers are used to control the moments such that the computed control signal are subsequently transferred back to the 3 blades. These computed control signals are added onto the collective pitch control signal which is computed for controlling the speed of the wind turbine, see Bossanyi (2003) and Bossanyi et al. (2013). The following description of the IPC scheme is based on these references. A block diagram of the IPC scheme is illustrated by Fig. 4.7.

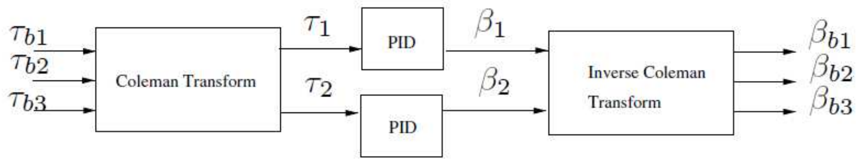

Figure 4.7: Illustration of the wind turbine control structure including the IPC scheme.

The used transformations are defined as given below. From $(\tau_{b1}, \tau_{b2}, \tau_{b3})$ to (τ_1, τ_2), denoted the Coleman transform.

$$\begin{bmatrix} \tau_1 \\ \tau_2 \end{bmatrix} = \frac{2}{3} \begin{bmatrix} \cos(\phi) & \cos(\phi + \frac{2\cdot\pi}{3}) & \cos(\phi + \frac{4\cdot\pi}{3}) \\ \sin(\phi) & \sin(\phi + \frac{2\cdot\pi}{3}) & \sin(\phi + \frac{4\cdot\pi}{3}) \end{bmatrix} \begin{bmatrix} \tau_{b1} \\ \tau_{b2} \\ \tau_{b3} \end{bmatrix}. \tag{4.35}$$

Two PID controllers are used to control the values of τ_1 and τ_2, the computed control signal from these controllers denoted as β_1 and β_2 are subsequently transferred back to the three pitch actuator control signals β_{b1}, β_{b2} and β_{b3}, using the following transformation, which is denoted as the inverse Coleman transformation.

$$\begin{bmatrix} \beta_{b1} \\ \beta_{b2} \\ \beta_{b3} \end{bmatrix} = \begin{bmatrix} \cos(\phi) & \sin(\phi) \\ \cos(\phi + \frac{2\cdot\pi}{3}) & \sin(\phi + \frac{2\cdot\pi}{3}) \\ \cos(\phi + \frac{4\cdot\pi}{3}) & \sin(\phi + \frac{4\cdot\pi}{3}) \end{bmatrix} \begin{bmatrix} \beta_1 \\ \beta_2 \end{bmatrix}. \tag{4.36}$$

The collective pitch reference computed in order to control the generator speed is added to the individual pitch control signals. (β_{b1}, β_{b2} and β_{b3}).

4.3.2 Application to Study Case

A model-based scheme for detecting faults in this sensor has previously been designed for the application of a high end fault diagnosis and fault tolerant control of wind turbines benchmark model, see Sanchez et al. (2015a). This fault diagnosis scheme is improved and integrated with a fault accommodation scheme which enables and disables the individual pitch algorithm based on the fault detection. Proceeding in this way, the blade and tower loads are not increased due to an individual pitch control algorithm operating with faulty azimuth angle inputs. The azimuth diagnosis scheme detects faults as bit errors in the binary signal from the encoder. This detection cannot directly be used for fault accommodation as the IPC scheme needs to be able to rely on the azimuth angle and not on/off values. The solution is to feed the detection signal to a new decision function which provides a persistent fault indication signal if a fault (e.g. bit error) has been detected in a window of length L, which in this case is equal one rotation of the rotor. This bit error is modeled by randomly adding an offset to the measurement that corresponds to the bit on which the error is present (Odgaard and Johnson, 2013). In case this decision function provides an active fault indication, the IPC schemes component to the pitch references are set to 0, as they are based on a faulty azimuth sensor signal.

The next step is to integrate the results of the fault diagnosis scheme shown in 4.14 with the proposed fault tolerant control scheme detailed below.

A function mapping from $\gamma(k)$ to $\alpha(k)$ is defined.

$$\alpha(k) = \begin{cases} 1 & \text{if } \sum_{i \in k-L \cdots k} \gamma(i) > 0, \\ 0 & \text{otherwise,} \end{cases} \tag{4.37}$$

where L is set equal to the number of samples found in the time signal of one rotor revolution, covering all errors on all bits.

In case $\alpha(k)$ is equal 1, the IPC pitch reference components are ignored. The new pitch references to each blade $\beta_1,\ \beta_2,\ \beta_3$ are given as

$$\beta_1(k) = \beta(k) + (1-\alpha) \cdot \beta_{b1}(k), \tag{4.38}$$

$$\beta_2(k) = \beta(k) + (1-\alpha) \cdot \beta_{b2}(k), \tag{4.39}$$

$$\beta_3(k) = \beta(k) + (1-\alpha) \cdot \beta_{b3}(k). \tag{4.40}$$

A general scheme showing the integration of the fault diagnosis and fault tolerance for IPC is presented in Fig. 4.8.

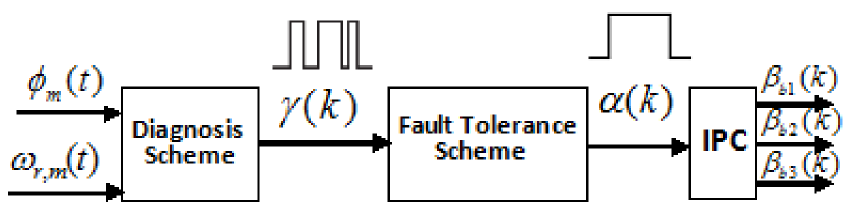

Figure 4.8: General Scheme of FD and FTC for IPC

4.3.3 Fault Tolerant Approach results

In this work an individual pitch controller tuning for the NREL 5 MW reference turbine has been used, see Dunne et al. (2012). In Figure 4.1 presents a block diagram of the wind turbine simulation model, provided with the benchmark, including the feedback loops corresponding to the pitch, yaw and torque variables.

According to Odgaard and Johnson (2013), the fault in the azimuth encoder consists of a bit error which is modeled by randomly adding an offset to the measurement that corresponds to the bit on which the error is present. This fault occurs in the time period from 295s to 320s.

In Fig. 4.9 it can be seen the detection signal resulting from the analytical redundant relation (4.14) and the function mapping defined in (4.37). It is observed that a persistent detection signal is obtained, this is useful for integrating the fault diagnosis scheme with the fault tolerant scheme because the new persistent detection signal is used to activate and deactivate the IPC components when the fault is present.

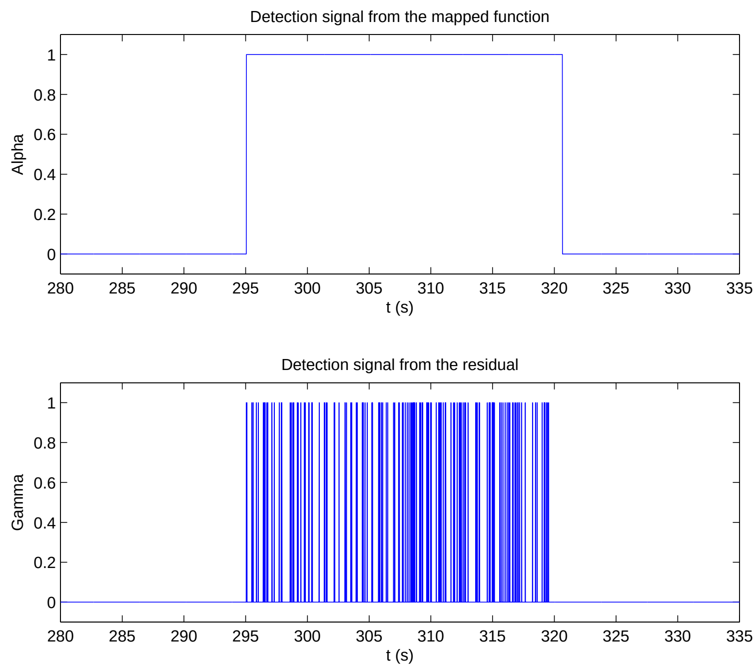

Figure 4.9: Detection signal obtained from the ARR and the mapping function

The Fault Tolerant scheme for IPC is shown in Fig. 4.10, it is observed how the IPC component for blade 1 is deactivated when the fault in the azimuth encoder is present. It is also shown that the tower loads are not increased when the fault is present as a result of the deactivation of the IPC component avoiding that IPC algorithm reads faulty azimuth angle values from the sensor.

4.4 Conclusions

In this chapter, a model based diagnosis approach using interval based ARRs (static and dynamic) and observers has been applied to an advanced wind turbine benchmark, in which a set of fault scenarios was defined. In most of the cases, the obtained ARRs proved to be able to detect the different fault scenarios of different types (scaling, offset and stuck) taken into account the uncertainty in the models parameters and the noise in the sensors proposed in the benchmark. The quality of the models used for fault detection is of primary importance. In case that theoretical models do not present a good approximation of the observed dynamics, an experimental model can be used if it is correctly estimated using data.

The fault isolation techniques based on column and row reasoning applied to the signature matrix obtained from the simulation tests, have shown that only some of the faults were completely isolable. The limitation of column reasoning is that in case that not all the residuals activate, no ex-

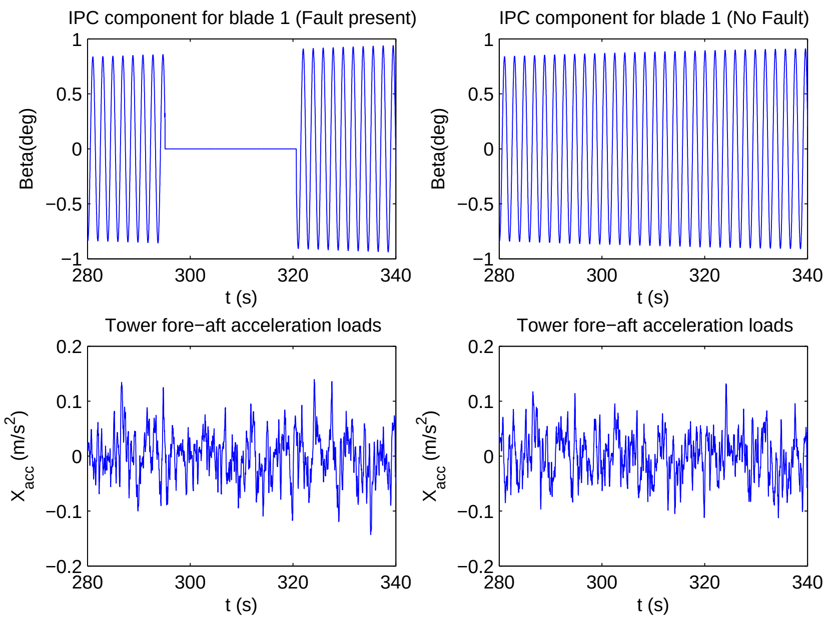

Figure 4.10: Fault Tolerant Control scheme for IPC and the tower loads when the scheme is activated and deactivated

act match with theoretical FSM is obtained and therefore the isolation is not very robust. Instead, the DX row based reasoning is more robust since it allows to isolate faults even though not all the theoretical residuals are activated.

Also a diagnosis and fault tolerant scheme for IPC of wind turbines has been proposed. The proposed scheme uses the azimuth angle sensor readings, to activate and deactivate the IPC component for the blades in the wind turbine control strategy. The schemes were tested on the FAST aero-elastic code provided by NREL where it was shown that the programmed fault tolerant scheme could achieve a persistent fault detection signal that is useful for the IPC control strategy. The correct detection signal read by the IPC scheme during the presence of the fault allowed the system to deactivate the IPC component during the fault avoiding wrong lectures from the faulty sensor signal and therefore achieving that loads such as the tower ones were not increased.

Chapter 5

Fatigue Estimation and Prognostics of Wind Turbines

The content of this chapter is based on the following works:

- Sanchez et al. (2016) Sanchez, H., Sankararaman, S., Escobet, T., Puig, V., Frost, S., and Goebel, K. (2016). Analysis of two modeling approaches for fatigue estimation and remaining useful life predictions of wind turbine blades. In *Third European Conference of the PHM Society - PHME16*, 451–461. Bilbao, Spain.

Wind turbine blades are components that are subject to highly irregular loading and extreme environmental conditions, especially those located offshore.

One of the aspects that are desirable from operators and original equipment manufacturers (OEMs) perspective is to have information about the damage and remaining useful life predictions provided by condition or health monitoring systems (Frost et al., 2013). Structural health information is necessary for the wind turbine to continue operating and producing power without exceeding some damage thresholds resulting in unscheduled downtime.

The challenge is thus to decide maintenance actions on components on the way to continuously reduce and eliminate costly unscheduled downtime and unexpected breakdowns, see Iung et al. (2008).

For offshore wind turbines, the higher operation and maintenance costs represent a larger overall proportion of the cost of energy than for onshore turbines, even when the large initial investment required for the installation of offshore turbines is included. One of the reasons that these costs are likely to be higher offshore is that the offshore environment will bring with it increased work loading which is relatively uncharacterized due to the lack of existing offshore installations (Myrent et al., 2013).

An understanding of the fatigue behavior of a wind turbine rotor blade is also valuable for the improvement of product development practices. Product development practice up to now has been based on an iterative process whereby a prototype rotor blade is built and tested against real, or realistic, loading patterns. However, this process is costly and time-consuming. The ability to simulate the fatigue behavior of the material, the blade structural component and/or the wind turbine rotor blade reduces the cost and allows the development of a wider range of products without the need for increasing the number of physical prototypes (Vassilopoulos, 2013).

In this work, fatigue in the blade root is analyzed. This component has been identified as a critical area for fatigue in several works such as Sutherland (1999) which shows, that the edgewise blade root bending moment frequency distribution from a small turbine contains two peaks; one originating from the wind loading, the other a result of the blade being loaded by its own weight. Caprile et al. (1995) present histograms of mid-size wind turbine blade edgewise and flapwise blade root moments, showing the same peak for the edgewise loading. For larger rotor blades, the edgewise gravity fatigue loading becomes increasingly relevant for life prediction. Kensche and Seifert (1990) gives typical root bending moments from measurements on wind turbine blades, both the flap and edgewise direction. Several methods for fatigue estimation in wind turbines have been analyzed in Barradas-Berglind and Wisniewski (2016) where the methods are classified into four general groups: cycle counting, spectral, stochastic and hysteresis.

Experimental evidence (Nijssen, 2006) has shown that typical composite materials used in wind turbine rotor blades exhibit strength degradation trends. The degradation of those materials in fatigue conditions has been thoroughly studied in Vassilopoulos and Nijssen (2010).

Different methods have been proposed to the degradation of composite materials used in the wind turbine blades. Some of them are based on phenomenological life predictions while others consider the actual mechanical damage modeling. In this work, one phenomenological method and one fatigue damage model are analyzed for wind turbine blades life predictions, these are the rainflow counting and a fatigue stiffness degradation model respectively. Both methods are tested in a high fidelity wind turbine simulator.

5.1 Fatigue Estimation Background for Wind Turbine Blades

This section provides a brief theory background for both of the analyzed techniques. The first subsection explains the rainflow counting method and the second subsection explains the stiffness degradation theories from which is proposed the fatigue damage model used in this work to study the stiffness degradation of the blade.

5.1.1 Rainflow Counting Method

Fatigue is the damage accumulation process on a component produced by cyclic loading. Exposing a material to cyclic loading of constant amplitude will cause fatigue failure after a certain number of cycles. In reality amplitudes of cyclic loading are rarely constant. Most components are exposed to random load fluctuations. A common method to quantify the fatigue impact of fluctuating loads is the combination of a rainflow counting algorithm and a damage equivalent load approach, enabling the relative comparison of different load samples (Martinen et al., 2014).

Rainflow counting (RFC) method, first introduced by Endo et al. (1967), has a complex sequential and nonlinear structure in order to decompose arbitrary sequences of loads into cycles. The rainflow cycle distributions (often simply called cycle distributions or rainflow spectra) represent the occurrence probability of load cycles with different ranges. Usually, to compute a lifetime estimate from a given stress input signal, the RFC method is applied by counting cycles and maxima, jointly with the Palmgren-Miner rule to calculate the expected damage. The input signal is obtained from time history of the loading parameter of interest, such as force, torque, stress, strain, acceleration, or deflection Lee et al. (2005). The Fig. 5.1 depicts the described procedure.

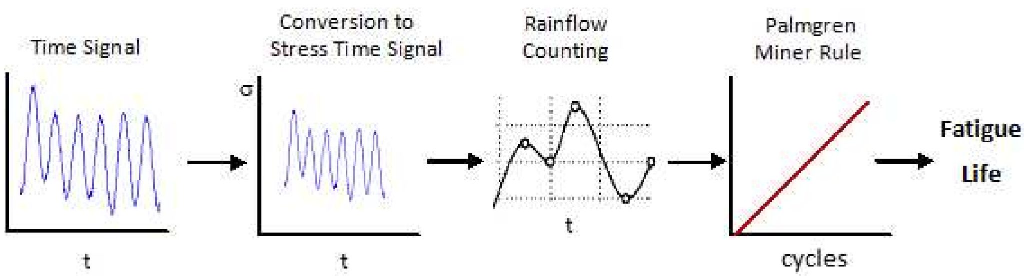

Figure 5.1: Rainflow counting damage estimation procedure

Different types of RFC algorithms have been proposed in the literature (Downing and Socie, 1982; Rychlik, 1987). The algorithm used in this paper is introduced in Niesłony (2009), and is implemented as a Matlab code. A previous applications of this code to integrate fatigue estimation with model predictive control has been performed in Sanchez et al. (2015b). This algorithm calculates the stress for each rainflow cycle in four steps:

- the stress history is converted to an extremum sequence of alternating maxima and minima;
- for each local maximum M_j, the left and right region where all stress values are below M_j is identified, denoted respectively as m_j^- and m_j^+;
- the minimum stress value is computed as:
  $m_j = min\{m_j^-, m_j^+\}$;
- the equivalent stress per rainflow cycle s_j associated with M_j is given by the amplitude $s_j = M_j - m_j$ or the mean value $s_j = \frac{M_j+m_j}{2}$.

The damage, D, at each stress cycle is computed using S-N curve Hammerum et al. (2007). The S-N curve is a graphical representation of the stress, s, versus the number of stress cycles, N. An often-used model for the S-N curve is

$$s^{cw} N = K, \tag{5.1}$$

where the quantities K and c_W are material properties, being c_W the Wöhler-coefficient. The damage imposed by a stress cycle with a range s_j is computed as

$$D_j \equiv \frac{1}{N_j} = \frac{1}{K} s_j^{c_W}. \tag{5.2}$$

The linear damage accumulation after N cycles can be computed using the Palmgren-Miner's damage rule, given by

$$D_{ac} = \sum_{j=1}^{N} \frac{1}{K} s_j^{c_W}. \tag{5.3}$$

The algorithm steps are illustrated with an example shown in Figure 5.2. On the top left of Figure 5.2 the time signal of the input stress is shown. Then the signal is converted into a sequence of maxima and minima (turning points) shown in the top right. In the bottom left part it is shown the calculated damage for each rainflow cycle individually. Finally, the accumulated damage is shown on bottom right part.

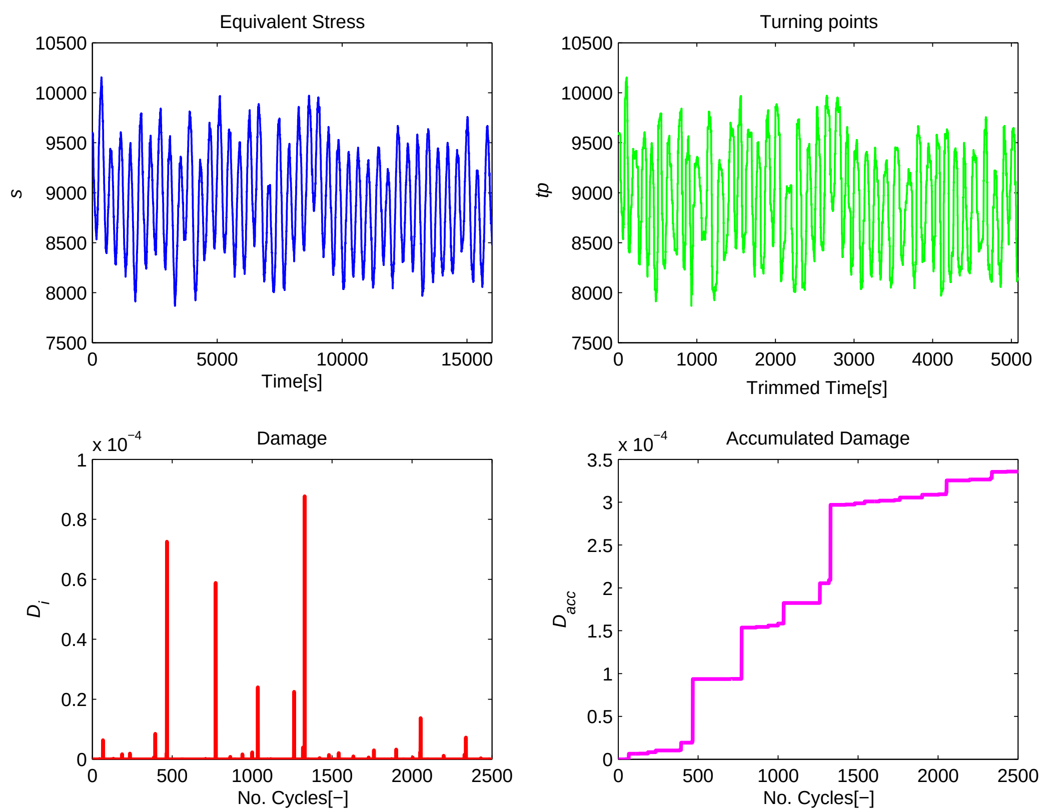

Figure 5.2: Example of the application of rainflow counting procedure on blade root moment stress signal

A common criterion accepted to determine failure when using Palmgren-Miners rule is when the cumulative damage expressed in the equation 5.3 reaches the value $D_{ac} = 1$.

In previous works has been explored how to calculate life predictions using the rainflow counting method, see Baek et al. (2008). The way to calculate life for a repeated stress signal implemented in this work is be given by:

$$Life = N_f \left(1 - \sum_{j=1}^{N} \frac{1}{K} s_j^{c_W} \right), \tag{5.4}$$

where N_f is the lifetime in cycles. The approach presented in equation to calculate the life in cycles is valid only when a constant load is applied and the accumulated damage expressed in equation (5.3) is in the range of [0,1].

5.1.2 Stiffness Degradation Fatigue Theories

As explained in Vassilopoulos (2013) strength and stiffness degradation fatigue theories have been introduced in order to model and predict the fatigue life of composite materials by taking into account the actual damage state, expressed by a representative damage metric of the material status. The damage metric is usually the residual strength or the residual stiffness. Failure occurs when one of these metrics decreases to such an extent that a certain limit is reached (Brondsted and Nijssen, 2013). Stiffness degradation theories are not linked to the macroscopic failure (rupture) of the examined material but rather to the prediction of its behavior in terms of stiffness degradation. Failure can be determined in various ways, e.g. when a predetermined critical stiffness degradation level is reached; or when stiffness degrades to a minimum stiffness designated by the design process in order to meet operational requirements for deformations; or even as a measure of the actual cyclic strains, e.g. failure occurs when the cyclic strain reaches the maximum static strain (Zhang et al., 2008). Methods that are able to assess the development of the remaining stiffness degradation of a material or a structural component during fatigue life are valuable for damage tolerant design considerations. In situations like this, the effect of local failure and the stiffness degradation caused by the failure must be investigated to ensure structural integrity under the given (acceptable) damage. Life prediction schemes for composite laminates have been developed based on these concepts (Eliopoulos and Philippidis, 2011). In addition, this effective medium description requires the gradual strength and stiffness degradation assessment due to cyclic loading. It is obvious that important experimental effort is necessary for the parameter estimation of such a hybrid (strength and stiffness degradation) modeling process.

According to Van Paepegem and Degrieck (2002), it is commonly accepted that for the vast majority of fibre-reinforced composite materials, the modulus decay can be divided into three stages: initial decrease, approximately linear reduction and final failure (see Figure 5.3), where E_0 is the undamaged stiffness, E is the stiffness at a certain moment in fatigue life, N is the number of testing cycles and N_f is the fatigue life in cycles.

In the work of Schulte (1984) three distinctive stages are distinguished:

- The initial region (stage I) with a rapid stiffness reduction of 2-5%. The development of transverse matrix cracks dominates the stiffness reduction ascertained in this first stage.
- An intermediate region (stage II), in which an additional 1-5% stiffness reduction occurs in an approximately linear fashion with respect to the number of cycles. Predominant damage mechanisms are the development of the edge delaminations and additional longitudinal cracks along the fibres.
- A final region (stage III), in which stiffness reduction occurs in abrupt steps ending in specimen fracture. In stage III, a transfer to local damage progression occurs, when the first initial fibre fractures lead to strand failures.

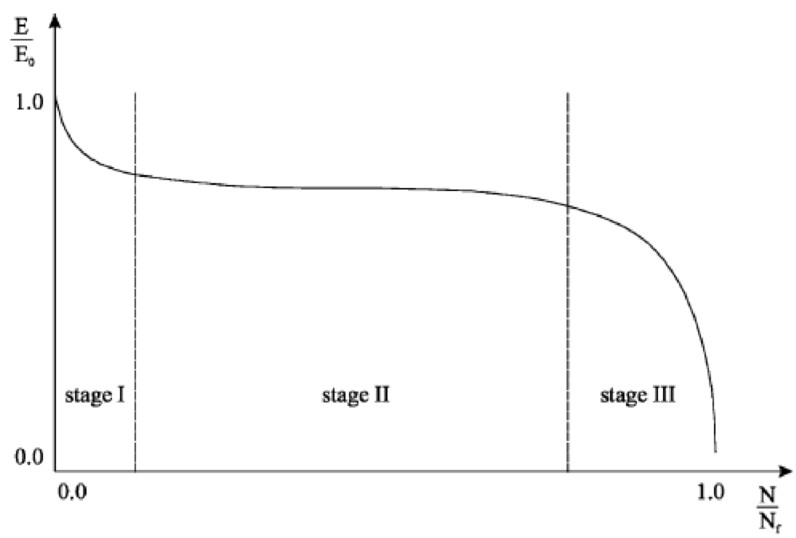

Figure 5.3: Typical stiffness degradation curve for a wide range of fibre-reinforced materials

5.2 Application to Wind Turbine Blade Prognostics

This section analyzes the application of the rainflow counting algorithm and the fatigue stiffness degradation model for fatigue estimation and remaining useful life prediction of a wind turbine blade. Figure 5.4 shows the process of applying the rainflow counting algorithm and the fatigue stiffness degradation model to estimate fatigue and calculate remaining useful life predictions for the wind turbine blade using the blade root moment sensor information from the high fidelity wind turbine simulator FAST (Fatigue, Aerodynamics, Structures and Turbulence), (Jonkman and Buhl, 2005).

To analyze the two approaches three different blade root moment bending loads are obtained from the wind turbine simulator working on three different constant wind speeds of 14, 16 and

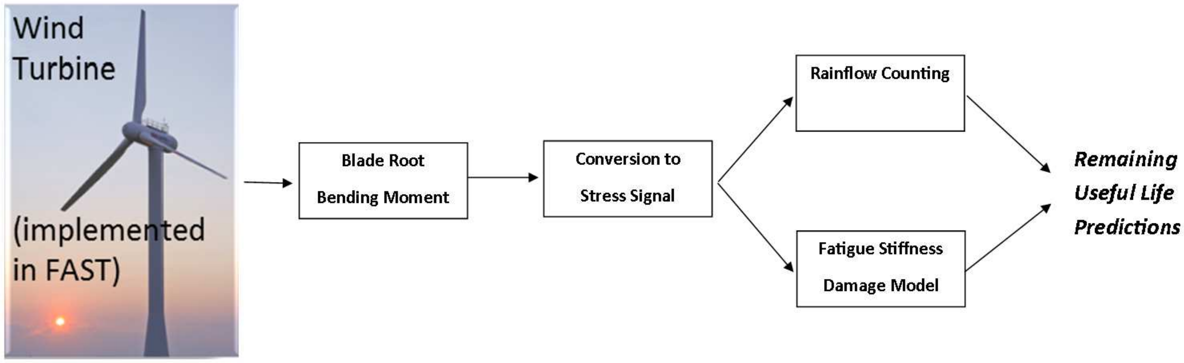

Figure 5.4: Scheme of the application of the analyzed approaches for wind turbine blade remaining useful life predictions

18 m/s. Figure 5.5 presents three different blade root moment (BRM) bending loads (obtained from FAST simulator) corresponding to the different wind speeds. The blade root moment signals present a sinusoidal wave due to the cyclic behavior of wind turbines and with different mean values because of the different wind speeds considered. These loads are converted in stresses dividing by the appropriate section modulus in order to be used as inputs for the rainflow counting algorithm and the fatigue degradation damage model.

5.2.1 Life prediction approach based on rainflow counting algorithm

For real-time applications, applying the traditional rainflow counting algorithm is very challenging and computationally heavy. Significant amounts of data must be stored and processed periodically to obtain a magnitude of the data in equivalent regular cycles. In addition, the algorithm must be applied to a stored set of data.

Loads in wind turbine structure arise from several factors (Jelavic et al., 2008), being the main cause the spatial variations of wind speed caused by the turbulent nature of wind.

The paper of Jelavic et al. (2008) concludes that the most pronounced contribution to the blade root loading happens at the frequency given by the blades speed, and this loading is the main source of fatigue at the blades.

Using the RFC method the accumulated damage is obtained as a function of the cycles of the blade root moment stress signal. In case that the input signal is expressed as bending moments it is necessary to convert the fatigue load to fatigue stress dividing by the appropriate section modulus (Burton et al., 2011). Some previous works such as Burton et al. (2011) and Vassilopoulos (2013) for wind turbine blade fatigue assessment and life prediction that describe the rainflow counting algorithm have been reviewed. A number of subproblems must be solved sequentially in order to produce the final result, the steps applied in this work are the following:

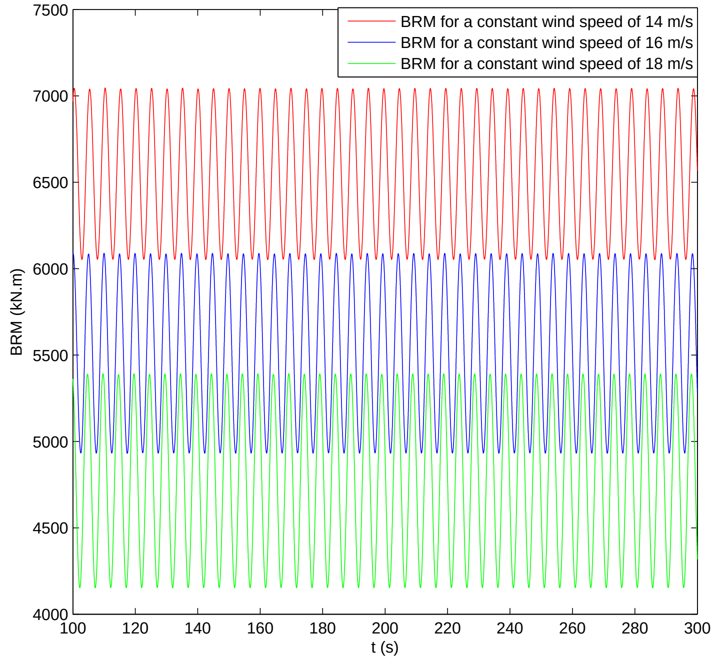

Figure 5.5: Blade root moment bending loads obtained in FAST for constant wind speeds of 14, 16 and 18 m/s

1. Derive the individual fatigue load spectra for each mean wind speed and for each radius. In this work, the wind and load information is obtained from the wind turbine FAST simulator.

2. Synthesize the complete fatigue load spectrum at each radius from the separate load spectra for each mean wind speed.

3. Convert the fatigue load cycles (expressed as bending moments) to fatigue stresses by dividing by the appropriate section modulus. The section modulus with respect to a particular principal axis is defined as Second Moment of Area of the cross-section about that axis divided by the distance of the point under consideration from the axis. The blade root bending moments are divided by the section corresponding to a wind turbine blade root.

4. Find an appropriate S-N curve for the material considered.

5. Cycle counting. This is done by applying rainflow counting algorithm.

6. Adoption of the fatigue failure criterion.

7. Calculate the cumulative damage according to Miners rule and obtain the fatigue life prediction. In section 5.3.2, is explained the damage assessment and assumptions that result in a prediction in the scope of this work.

5.2.2 Prognostics approach based on fatigue stiffness degradation model

This section analyzes a fatigue stiffness damage model application based on the model proposed by Van Paepegem and Degrieck (2002). In order to apply this model, it is assumed that the blade is a solid beam. This assumption simplifies the application of the stiffness damage model which is derived for a specific material fiberglass which is commonly used in wind turbine blades. The blade root bending moment sensor information from the high fidelity simulator as the input load which translates in compressive stress. The damage model is used to obtain remaining useful life predictions subject to different wind speed scenarios generated by the wind turbine high fidelity simulator FAST.

The model proposed in Van Paepegem and Degrieck (2002) defines the model as the sum of an initiation function and a propagation function based on theoretical considerations and a sound modeling of the observed fatigue damage mechanisms, it proposes models for the tensile and the compressive stresses. The model used in this work is the one proposed for the compressive stresses since the damage loads considered for this study are the ones that come from the flapwise bending moments at the blade root. Therefore, choosing the flapwise bending moments as the considered damage loads involves the use of the model for compressive stresses. This model has been tested for bending fatigue experiments in Van Paepegem and Degrieck (2002). The impact of control contingency strategies for reducing flapwise blade root moment damage loads have been previously studied in the work of Frost et al. (2013), which makes these type of loads interesting for future research work in damage reduction and the increase of remaining useful life of wind turbine blades. The damage initiation function f_i simulates the sharp decline of the stiffness in the first stage of fatigue life. Matrix cracking is the predominant mechanism in this stage and according to Van Paepegem and Degrieck (2002). The damage propagation function f_p is a function that describes the second and third stage of damage propagation and final failure, respectively.

The damage initiation function f_i is defined as

$$f_i\left(\sigma, D\right) = \left[c_1 \sum\ \left(\sigma, D\right)\ \exp\left(-c_2 \frac{D}{\sqrt{\sum\ \left(\sigma, D\right)}}\right)\right]^3, \tag{5.5}$$

and the damage propagation function f_p is defined as

$$f_p\left(\sigma, D\right) = c_3\, D\, \Sigma(\sigma, D)^2 \left[1 + \exp\left(\frac{c_5}{3}\left(\Sigma\left(\sigma, D\right) - c_4\right)\right)\right], \tag{5.6}$$

where $\sum(\sigma, D)$ is the failure index which is a function of the damage variable D defined as a measure for the stiffness reduction in the considered material element due to matrix cracks and σ is the stress measure.

The fatigue failure index for the purposes of this work is given by

$$\sum\left(\sigma, D\right) = \frac{\sigma}{(1-D)X_C}. \tag{5.7}$$

Practical implementations of equations 5.5 and 5.6, requires to make a distinction on the level of the damage growth rate equation dD/dN, because the damage increment is calculated after each cycle and this damage increment is extrapolated to the next simulated cycle. The final layout of the fatigue damage model states as follows

$$\frac{dD}{dN} = \left[c_1 \Sigma \exp\left(-c_2 \frac{D}{\sqrt{\Sigma}}\right)\right]^3 + c_3 D \Sigma^2 \left[1 + \exp\left(\frac{c_5}{3}\left(\Sigma - c_4\right)\right)\right], \tag{5.8}$$

where the damage variable, X_C is the ultimate compressive static strength, the constant c_1 determines the amplitude of the damage initiation rate, while the exponential function is a decreasing function of damage D. Constant c_2 together with c_1 are used to model the first stage decrease of the stiffness. Once a certain damage value has been reached, the contribution of the damage initiation function becomes negligible. c_3 is the damage propagation rate, c_4 is a sort of threshold below which no fibre initiates and c_5 is a model parameter used to keep the exponential function strongly negative as long as failure index $\sum(\sigma, D)$ remains below the threshold c_4, but switches to a large positive value once the threshold has been crossed. In Van Paepegem and Degrieck (2002) the model is tested for different values of the damage propagation rate c_3, which shows that final failure occurs much earlier if this parameter is increased. In the case of the simulations shown in this chapter, the value for the parameter was chosen as $c_3 = 4 \times 10^{-4}$ (1/cycle).

Table 5.1: Material and model parameters

Material parameters	Model parameters
$X_c = 341.5 \quad (\mathrm{MPa})$	$c_1 = 0.002 \quad (1/\mathrm{cycle})$
	$c_2 = 30 \quad (-)$
	$c_3 = 4 \times 10^{-4} \quad (1/\mathrm{cycle})$
	$c_4 = 0.85 \quad (-)$
	$c_5 = 93 \quad (-)$

5.2.3 Damage prognostics

For predicting remaining useful life (RUL) of a composite structure such as a wind turbine blade, we are interested in predicting the time when the damage grows beyond a predefined acceptable threshold (Saxena et al., 2010). The time or cycle at which it occurs is known as the expected end of life (EOL).

The wind turbine is expected to continue operating and producing power without exceeding the end of life (EOL) threshold for the blade given by the accumulated stiffness fatigue damage $D = 0.8$ provided by equation 5.8, which is set as the maximum stiffness reduction allowed for the purpose of this work.

Once the (EOL) threshold is determined, the remaining useful life can be readily obtained as $RUL_n = EOL - n$, where n stands for the current time or cycle.

A simplified algorithmic description for the RUL prediction is provided below.

1. The stiffness damage at the current cycle and the future loads are required.

2. Calculate damage for the next cycle provided by equation (5.8).

3. Increase the number of cycles to failure.

4. If the current damage is less than EOL repeat steps 2-4.

5. If the current damage is greater than EOL the RUL is equal to the number of cycles to failure accumulated.

5.3 Application to Case Study

In this section, both methods are tested to estimate fatigue damage accumulation and calculate remaining useful life predictions using the blade root bending loads given by the wind turbine simulator FAST, in three different constant wind speeds scenarios. In section 5.3.1 is simulated the damage progression with the fatigue stiffness degradation model which is later embedded into a prognostics algorithm to calculate remaining useful life predictions. Section 5.3.2 tests the rainflow counting method with the same blade root moment loads used in the stiffness degradation model, the cumulative damage for the three wind scenarios is obtained as well.

5.3.1 Fatigue stiffness degradation model

Figure 5.6 shows the damage progression for different wind speeds using the stiffness degradation damage model of equation 5.8. The parameters used for simulation are the ones shown in Table 5.1.

From Figures 5.7-5.9, it can be observed the curves for remaining useful life predictions for the wind turbine blade on three different wind scenarios of constant wind speeds of 14, 16 and 18 m/s. The remaining useful life predictions shown are the mean value of 500 samples and the value $\alpha = 0.9$.

The results show that the damage progression is faster for lower wind speeds, resulting in the reach of the end of life threshold earlier as it can be seen in the Figure 5.6. This is due to the fact that wind turbine is operating in control region 3. In region 3, the wind turbine rotational speed is maintained constant at the rated speed by pitching the turbine blades (Frost et al., 2013). In lower wind speeds the angle of attack of the blades against the wind is higher and that translates into higher flapwise blade root bending loads. When the wind speed is higher the angle of attack of the blades needs to be lower to maintain the wind turbine rotating at the rated speed, therefore the flapwise damage loads are lower. When the flapwise damage loads are lower at the blade root (i.e. lower stress input to the stiffness degradation model) and consequently in Figures 5.7-5.9 it is observed that the RUL predictions for lower wind speeds in control region 3 are shorter while the RUL predictions for higher wind speeds are higher.

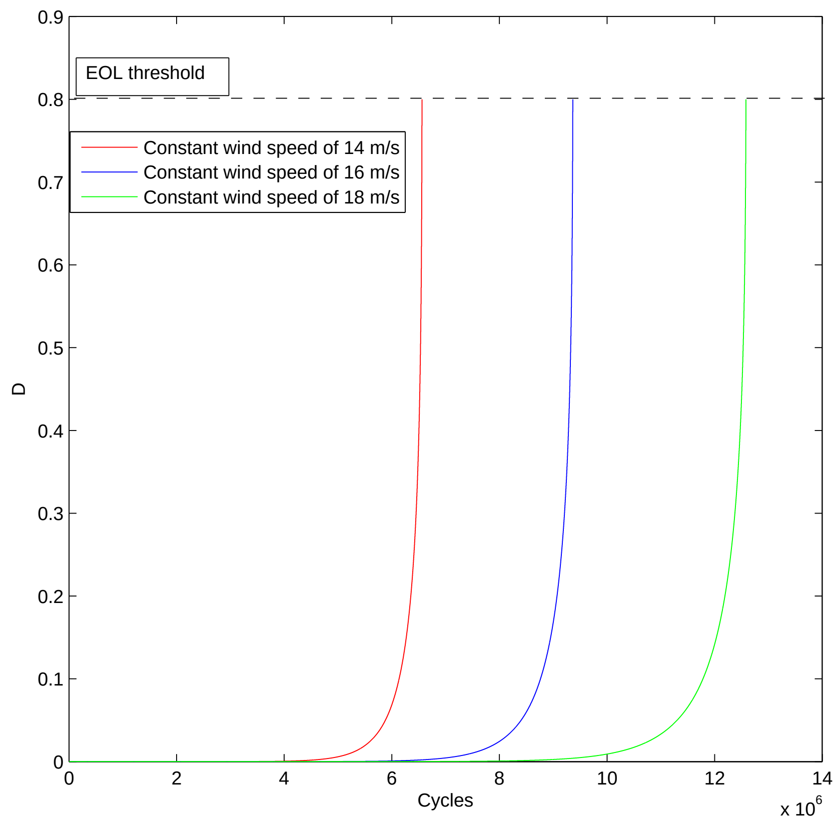

Figure 5.6: Damage progression in the stiffness degradation model for different loads due to three different wind speed scenarios

5.3.2 Rainflow counting algorithm

In the Figure 5.10, it is shown the cumulative damage obtained applying the rainflow counting algorithm for the case of three different loads due to three different wind speeds scenarios of 14, 16 and 18 m/s. The parameters used in this work are $c_w = 10$ which is a common value for glass fibre composite materials Burton et al. (2011). Wind turbine rotor blades will probably be required to sustain 10^9 fatigue cycles during the 25 years of their expected operational life (Vassilopoulos, 2013) which translates in $N = 10^9$, assuming $K = 7.0173 \times 10^{76}$, see eq. 5.1.1.

Figure 5.10 shows that the slope of damage is higher for lower winds which have a higher mean stress values, this translates into a faster damage accumulation, i.e. a shorter life of the blade. It is assumed that future wind speed will remain constant for the purpose of the rainflow counting application in this work. The results are presented in Table 5.2, showing the calculated life predictions for each wind scenario.

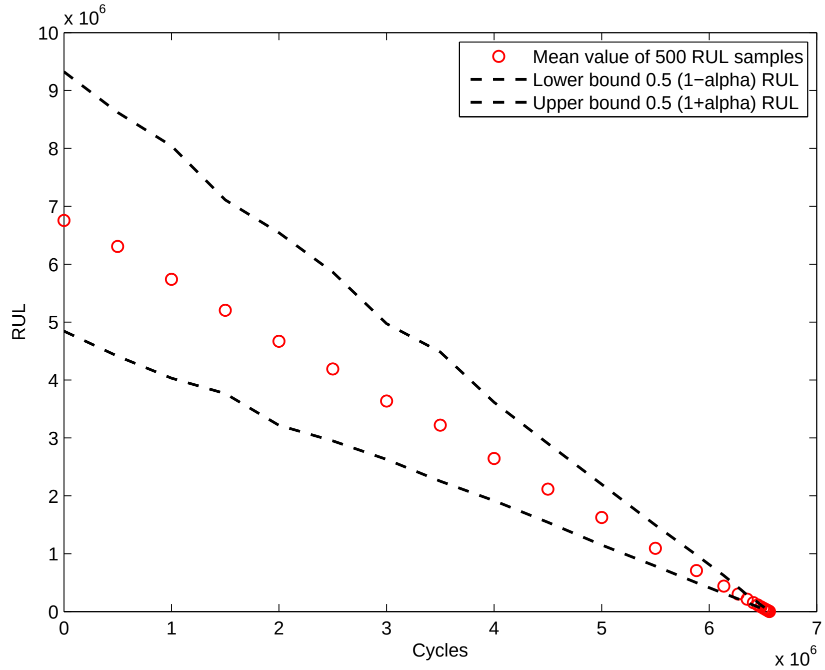

Figure 5.7: Remaining useful life predictions for different cycles on a wind speed of 14 m/s

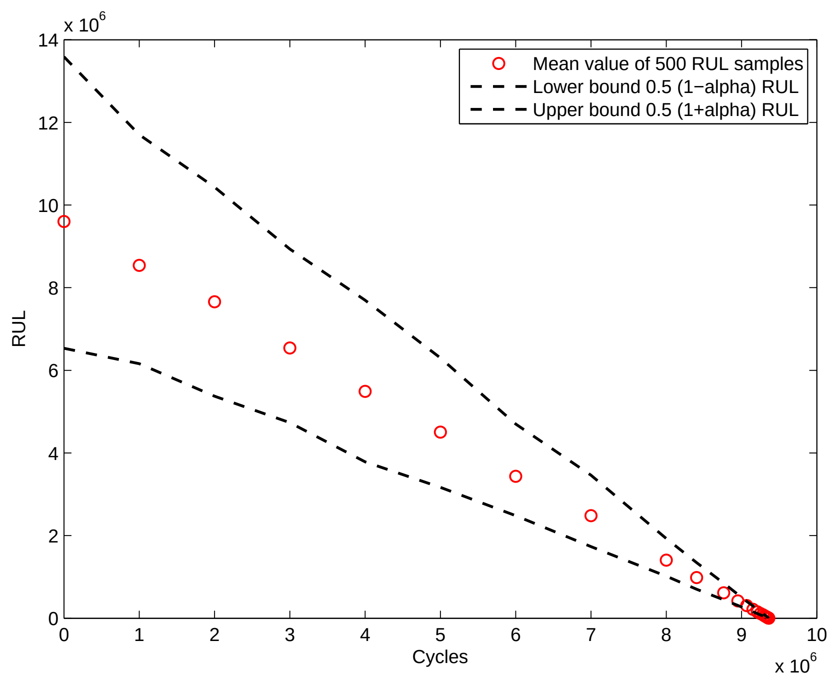

Figure 5.8: Remaining useful life predictions for different cycles on a wind speed of 16 m/s

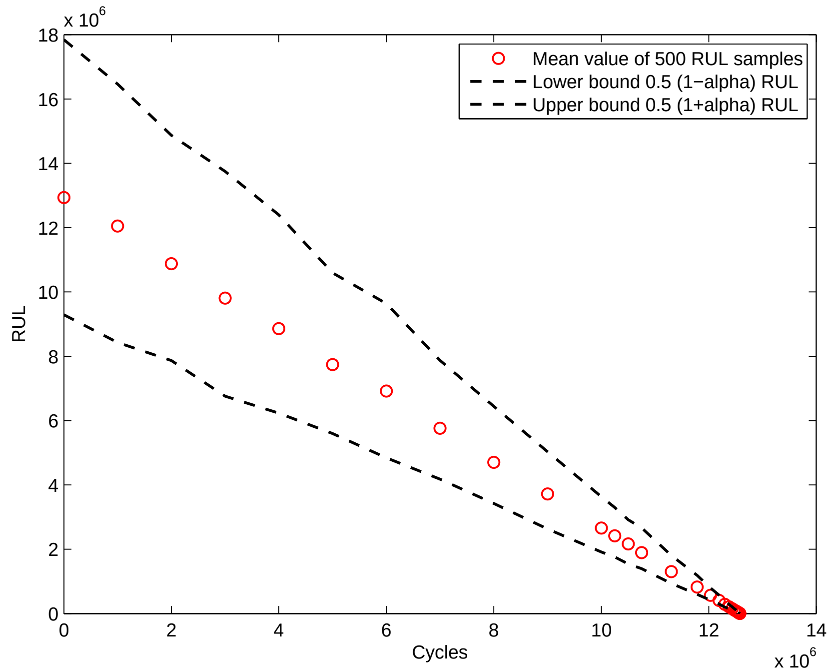

Figure 5.9: Remaining useful life predictions for different cycles on a wind speed of 18 m/s

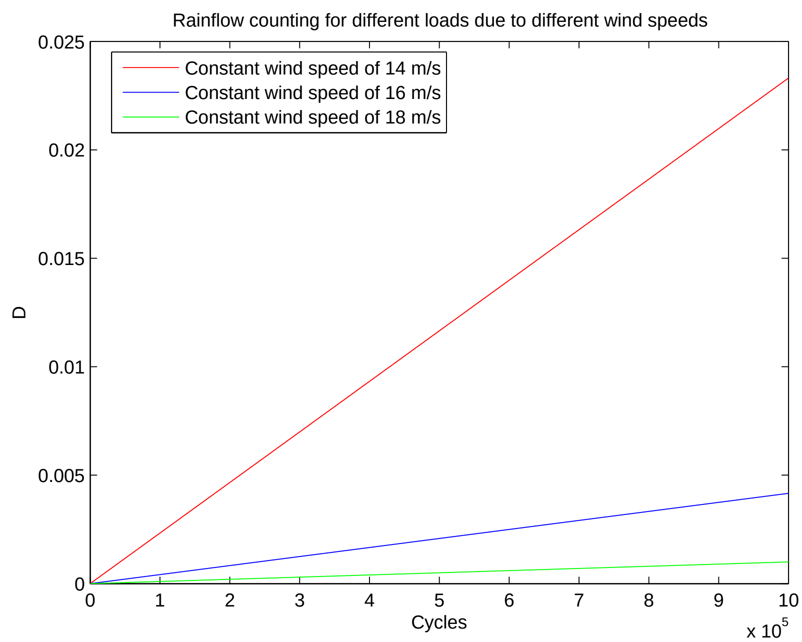

Figure 5.10: Cumulative Damage obtained with rainflow counting algorithm for different loads due to three different wind speed scenarios

Table 5.2: Results of life predictions using the rainflow counting method

Wind speed (m/s)	Life prediction (cycles)
14	9.77×10^8
16	9.96×10^8
18	9.99×10^8

5.3.3 Comparison of the approaches

There is extensive research that has been performed analyzing rainflow counting algorithm and the stiffness degradation models (see Nijssen (2006); Vassilopoulos and Nijssen (2010); Vassilopoulos (2013)).

In this section, a brief summary collected from the mentioned literature for both of the approaches analyzed in this work is provided based on the input information that they require, the output information we get from them and the advantages and disadvantages that each one presents.

Advantages and Disadvantages of Rainflow Counting Method

The main advantage of rainflow counting method is that the estimation of the model parameters is based on linear regression analysis that can be performed by simple hand calculations.

The rainflow counting method presents the following disadvantages:

- Needs experimental data for the specific material in order to have an S-N curve for the specific material.
- Different model parameters should be determined for different loading conditions.
- Do not take into account any of the failure mechanisms that develop during the failure process.
- As an empirical method, its predictive ability is strongly affected by the selection of a number of parameters that must be estimated or even, in some cases, assumed.
- The linear behavior observed in cumulative damage methods based on Miner's rule such as the rainflow counting is not an accurate representation fit to the behavior observed in realistic scenarios.

Advantages and Disadvantages of the Fatigue Stiffness Degradation Model

Among the advantages of fatigue stiffness degradation model can be mentioned the following:

- The ability to quantify the stiffness reduction at any point during realistic loading applied to the structure constitutes the major advantage of stiffness degradation methods for life prediction.
- Modeling the loss of stiffness of a material after cyclic loading can be a powerful tool in the development of life prediction schemes, especially when dealing with variable amplitude

or spectrum loading, since it offers a meaningful physical alternative to empirical damage accumulation rules such as the Palmgren-Miner rule.

- The remaining useful life can be assessed by nondestructive evaluation since the stiffness degradation theories are based on a damage metric that does not need the failure of the material in order to derive it.

- Stiffness degradation exhibits greater changes during the entire fatigue life.

One of the disadvantages of stiffness degradation models is the important experimental effort that is necessary for the parameter estimation of the fatigue damage model.

In Table 5.3 is summarized the input and output information for both of the approaches analyzed in this work.

Table 5.3: Input-output information for Rainflow Counting Algorithm and the Fatigue Stiffness Degradation Model

Approach	**Input Information**	**Output Information**
Rainflow Counting	-Numbers of cycles to failure on current load condition. -Strain or stress measure for each cycle.	Calculated damage for each load cycle.
Stiffness Degradation Model	- Current state of stiffness damage. -Stress measure for the current cycle.	Stiffness damage increment for the current cycle and this damage increment is extrapolated to the next simulated cycle.

5.4 Conclusions

Two approaches for fatigue estimation and remaining useful life predictions for wind turbine blades were analyzed and tested in this paper. The advantages and disadvantages of both methods were investigated and both methods were tested using a blade root moment bending signal given by a high fidelity wind turbine simulator.

The damage definition used in the two methods is different. In the fatigue stiffness damage model, the damage is defined as the stiffness reduction in the material due to cyclic loading while the damage in the case of the rainflow counting algorithm it is not explicitly related to a physical characteristic of the material or the considered structure. Therefore, the numerical results obtained for each one of the methods cannot be directly compared or analyzed. However both of the approaches demonstrated that the higher is the mean stress value due to wind speed, the damage accumulation occurs faster which translates in shorter life and RUL predictions for the wind turbine blade.

As a future work, other methods such the ones proposed by Bendat (1964) or Dirlik (1985) could also be considered for comparison. Moreover, the results of the analysis and tests done in this work can be used to assess the design of a wind turbine controller that can be capable of adapting the damage and remaining useful life predictions provided by the models in order to enable a damaged turbine to operate in a reduced capacity and optimize the trade-off between the remaining useful life predictions of a wind turbine blade and energy production demands.

Chapter 6

Health Aware Model Predictive Control

The content of this chapter is based on the following works:

- Sanchez et al. (2017) Sanchez, H., Escobet, T., Puig, V., and Odgaard, P. (2017). Health-aware model predictive control of wind turbines using fatigue prognosis. *Int J Adapt Control Signal Process.* URL `https://doi.org/10.1002/acs.2784`.

- Sanchez et al. (2015b) Sanchez, H., Escobet, T., Puig, V., and Odgaard, P. (2015b). Health-aware model predictive control of wind turbines using fatigue prognosis. In *9th IFAC Safe-process*, 1363–1368. Paris, France.

This chapter describes the proposed approach named health-aware model predictive control (HAMPC) which integrates the approaches to calculate fatigue and remaining useful life (RUL) predictions of the blade explained in chapter 5 with the proposed HAMPC. Considering the trade-off between power production and reduction of damage or extension of the RUL for the analyzed component, the blade.

The main contribution relies on the development of HAC approach based on MPC with application to wind turbines. This approach integrates fatigue-based prognostics with the aim of minimizing the damage of wind turbine components (the blades) while still maximizing the extracted wind power from the wind. The integration of a system health management module with MPC control is done by developing a fatigue-based model using the rain-flow counting approach and adding an extra criterion in the control objective function that takes into account the accumulated damage. This provides the wind turbine a mechanism to operate safely and optimize the trade-off between components life and energy production. The proposed approach is implemented and tested using a high fidelity simulator of a utility-scale wind turbine called FAST.

The main objective of operational control of wind turbines is to maximize the extracted wind power from the wind. However, wind turbines components are subject to considerable fatigue due to extreme environmental conditions to which are exposed, especially those located offshore. For this reason, interest in the integration of control with the fatigue-based prognostics of components has increased in recent years, as described in Section 2.4.

The research presented in this chapters contributes to a new control paradigm, named "*health-aware control*" (HAC) that considers the information about the system health to adapt the objectives of the control law to extend the system remaining useful life (RUL) (Escobet et al., 2012). In this way, the control actions are generated to fulfill the control objectives/constraints but at the same time to extend the life of the system components. So, HAC tries to achieve maximum performance while not degrading the system so much. In case that the controller is implemented using MPC, the trade-off is based on modifying the control objective function including new terms that take care of the system health. This leads to solve a multi-objective optimization problem where a trade-off between system health and performance should be established (Bento-Pereira et al., 2010). The health-aware control has been investigated for an application to a subsea gas compression system, where information of the compressor degradation has been included in the MPC control (Verheyleweghen and Jäschke, 2016). Controllers designed with standard procedures aim to maximize performance without caring about whether the resulting action will deteriorate very fast the system life (Bento-Pereira et al., 2010).

6.1 Model Predictive Control

6.1.1 Standard MPC

MPC uses a mathematical model to calculate the optimal control actions according to a given cost function (Maciejowski, 2002). In this Thesis, it is assumed that the system behavior can be described at each time instant $k \in \mathbb{Z}$ by the discrete-time model (3.97).

It is also considered that the system is subject to state and input constraints, which can be posed as

$$x(k) \in \mathbb{X} \triangleq \{x(k) \in \mathbb{R}^{n_x} \,|\, \underline{x} \leq x(k) \leq \overline{x},\ \forall k\}, \tag{6.1a}$$

$$u(k) \in \mathbb{U} \triangleq \{u(k) \in \mathbb{R}^{n_u} \,|\, \underline{u} \leq u(k) \leq \overline{u},\ \forall k\}. \tag{6.1b}$$

The control goal is to minimize a convex (possible multi-objective) cost function $\ell(x,u) : \mathbb{X} \times \mathbb{U} \to \mathbb{R}$, which might bear any functional relationship to the operating cost of the system. From the model in (3.97), let $\hat{w}(k : k+H_p-1) \triangleq (\hat{w}(k), \hat{w}(k+1|k), \ldots, \hat{w}(k+H_p-1|k))$ be the sequence of disturbances over a fixed time prediction horizon $H_p \in \mathbb{Z}_+$. The first element of the sequence is measured, while the rest of the elements, i.e., $\hat{w}(k+i|k)$, denote estimates of future disturbances computed by an exogenous system and available at each time instant k. Hence, the MPC controller design is based on the solution of the following finite horizon optimization problem (FHOP)

$$\min_{\mathbf{u}_k} \sum_{i=0}^{H_p-1} [\|e(k+i|k)\|^2_{W_e} + \|u(k+i|k)\|^2_{W_u} + \|\Delta u(k+i|k)\|^2_{W_{\Delta u}}], \tag{6.2a}$$

subject to

$$x(k+i+1|k) = Ax(k+i|k) + Bu(k+i|k) + E\hat{w}(k+i|k), \tag{6.2b}$$

$$e(k+i+1|k) = r(k+i+1|k) - Cx(k+i|k), \tag{6.2c}$$

$$\Delta u(k+i|k) = u(k+i|k) - u(k+i-1|k), \tag{6.2d}$$

$$u(k+i|k) \in \mathbb{U}, \tag{6.2e}$$

$$x(k+i|k) \in \mathbb{X}, \tag{6.2f}$$

$$(x(k|k), u(k-1|k), \hat{w}(k|k)) = (x_k, u_{k-1}, w_k), \tag{6.2g}$$

for all $i \in \mathbb{Z}_{[0,H_p-1]}$, where $\mathbf{u}_k = \{u_{k+i|k}\}_{i\in\mathbb{Z}_{[0,H_p-1]}}$ are the decision variables, with $\mathbf{u}_k$ being the sequence of controlled inputs. Moreover, $r_{k+i|k}$ are the set-points for the controlled variables and $\hat{w}_{k+i|k}$ are the forecasted disturbances for the i-step ahead from k. Weighting matrices $W_e \in \mathbb{R}_+^{n_y\times n_y}$, $W_u \in \mathbb{R}_+^{n_u\times n_u}$ and $W_{\Delta u} \in \mathbb{R}_+^{n_u\times n_u}$ are used to establish the priority of the different control objectives, that are, tracking error, control effort and smoothness, respectively. Constraint (6.2g) represents the measurements available at time step k.

From the optimal solution of (6.2), $\mathbf{u}_k^\star$, at time step k, only the first optimal control action is applied, i.e., $u_k = u_{k|k}^\star$, following the MPC receding horizon philosophy. Then, the new measurements are collected to initialize initial conditions (6.2g) and the optimization problem (6.2) is solved again. This procedure is repeated at each time step k.

6.2 Health-aware MPC using Rainflow Counting approach

In this section, the rainflow counting algorithm explained in section 5.1.1 is integrated with MPC control of the wind turbine. The wind turbine stress information is included in the model used by the MPC law as an additional output of the system.

6.2.1 Application to the wind turbine case study

The case study used to illustrate both of the approaches proposed in this chapter are based on the wind turbine benchmark model introduced in Odgaard and Johnson (2013). The wind turbine model is implemented in FAST simulator and it is based on a 5 MW three-bladed variable speed wind turbine developed by NREL for scientific research (Jonkman and Buhl, 2005). This model has been used to establish the reference specifications for a number of research projects supported by the U.S. DOEs Wind and Hydropower Technologies Program, the integrated European Union UpWind research program and the International Energy Agency (IEA).

For real-time applications, applying the traditional rainflow counting algorithm is very challenging and computationally expensive. Significant amount of data must be stored and processed periodically to obtain a magnitude of the data in equivalent regular cycles. In addition, the algorithm must be applied to a stored set of data. To address this challenge, an approach based on the rainflow counting algorithm that can operate in real time has been proposed. In previous works, efficient rainflow counting implementations have been proposed, see for example (Musallam and Johnson, 2012).

Loads in wind turbine structure arise from several factors (Jelavic et al., 2008), being the main cause the spatial variations of wind speed caused by the turbulent nature of wind. This spatial difference in wind speeds upon blades results in different loading of the wind turbine blades depending on their intermittent position. Jelavic et al. (2008) concludes that the most pronounced contribution to the blade root loading happens at the frequency given by the blades speed, and this loading is the main source of fatigue at the blades and the hub. In case that the input signal is expressed as bending moments, it is necessary to convert the fatigue load to fatigue stress dividing by the appropriate section modulus Burton et al. (2011).

Using the RFC method, the accumulated damage is obtained as a function of the cycles of the blade root moment stress signal. In order to have available an accumulated damage variable that can be integrated with a linear MPC model, a simplified approach to calculate fatigue using a time series signal is proposed based on RFC theory explained in Section 5.1.1. The result of this approach is such that the accumulated damage is obtained as a function of time instead of the number of cycles. The proposed approach detects the changes of sign which corresponds to a cycle in the stress time signal. The obtained function at each sample step k is the following

$$D(k) = \begin{cases} 0 & if \quad I(k) = I(k-1), \\ \frac{1}{K}(s(k))^{cW} & if \quad I(k) \neq I(k-1), \end{cases} \tag{6.3}$$

where $s(k)$ is the stress at time k

$$s(k) = \frac{1}{L} \sum_{p=k-L}^{k} M_{B,i}(p), \tag{6.4}$$

$I(k)$ is the signal adapted to detect cycles

$$I(k) = M_{B,i}(k) - s(k), \tag{6.5}$$

L is the number of samples per cycle and $M_{B,i}$ is the blade root moment of blade i.

The accumulated damage is calculated as follows

$$\hat{D}_{acc}(k) = \hat{D}_{acc}(k-1) + D(k). \tag{6.6}$$

In this chapter, the RFC method applied to the wind turbines considers the blade root moment as the time stress signal in (6.3). Figure 6.1 shows the accumulated damage value obtained with the RFC method and by means of (6.6). Notice that at the end of the scenario the accumulated damage is almost the same. The difference as explained before relies on the fact that the damage obtained by RFC method is expressed as a function of the cycles count while the method that uses (6.1) considers the damage as a function of time.

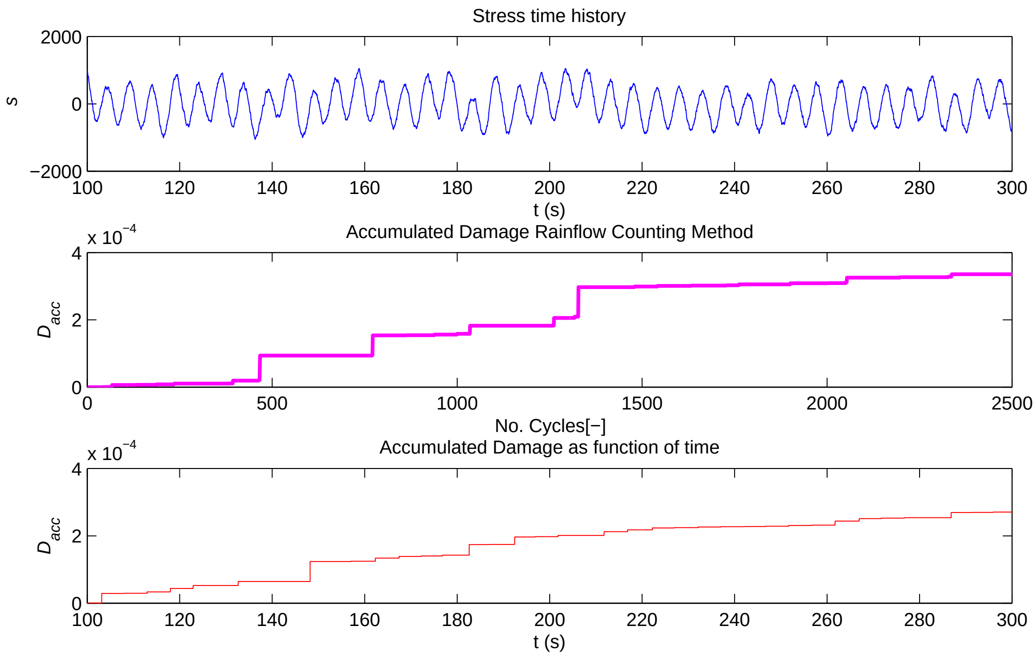

Figure 6.1: Accumulated Damage Comparison

Figure 6.2 presents a block diagram of the wind turbine simulation model, provided with the benchmark, including the feedback loops corresponding to the pitch, yaw and torque variables. It is shown the fatigue model block which provides a damage estimate used to feedback the MPC controller.

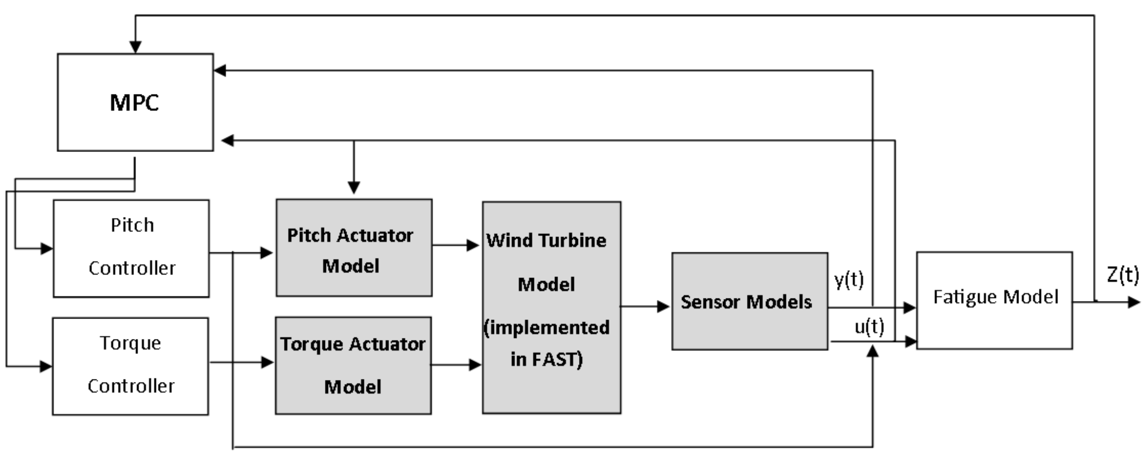

Figure 6.2: Block diagram of wind turbine simulation and fatigue model

6.2.2 Health-aware MPC formulation

As described in Section 6.2.1, the degradation process of the wind turbine blade can be evaluated using the blade root moment sensor information. In order to include a new objective in the MPC that aims to reduce the accumulated damage, the RFC model is approximated by means of a linear model.

As a first approximation, after observing that the proposed approach gives a very close approximation of the accumulated damage obtained by the RFC method (Figure 6.1), the slope m of the accumulated damage curve in function of time is calculated. This function is approximated by means of a linear fatigue damage model.

In a preliminary work Sanchez et al. (2015a), after conducting several tests performed on the wind turbine benchmark implemented in FAST simulator, an experimental model that relates the mean values of the blade root moment and pitch angle signals in steady state was proposed. In a subsequent work Sanchez et al. (2016), the maximum values of the blade root moment signal were used as inputs to a stiffness degradation model and the rainflow counting to calculate fatigue and remaining useful life of wind turbine blades.

Equation (6.7) proposes a linear model between the maximum blade root moment as a function of the generated power and the wind. The power is a function of the generator speed and torque, therefore the proposed model considers the influence of the rotor speed, a control variable which is the applied torque and the wind in the blade root moment. The proposed model for the blade root moment dynamics is a first order blade root moment model with the parameters a_0, a_1 and a_2 as follows

$$M_{B,i}(k) = a_0 + a_1 P_{g,m}(k) + a_2 v_w(k), \tag{6.7}$$

after the substitution of the linear expression for the power (6.15) the proposed model is

$$M_{B,i}(k) = a_0 + a_1 \tfrac{\partial P_g}{\partial \omega_r}\omega_r(k) + a_1 \tfrac{\partial P_g}{\partial T_g} T_g(k) + a_2 v_w(k). \tag{6.8}$$

The model parameters are estimated applying least squares algorithm, for wind speeds in the control region 3 and different rated powers obtaining the following values for the parameters $a_0 = 6468.48$, $a_1 = 757.52$ and $a_2 = -248.83$.

Assuming a cycle with a constant wind speed and knowing the sampling time T_s, the number of samples per cycle L can be determined. The proposed linear fatigue damage model establishes a relation between a control signal T_g, the system state ω_r and a disturbance v_w with the damage of the blade root moment:

$$z(k) = \frac{m}{L}(a_0 + a_1 \tfrac{\partial P_g}{\partial \omega_r}\omega_r(k) + a_1 \tfrac{\partial P_g}{\partial T_g} T_g(k) + a_2 v_w(k)), \tag{6.9}$$

$$Z_{acc}(k+1) = Z_{acc}(k) + z(k), \tag{6.10}$$

where $z(k)$ and $Z_{acc}(k)$ are the estimated damage and accumulated damage of the blade root moment, respectively. Equation (6.9) can be included in the MPC as a new output of the state space model and an additional objective is added to the MPC cost function (6.2a) to minimize the damage.

Figure 6.3 presents the fitting between the RFC approximation as a function of time presented in Section 6.2.1 and the linear Z_{acc} approximation model introduced in (6.10). According to Vassilopoulos (2013), it is expected that a wind turbine blade would be required to sustain 10^9 fatigue cycles in 25 years of operational life. Figure 6.3 shows the accumulated damage for a time frame that is of interest for the MPC controller in terms of the prediction and control horizon, the slope of the curves shown would be maintained until the end of the fatigue life if the wind turbine continues to operate with the loads for the wind scenario considered in the simulation.

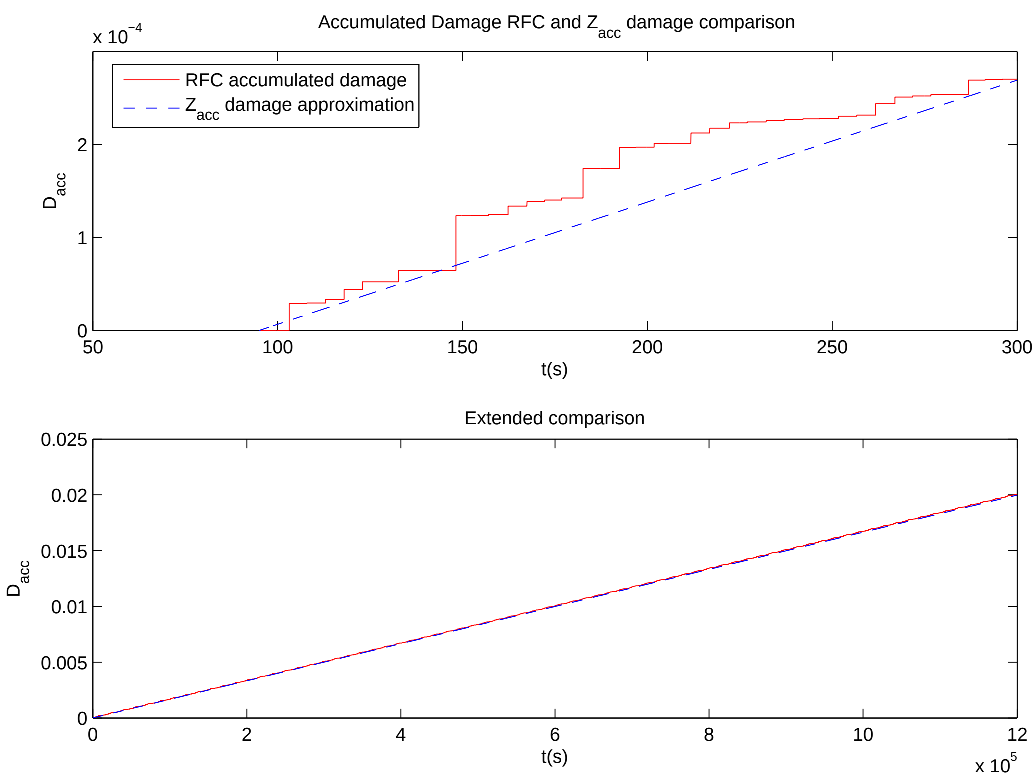

Figure 6.3: Accumulated damage RFC as a function of time and Z_{acc} damage approximation

Figure 6.4 shows the proposed linear damage model formulated in 6.9 as function of the produced power P_g and the mean wind speed v_w. This model is proposed for winds speeds in control region 3 and it can be observed than the maximum damage is obtained when the wind turbine is operating at the maximum rated power of 5MW and at the lower mean wind speed of 13 m/s. The minimum damage is obtained when the wind turbine is operating in a derated power of 2.75 MW and the higher mean wind speed of 25 m/s.

Taking into account (6.9), the MPC problem (6.2) can be formulated as follows

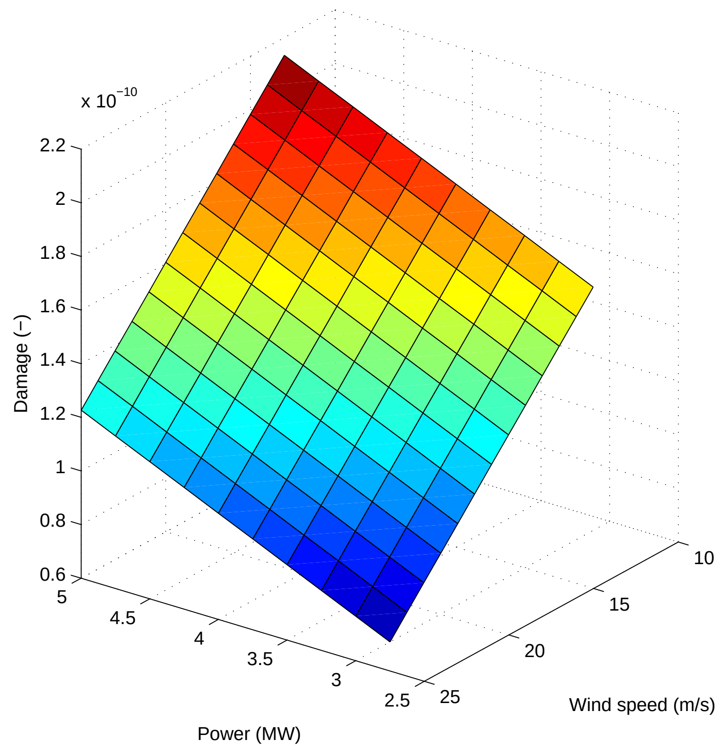

Figure 6.4: Damage $z(k)$ as a function of produced power and mean wind speed

$$\min_{\mathbf{u}_k} \sum_{i=0}^{H_p-1} [\|e(k+i|k)\|^2_{W_e} + \|u(k+i|k)\|^2_{W_u} + \|\Delta u(k+i|k)\|^2_{W_{\Delta u}} + \|z(k+i|k) - z_{ref}\|^2_{W_z}], \quad (6.11a)$$

subject to

$$x(k+i+1|k) = Ax(k+i|k) + Bu(k+i|k) + E\hat{w}(k+i|k), \quad (6.11b)$$

$$e(k+i+1|k) = r(k+i+1|k) - Cx(k+i|k), \quad (6.11c)$$

$$z(k+1) = \frac{m}{L}(a_0 + a_1 \tfrac{\partial P_g}{\partial \omega_r}\omega_r(k) + a_1 \tfrac{\partial P_g}{\partial T_g} T_g(k) + a_2 v_w(k)) \quad (6.11d)$$

$$\Delta u(k+i|k) = u(k+i|k) - u(k+i-1|k), \quad (6.11e)$$

$$u(k+i|k) \in \mathbb{U}, \quad (6.11f)$$

$$x(k+i|k) \in \mathbb{X}, \quad (6.11g)$$

$$(x(k|k), u(k-1|k), \hat{w}(k|k)) = (x_k, u_{k-1}, \hat{w}_k), \quad (6.11h)$$

where an additional objective with the corresponding weight W_z is added to the MPC cost function (6.2a) to track the reference z_{ref} and minimize the damage.

6.2.3 Implementation of MPC with damage objective

The health-aware MPC is implemented using Matlab MPC toolbox considering the reduced wind turbine linear model introduced in Section 3.4 and adding the linear damage model (6.9) as a new output.

$$x(k+1) = Ax(k) + Bu(k) + E_d w_d(k), \tag{6.12}$$

$$y_d(k) = C_d x(k) + F_d w_d(k), \tag{6.13}$$

where the new output vector is given by $y_d = \left[P_{g,m} - P_g^* \; v_{t,m} - v_t^* \; \omega_{r,m} - \omega_r^* \; z\right]^T$ and the disturbance vector is $w_d = [v_w - v_w^* \; a_0]^T$. The new matrices are defined as

$$E_d = \begin{bmatrix} \frac{T_s}{J}\frac{\partial T_a}{\partial v_\omega} & 0 & \frac{T_s}{M_t}\frac{\partial F_t}{\partial v_\omega} & 0 & 0 \\ 0 & 0 & 0 & 0 & 0 \end{bmatrix}^T, \tag{6.14}$$

$$C_d = \begin{bmatrix} T_s\frac{\partial P_g}{\partial \omega_r} & 0 & 0 & 0 & T_s\frac{\partial P_g}{\partial T_g} \\ 0 & 0 & 1 & 0 & 0 \\ 1 & 0 & 0 & 0 & 0 \\ \frac{m\,a_1}{LT_s}\frac{\partial P_g}{\partial \omega_r} & 0 & 0 & 0 & \frac{m\,a_1}{LT_s}\frac{\partial P_g}{\partial T_g} \end{bmatrix}, \tag{6.15}$$

$$F_d = \begin{bmatrix} 0 & 0 & 0 & \frac{m\,a_2}{LT_s} \\ 0 & 0 & 0 & \frac{m}{LT_s} \end{bmatrix}^T. \tag{6.16}$$

MPC has been implemented using prediction horizon $H_p = 200$ with a sampling time of $T_s = 0.05$ s. The MPC objective function (6.20a) considers the following objectives: track the reference power $P_{g,ref}$, rotor speed $\omega_{r,ref}$, damage reference z_{ref} while the damage evaluated as (6.9) is minimized.

6.2.4 Health-aware MPC using RFC Results

The health-aware MPC controller results are presented when the wind turbine is operating in the pitch control region 3 for several wind speeds and varying the weight of associated to the blades damage W_z.

In figure 6.5 is shown the evolution of the accumulated damages for a turbulent wind of 14 m/s mean speed and the performance of the system assessed in terms of different wind turbine variables such as the rotor speed, the pitch angle and the generated power.

When a higher emphasis is placed on the damage term z the health-aware MPC derates the wind turbine producing less power, rotating at a lower speed and pitching the blades to a higher angle. A higher blade pitch angle is equivalent to a lower angle of attack of the blades against the wind which leads to reduced blade root moment loads and therefore a reduced accumulated damage is obtained. The inclusion of the fatigue objective mitigates the damage (assessed with the blade root moment and the rain-flow counting approach).

Figure 6.6 shows the evolution of the accumulated damage Z_{acc} in more detail and the Pareto front when varying the weight corresponding to the damage term z. It can be observed that the maximum accumulated damage, as well as the maximum extracted power, is obtained when the minimum weight (W_z) is assigned to the damage term of the health-aware MPC controller (see Figure 6.6.a). When the damage term is gradually augmented, the accumulated damage is reduced at the same time that the extracted power in the wind turbine is reduced. The Pareto front (Figure 6.6.b) shows the trade-off between maximizing the extracted power and minimizing the accumulated damage in the blades.

It is an open research topic to find the best trade-off between maximum power while reducing the accumulated damage.

Tables 6.1 and 6.2 summarize the values of different wind turbine variables altogether with the accumulated damage Z_{acc} for different values on the damage weight W_z (0, 2×10^8 and 3×10^8) of the MPC controller and two different wind speed scenarios (14 m/s and 17 m/s) on a 900 seconds simulations are analyzed.

From these tables, it can be observed that increasing the value of weight W_z the accumulated damage is reduced but at the price of decreasing the generated power.

Table 6.1: Table showing the results of the accumulated damage and system performance variables for different weights of the MPC control for a turbulent wind with mean speed of 14 m/s.

Weight W_z	**BRM (kN m)**	**Power (MW)**	**Rotor speed (rpm)**	**Accumulated Damage**
0	8247	5	12.1	1.465×10^{-5}
2×10^8	7694	4.73	11.43	1.424×10^{-5}
3×10^8	7229	4.43	10.71	1.377×10^{-5}

Table 6.2: Table showing the results of the accumulated damage and system performance variables for different weights of the MPC control for a turbulent wind with mean speed of 17 m/s.

Weight W_z	**BRM (kN m)**	**Power (MW)**	**Rotor speed (rpm)**	**Accumulated Damage**
0	7135	5	12.1	1.302×10^{-5}
2×10^8	6726	4.75	11.51	1.267×10^{-5}
3×10^8	6266	4.50	10.87	1.255×10^{-5}

6.3 Health-aware MPC with RUL predictions approach

In this section, the remaining useful life (RUL) predictions calculated as explained in section 5.2.3 are integrated with MPC control of the wind turbine. The wind turbine stress information is included as an input of the stiffness degradation model which is embedded in a prognostics algorithm to calculate the remaining useful life (RUL) predictions of the blade. An approximated RUL model is formulated as an additional output of the system in the MPC controller.

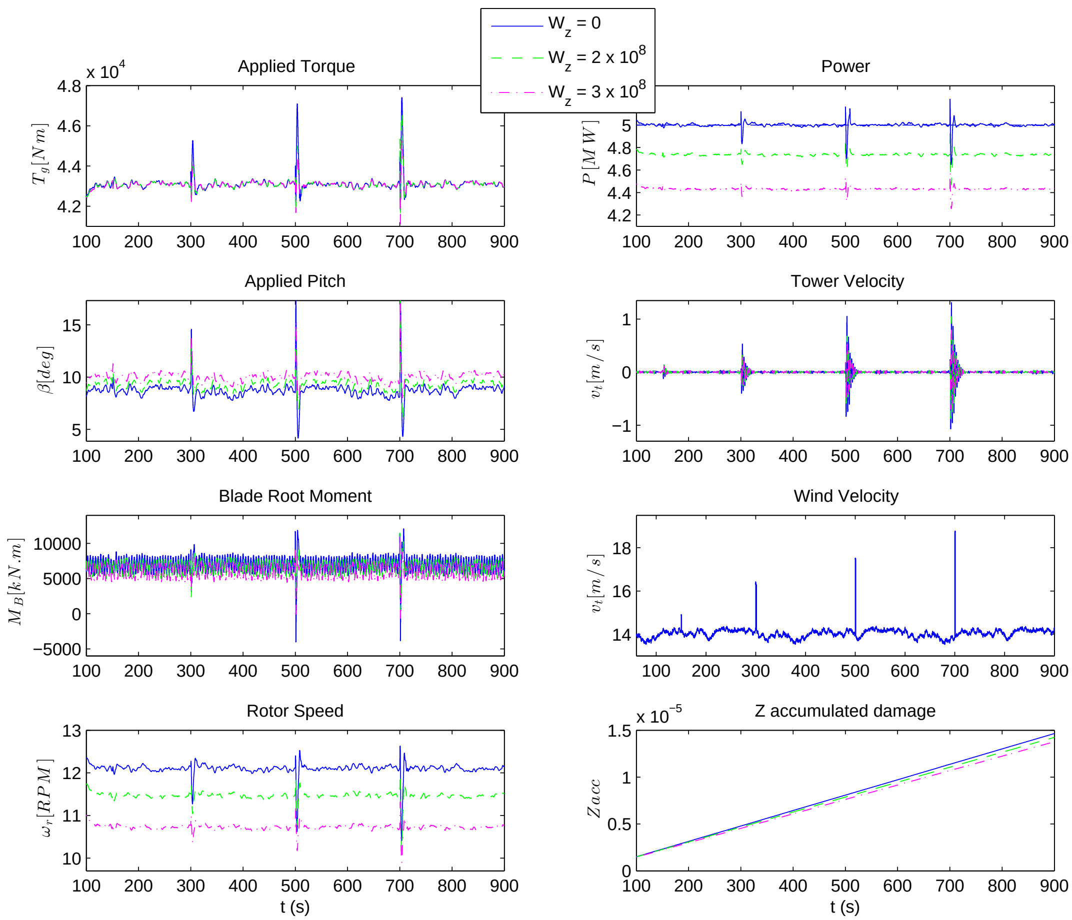

Figure 6.5: Evolution of the wind turbines variables and the accumulated damages for a turbulent wind of 14 m/s mean speed

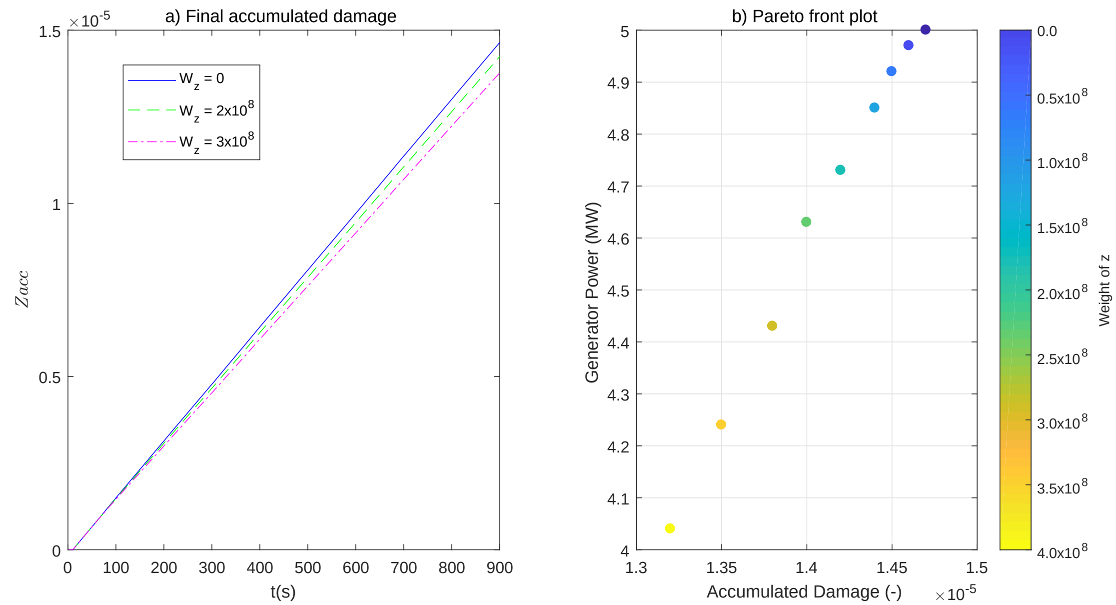

Figure 6.6: Detail of the accumulated damage Z_{acc} and the Pareto front showing the trade-off between power produced and accumulated damage for a turbulent wind of 14 m/s mean speed

6.3.1 Application to the wind turbine case study

Using the stiffness degradation model shown in (5.8) that is embedded into a prognostics algorithm as the one described in Section 5.2.3, the RUL predictions of the blade are obtained as a function of the blade root moment stress signal. In order to have available an RUL variable that can be integrated with a linear MPC model, a simplified approach to calculate RUL predictions using the blade root moment time signal is proposed. The result of this approach is such that approximated RUL predictions are obtained as a function of time instead of the number of cycles.

In this section, the stiffness degradation model 5.8 applied to the wind turbine considers the blade root moment stress signal as the input of the model as it can be seen in Figure 5.4.

Figure 6.7 presents a block diagram of the wind turbine simulation model, provided with the benchmark, including the feedback loops corresponding to the pitch, yaw and torque variables. In the figure 6.7 is shown the block diagram with the prognostics architecture block that includes the approximated RUL model 6.18 which calculates the approximated RUL that is used to feedback the MPC controller.

6.3.2 Health-aware MPC formulation

As described in Section 6.2.1, the degradation process of the wind turbine blade can be evaluated using the blade root moment sensor information. In order to include a new objective in the MPC that aims to extend the remaining useful life (RUL) of the blade, a RUL prediction model is approximated by means of a linear function.

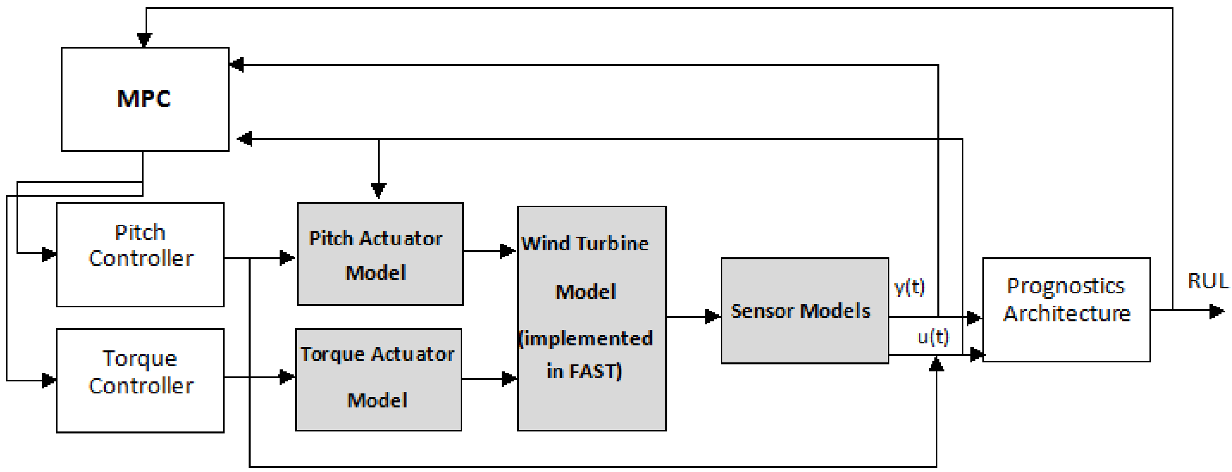

Figure 6.7: Block diagram of wind turbine simulation and prognostics architecture

As a first approximation, it was observed that the proposed approach gives a very close approximation of the RUL predictions obtained using the actual damage model 5.8.

In a the work of Sanchez et al. (2016), the maximum values of the blade root moment signal were used as inputs to the stiffness degradation to calculate the remaining useful life (RUL) predictions of wind turbine blades.

Equation (6.17) proposes a linear model between RUL predictions as a function of the generated power and the wind. The power is a function of the generator speed and torque, therefore the proposed model considers the influence of the rotor speed, a control variable which is the applied torque and the wind speed at the hub height. The proposed model to approximate the RUL predictions is a first order model with the parameters a_0, a_1 and a_2 as follows

$$RUL(k) = a_0 + a_1 P_{g,m}(k) + a_2 v_w(k), \tag{6.17}$$

after the substitution of the linear expression for the power (6.15) the proposed model is

$$RUL(k) = a_0 + a_1 \tfrac{\partial P_g}{\partial \omega_r}\omega_r(k) + a_1 \tfrac{\partial P_g}{\partial T_g}T_g(k) + a_2 v_w(k). \tag{6.18}$$

The model parameters are estimated applying least squares algorithm, for wind speeds in the control region 3 and different rated powers obtaining the following values for the parameters $a_0 = 9.1094 \times 10^9$, $a_1 = -2.1451 \times 10^9$ and $a_2 = 2.4323 \times 10^8$.

Assuming a cycle with a constant wind speed and knowing the sampling time T_s, the number of samples per cycle L can be determined. The proposed linear RUL prediction model establishes a relation between a control signal T_g, the system state ω_r and a disturbance v_w with the RUL prediction of the blade

$$RUL(k)^* = \frac{m}{L}(a_0 + a_1 \tfrac{\partial P_g}{\partial \omega_r}\omega_r(k) + a_1 \tfrac{\partial P_g}{\partial T_g}T_g(k) + a_2 v_w(k)), \tag{6.19}$$

where $RUL(k)^*$ is the approximated RUL prediction and m is a scaling factor used in the implementation of the linear approximated model in the MPC formulation. Equation (6.19) can be included in the MPC as a new output of the state space model and an additional objective is added to the MPC cost function (6.2a) to increase the remaining useful life (RUL). Figure 6.8 shows the proposed linear RUL prediction model formulated in (6.17) as function of the produced power P_g and the mean wind speed v_w. This model is proposed for winds speeds in control region 3 and it can be observed than the minimum RUL prediction is obtained when the wind turbine is operating at the maximum rated power of 5MW and at the lower mean wind speed of 13 m/s. The maximum RUL prediction is obtained when the wind turbine is operating in a derated power of 2.75 MW and at the higher mean wind speed of 25 m/s. The figure is obtained for RUL predictions calculated at starting damage $D = 0$, end of life threshold $EOL = 0.2$ representing a 20% stiffness reduction where the parameters of the stiffness degradation model are shown in Table 5.1 with $c_3 = 4 \times 10^{-6}$.

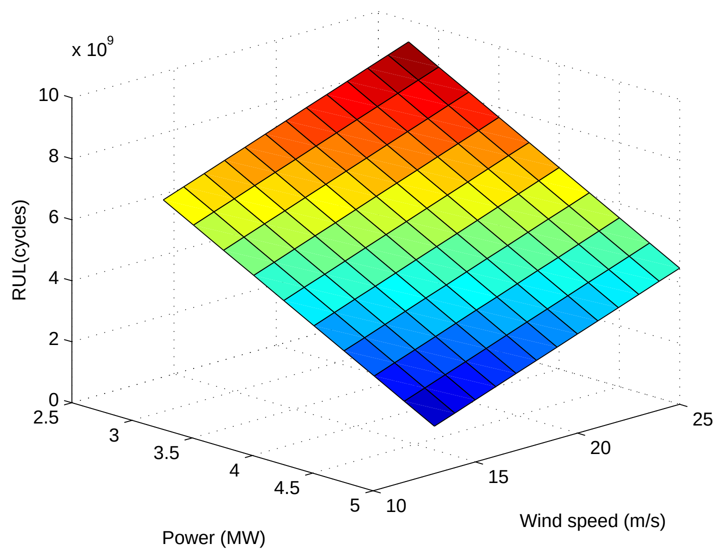

Figure 6.8: Remaining useful life $RUL(k)$ as a function of produced power and mean wind speed

Taking into account (6.19), the MPC problem (6.20) can be formulated as follows:

$$\min_{\mathbf{u}_k} \sum_{i=0}^{H_p-1} [\|e(k+i|k)\|^2_{W_e} + \|u(k+i|k)\|^2_{W_u} + \|\Delta u(k+i|k)\|^2_{W_{\Delta u}} + \|RUL^*(k+i|k) - K_{RUL}\|^2_{W_{RUL}}], \tag{6.20a}$$

subject to

$$x(k+i+1|k) = Ax(k+i|k) + Bu(k+i|k) + E\hat{w}(k+i|k), \tag{6.20b}$$

$$e(k+i+1|k) = r(k+i+1|k) - Cx(k+i|k), \tag{6.20c}$$

$$RUL^*(k) = \frac{m}{L}(a_0 + a_1\tfrac{\partial P_g}{\partial \omega_r}\omega_r(k) + a_1\tfrac{\partial P_g}{\partial T_g}T_g(k) + a_2 v_w(k)) \tag{6.20d}$$

$$\Delta u(k+i|k) = u(k+i|k) - u(k+i-1|k), \tag{6.20e}$$

$$u(k+i|k) \in \mathbb{U}, \tag{6.20f}$$

$$x(k+i|k) \in \mathbb{X}, \tag{6.20g}$$

$$(x(k|k), u(k-1|k), \hat{w}(k|k)) = (x_k, u_{k-1}, \hat{w}_k), \tag{6.20h}$$

where an additional objective of tracking a higher constant value K_{RUL} for the $RUL^*(k)$ is defined with the corresponding weight W_{RUL} added to the MPC cost function (6.2a) to increase the remaining useful life (RUL).

6.3.3 Implementation of MPC with RUL objective

The health-aware MPC is implemented using Matlab MPC toolbox considering the wind turbine linear model introduced in Section 3.4 and adding the linear RUL prediction model (6.19) as an output of the system.

$$x(k+1) = Ax(k) + Bu(k) + E_d w_d(k), \tag{6.21}$$

$$y_d(k) = C_d x(k) + F_d w_d(k), \tag{6.22}$$

where the new output vector is given by $y_d = \begin{bmatrix} P_{g,m} - P_g^* & v_{t,m} - v_t^* & \omega_{r,m} - \omega_r^* & RUL^* \end{bmatrix}^T$ and the disturbance vector is $w_d = [v_w - v_w^* \ \ a_0]^T$. The new matrices are defined as

$$E_d = \begin{bmatrix} \frac{T_s}{J}\frac{\partial T_a}{\partial v_\omega} & 0 & \frac{T_s}{M_t}\frac{\partial F_t}{\partial v_\omega} & 0 & 0 \\ 0 & 0 & 0 & 0 & 0 \end{bmatrix}^T, \tag{6.23}$$

$$C_d = \begin{bmatrix} T_s\frac{\partial P_g}{\partial \omega_r} & 0 & 0 & 0 & T_s\frac{\partial P_g}{\partial T_g} \\ 0 & 0 & 1 & 0 & 0 \\ 1 & 0 & 0 & 0 & 0 \\ \frac{m\,a_1}{LT_s}\frac{\partial P_g}{\partial \omega_r} & 0 & 0 & 0 & \frac{m\,a_1}{LT_s}\frac{\partial P_g}{\partial T_g} \end{bmatrix}, \tag{6.24}$$

$$F_d = \begin{bmatrix} 0 & 0 & 0 & \frac{m\,a_2}{LT_s} \\ 0 & 0 & 0 & \frac{m}{LT_s} \end{bmatrix}^T. \tag{6.25}$$

MPC has been implemented using prediction horizon $H_p = 200$ with a sampling time of $T_s = 0.05$ s. The MPC objective function (6.20a) considers the following objectives: track the reference power $P_{g,ref}$ and rotor speed $\omega_{r,ref}$, while the RUL as (6.19) is maximized.

6.3.4 Health-aware MPC using RUL Results

This section presents the results of the health-aware MPC approach using RUL predictions proposed in section 6.3.

In the following the health-aware MPC controller results are presented for the RUL predictions approach when the wind turbine is operating in the pitch control region 3 for several wind speeds and varying the weight of associated to the blade health W_{RUL}.

Figure 6.10 presents the approximated RUL approximated predictions in a turbulent wind of 14 m/s mean speed and the performance of the system assessed in terms of different wind turbine variables such as the rotor speed, the pitch angle and the generated power. When a higher emphasis is placed on the RUL term $RUL^*(k)$ the health-aware MPC derates the wind turbine producing less power, rotating at a lower speed and pitching the blades to a higher angle. A higher blade pitch angle is equivalent to a lower angle of attack of the blades against the wind which leads to reduced flapwise blade root moment loads and therefore the RUL of the blade is increased. The inclusion of the RUL objective extends the remaining useful life of the blade (assessed with the blade root moment and the RUL predictions using a stiffness degradation model). Figure 6.11 shows the Pareto front when varying the weight corresponding to the RUL term W_{RUL}. It can be observed that the minimum remaining useful life (RUL) as well as the maximum extracted power, is obtained when the minimum weight (W_{RUL}) is assigned to the RUL term of the health-aware MPC controller (see Figure 6.11). When the RUL term is gradually augmented, the remaining useful life is extended at the same time that the extracted power in the wind turbine is reduced. The RUL predictions shown in Figures 6.10-6.11 are obtained assuming no initial damage in the blade and future loads obtained when operating around mean wind speeds values of 14 m/s. The same assumptions for the RUL predictions obtained in mean wind speeds scenarios of 17 m/s.

From Figures 6.9.(a)-6.9.(c), it can be observed the curves for remaining useful life predictions for the wind turbine blade for three different weights of the RUL term W_{RUL} (0, 6.25 and 10) of the MPC controller where the parameter $\alpha = 0.9$ is used to set the confidence level of the RUL predictions bounds at 95% confidence. The figures show that higher RUL predictions are obtained when the weight of the RUL term is increased.

The Pareto front (Figure 6.11) shows the trade-off between maximizing the extracted power and minimizing the remaining useful life predictions of the blades. It is an open research topic to find the best trade-off between maximum power while reducing the accumulated damage.

Tables 6.3 and 6.4 summarize the values of different wind turbine variables altogether with the remaining useful life RUL for different values on the weight W_{RUL} (0, 6.25 and 10) of the MPC controller. Two different wind speed scenarios (14 m/s and 17 m/s) on a 900 seconds simulations are analyzed. From these tables, it can be observed that increasing the value of the weight W_{RUL} the remaining useful life of the blade is increased but at the price of decreasing the generated power.

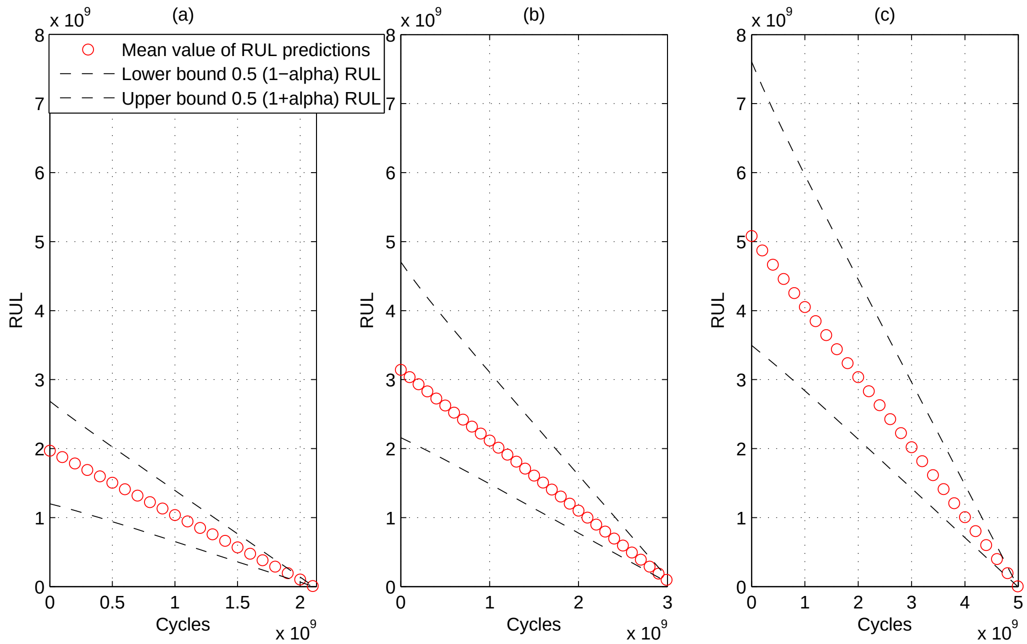

Figure 6.9: Remaining useful life predictions for different weight values of the RUL term in the cost function of the MPC controller. $W_{RUL} = 0$,$W_{RUL} = 6.25$ and $W_{RUL} = 10$ shown in (a,b,c) respectively

Table 6.3: Table showing the results of the RUL predictions and system performance variables for different weights of the MPC control for a turbulent wind with mean speed of 14 m/s.

Weight W_{RUL}	BRM (kN m)	Power (MW)	Rotor speed (rpm)	RUL(cycles)
0	8249.47	5	12.1	2.1087×10^9
6.25	6894.5	4.28	10.32	3.0860×10^9
10	5494.52	3.31	7.88	4.9927×10^9

Table 6.4: Table showing the results of the the RUL predictions and system performance variables for different weights of the MPC control for a turbulent wind with mean speed of 17 m/s.

Weight W_{RUL}	BRM (kN m)	Power (MW)	Rotor speed (rpm)	RUL(cycles)
0	7008.58	5	12.1	2.9804×10^9
6.25	6033.30	4.31	10.36	4.0950×10^9
10	4960.04	3.36	8.11	6.2008×10^9

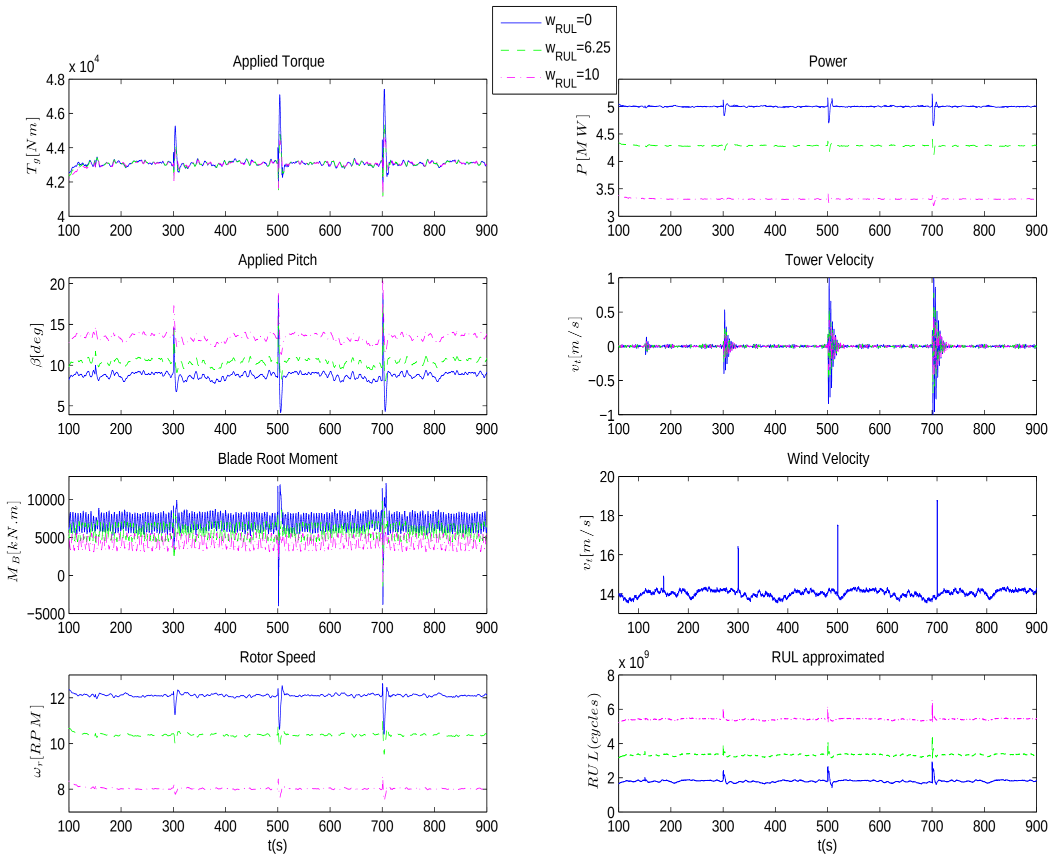

Figure 6.10: Evolution of the wind turbines variables and the approximated RUL for a turbulent wind of 14 m/s mean speed

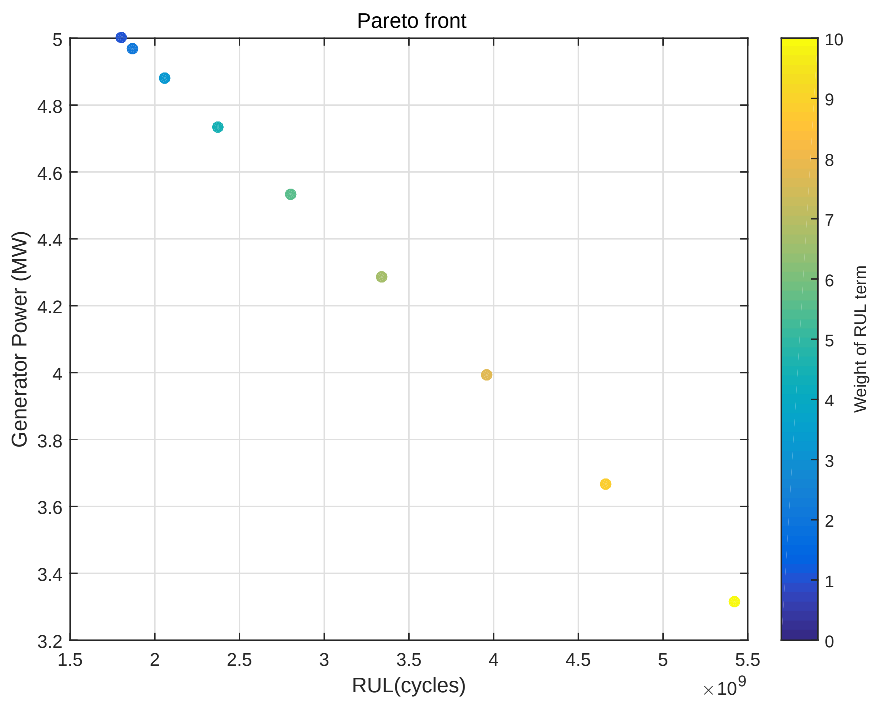

Figure 6.11: Pareto front showing the trade-off between power produced and remaining useful life of the blade for a turbulent wind of 14 m/s mean speed

6.4 Conclusions

The research presented in this chapter has explored the integration of MPC with fatigue-based prognostics to minimize the damage and increase the remaining useful life of wind turbine blades. The integration of a systems health management module with MPC control has provided the wind turbine with a mechanism to operate safely and optimize the trade-off between the blades life and energy production. The controller objective has been modified by adding an extra criterion that takes into account the damage and the remaining useful life predictions of the blade. The scheme has been satisfactorily implemented and tested using a high fidelity simulator of a utility-scale wind turbine. The results obtained show that exists a trade-off between maximum power and the minimization of the accumulated damage or maximization of the RUL of the blade.

Chapter 7

Conclusions and Future Work

This chapter summarizes the work and contributions made on this Thesis to the fields of fault diagnosis (FD), fault tolerant control and prognostics applied to wind turbines. It also summarizes the proposed advanced control approach named health-aware model predictive control (HAMPC) and explores the possibilities of future research.

7.1 Conclusions

The main contributions and conclusions of each chapter are set out below.

In Chapter 3 the high fidelity FAST simulator and the 5MW wind turbine reference model which are used as the realistic plant system has been explained. The nonlinear model models for each of the wind turbine sub-systems have been structured and detailed. In the end of the chapter a reduced linear control oriented has been derived around an operating point, which has later been used in the health-aware model predictive control formulation.

In Chapter 4, a model based diagnosis approach that utilizes interval based ARRs and observers has been applied to the wind turbine benchmark proposed by the scientific community that includes a set of the most common faults found in sensors and actuators of wind turbines. Static and dynamic ARRs have been derived, and uncertainty parameters for the bounds of the interval based observers have been estimated in order to diagnose the faults. Theoretical models from the literature have been used as the base to propose the ARRs to detect and isolate the faults. It has been observed that in some cases, the theoretical models did not adjust to the observed dynamics in the simulator and because of that, experimental models have been proposed using the data obtained from the wind turbine simulator FAST.

Fault isolation techniques based on column and row reasoning that were applied to the signature matrix shown that only a subset of the faults presented in the benchmark was completely isolable. The column reasoning approach has shown to be less robust compared to the row reasoning approach, while the first one needs that all the residuals activate to completely isolate the faults, the DX row reasoning approach has shown more robustness since it allows the isolation without the necessity of all the theoretical residuals activation.

Fault tolerant control has been investigated where a fault tolerant scheme based on individual pitch control (IPC) has been proposed. This scheme uses the azimuth angle sensor readings, to activate and deactivate the IPC component for the blades in the wind turbine control strategy. The fault tolerant scheme needed a persistent fault indication signal when the fault in azimuth angle sensor was detected. To achieve it, a decision function has been proposed to provide a persistent fault indication signal when the fault is detected in a window of determined length. The results have shown that when wrong lectures were detected in the azimuth angle sensor, the IPC component was deactivated resulting that tower loads were not increased. The schemes were tested on the FAST aero-elastic code provided by NREL where it has been demonstrated that the programmed fault tolerant scheme could achieve a persistent fault detection signal that is useful for the IPC control strategy.

In Chapter 5, two approaches for fatigue estimation and remaining useful life predictions for wind turbine blades have been analyzed and tested using the high fidelity wind turbine simulator FAST. The advantages, disadvantages, as well the input and output information they require have been analyzed for both methods. The approaches have been tested using the flapwise blade root moment bending signal as the input load where estimations of accumulated damage and remaining useful life (RUL) predictions have been obtained.

After extensive research, literature review and discussions, two different methods to obtain damage estimation and RUL predictions for wind turbine blades have been selected to analyze and to be implemented in the health-aware model predictive control proposed in this Thesis. The methods are the rainflow counting approach and a stiffness degradation model. The nature of the damage defined in the two methods is different, in the cumulative damage approach used on rainflow counting there is no physical meaning to the damage while in the stiffness degradation model the damage accounts for stiffness reduction of the blade material. The stiffness degradation model has been later embedded in a prognostics algorithm to calculate remaining useful life (RUL) predictions of the blade.

In the stiffness degradation model, the damage is defined as the stiffness reduction in the material due to cyclic loading while the damage in the case of the rainflow counting algorithm it is not explicitly related to a physical characteristic of the material or the considered structure.

The two approaches have been tested on different wind speed scenarios in control region 3, showing that reduced damage or increased RUL is obtained when the wind turbine is operating at higher wind speeds since the angle of attack of the blades is smaller for higher wind speeds. Three different wind scenarios have been used for testing both approaches on the wind turbine simulator FAST. The application to the wind turbine blades prognostics was achieved because both of the methods could use the flap-wise blade root moments loads measurements available in the wind turbine simulator FAST. The numerical results obtained for each one of the methods cannot be directly compared since the nature of the damage different in each one of them. However, both of the approaches demonstrated that the higher is the mean stress value due to wind speed, the damage accumulation occurs faster which translates in shorter life and RUL predictions for the wind turbine blade.

The results and analysis derived in **Chapter 5** have been useful to design the health-aware model predictive controller proposed in **Chapter 6** since the controller needs to derate the wind turbine (i.e. setting the wind turbine to operate in a reduced power respect to the maximum rated power that is capable of operating). The de-rating strategy causes the wind turbine to pitch the blades to a higher angle similarly as when it is operating in high wind speeds which result in reduced loads at the blade root, and that translates into reduced fatigue damage and increased RUL of the blade.

In **Chapter 6**, the integration of MPC with fatigue-based prognostics to minimize the damage and extend the remaining useful life of wind turbine blades has been explored.

The health-aware model predictive control (HAMPC) proposed in this work has been designed to include information from the two different damage estimation approaches, the rainflow counting approach and a stiffness degradation model that was used to calculate RUL predictions of the blade, both analyzed in **Chapter 5**.

The HAMPC uses an augmented state space model of the wind turbine adding the RUL predictions and damage as new outputs of the system which are included in the cost function with the objective of being reduced (damage) or increased (RUL).

Linear damage and RUL predictions models that fit the original approaches (rainflow counting and RUL predictions using a stiffness degradation model) have been proposed in order to be formulated in the HAMPC definition. These approximated models have shown a good fit respect to the original ones and have been proposed as functions of relevant variables of the wind turbine such as the generator power (i.e. generator torque and rotor speed) and the mean wind speed measured at the hub height. The trade-off between energy production and damage accumulation or RUL has been reflected in the HAMPC definition.

The results obtained have demonstrated the feasibility of the proposed HAMPC in terms of reducing damage or increasing the RUL predictions of the blades considering the trade-off with power production and have been validated using the wind turbine high fidelity simulator FAST subject to realistic wind scenarios with different gusts included.

7.2 Future Work

In this section are presented some ideas or possible extensions that can be done in the future regarding the efforts this Thesis has presented in the problems and challenges that exist in the fields of fault diagnosis, prognostics and the integration of control with prognostics and fault diagnosis of wind turbines.

In the fault diagnosis scheme proposed for the fault diagnosis and fault tolerant control wind turbine benchmark challenge in order to improve the fault isolation and robustness, it would be necessary to propose additional ARRs that could lead to a more complete fault signature matrix (FSM).

For fatigue damage estimation of wind turbine blades, other methods such the ones proposed by Bendat (1964) or Dirlik (1985) could also be considered for analysis and comparison. The health-aware model predictive controller (HAMPC) can be extended to include information about real-time energy costs in the optimization function, in order to have the cost of energy as an additional variable in the cost function and to assess the profitability in the trade-off that exists between power and fatigue damage reduction or increases in the remaining useful life of the blade. This additional variable would add another element to the optimization, trade-offs and consequently the decision-making process of the HAMPC. Also, a way to find the optimal tuning of this trade-off could be investigated using multi-objective optimization techniques with the inclusion of a business model that considers the cost of energy.

This thesis proposed some first efforts in including fatigue and remaining useful life predictions (RUL) information of the wind turbine blade in the MPC controller. Approximated linear models for the the rainflow counting approach and the calculation of RUL predictions were used to provide the HAMPC with the damage and RUL information respectively. Future efforts could be done in order to use the rainflow counting algorithm online and to find more efficient ways to calculate the blade RUL predictions using the actual stiffness degradation model in order to have the closed loop system composed by the FAST nonlinear wind turbine model, the HAMPC and the rainflow counting or the prognostics working online in an efficient manner.

Bibliography

(????).

Adegas, F., Wisniewski, R., and Sloth Larsen, L. (2013). Gain-scheduled model predictive control of wind turbines using laguerre functions. In *American Control Conference (ACC), 2013*, 653–658.

Alamo, T., Bravo, J., and Camacho, E. (2005). Guaranteed state estimation by zonotopes. *Automatica*, 41(6), 1035–1043.

Amirat, Y., Benbouzid, M., Bensaker, B., and Wamkeue, R. (2007). Condition monitoring and fault diagnosis in wind energy conversion systems: A review. In *IEEE International Electric Machines and Drives Conference*, volume 2, 1434–1439. Antalya, Turkey.

Amirat, Y., Choqueuse, V., Benbouzid, M., and Turri, S. (2011). Hilbert transform-based bearing failure detection in dfig-based wind turbines. *International Review of Electrical Engineering*, 6(3), 1249–1256.

Andrawus, J., Watson, J., and Kishk, M. (2007). Modelling system failures to optimise wind turbine maintenance. *Wind Engineering*, 31(6), 503–542.

Baek, S., Cho, S., and Joo, W. (2008). Fatigue life prediction based on the rainflow counting method for the end beam of freight car bogie. *International Journal of Automotive Technology*, 9(1), 95–101.

Bagajewicz, M. (2000). *Design and Upgrade of Process Plant Instrumentation*. Technomic Publishers, Lancaster.

Balaban, E., Narasimhan, S., Daigle, M., Roychoudhury, I., Sweet, A., Bond, C., and Gorospe, G. (2013). Development of a mobile robot test platform and methods for validation of prognostics-enabled decision making algorithms. *International Journal of Prognostics and Health Management*, 4(2).

Banjevic, D. (2009). Remaining useful life in theory and practice. *Metrika*, 69(2), 337–349.

Barradas-Berglind, J. and Wisniewski, R. (2016). Representation of fatigue for wind turbine control. *Wind Energy*, 19(12), 2189–2203.

Barradas-Berglind, J., Wisniewski, R., and Soltani, M. (2015). Fatigue damage estimation and data-based control for wind turbines. *IET Control Theory and Applications*, 9(7), 1042–1050.

Bendat, J. (1964). Probability functions for random responses. Technical report on contract NAS-5-4590, NASA (National Aeronautics and Space Administration).

Bento-Pereira, E., Harrop-Galvão, R., and Yoneyama, T. (2010). Model predictive control using prognosis and health monitoring of actuators. In *IEEE International Symposium on Industrial Electronics (ISIE)*, 237–243. Bari, Italy.

Bernal-Perez, S., Ano-Villalba, S., Blasco-Gimenez, R., and Rodriguez-D'Derlee, J. (2013). Efficiency and fault ride-through performance of a diode-rectifier- and vsc-inverter-based hvdc link for offshore wind farms. *IEEE Transactions on Industrial Electronics*, 60(6), 2401–2409.

Bianchi, F., De Battista, H., and Mantz, R. (2007). *Wind Turbine Control Systems. Principles, Modelling and Gain Scheduling Design*. Springer, London.

Biswas, G., Cordier, M., Lunze, J., Travé-Massuyès, L., and Staroswiecki, M. (2004). Diagnosis of complex systems: Bridging the methodologies of the FDI and DX communities. *IEEE Transactions on Systems, Man, and Cybernetics*, 34(5), 2159–2162.

Blanke, M., Kinnaert, M., Lunze, J., and Staroswiecki, M. (2006). *Diagnosis and Fault-Tolerant Control.* Springer-Verlag Berlin Heidelberg.

Blesa, J., Puig, V., Romera, J., and Saludes, J. (2011). Fault diagnosis of wind turbines using a set-membership approach. In *18th IFAC World Congress*, 8316–8321. Milan, Italy.

Bossanyi, E. (2003). Individual blade pitch control for load reduction. *Wind Energy*, 6, 119–128.

Bossanyi, E., Fleming, P., and Wright, A. (2013). Validation of individual pitch control by field tests on two- and three-bladed wind turbines. *IEEE Trans. Control Systems Technology*, 21(4), 1067 – 1078.

British Standards, C. (1984). *British Standard Glossary of Maintenance Management Terms in Terotechnology*. British Standards Institution.

Brondsted, P. and Nijssen, R. (2013). *Advances in Wind Turbine Blade Design and Materials*. Woodhead Publishing, Cambridge.

Brown, D., Georgoulas, G., Bole, B., Pei, H., Orchard, M., Tang, L., Saha, B., Saxena, A., Goebel, K., and Vachtsevanos, G. (2009). Prognostics enhanced reconfigurable control of electro-mechanical actuators. In *1st Annual Conference of the PHM Society*. San Diego, United States of America.

Buhl, M. and Jonkman, J. (2007). *IECWind*. NREL National Renewable Energy Laboratory, Colorado, USA. URL `https://nwtc.nrel.gov/IECWind`.

Burton, T., Jenkins, N., Sharpe, D., and Bossanyi, E. (2011). *Wind Energy Handbook*. John Wiley and Sons, Ltd. Chichester.

Butterfield, S., Sheng, S., and Oyague, F. (2009). Wind energys new role in supplying the worlds energy: What role will structural health monitoring play? In *7th International Workshop on Structural Health Monitoring*. Stanford, USA.

Byon, E. and Ding, Y. (2010). Season-dependent condition-based maintenance for a wind turbine using a partially observed markov decision process. *IEEE Transactions on Power Systems*, 25(4), 1823–1834.

Campos-Gaona, D., Moreno-Goytia, E., and Anaya-Lara, O. (2013). Fault ride-through improvement of DFIG-WT by integrating a two-degrees-of-freedom internal model control. *IEEE Transactions on Industrial Electronics*, 60(3), 1133–1145.

Caprile, C., Sala, G., and Buzzi, A. (1995). Environmental and mechanical fatigue of wind turbine blades made of composites materials. *Journal of Reinforced Plastics and Composites*, 15(7), 673–691.

Casau, P., Rosa, P., Tabatabaeipour, S., and Silvestre, C. (2012). Fault detection and isolation and fault tolerant control of wind turbines using set-valued observers. In *8th IFAC Symposium on Fault Detection, Supervision and Safety of Technical Processes*, volume 45, 120–125. Mexico City, Mexico.

Caselitz, P. and Giebhardt, J. (2005). Rotor condition monitoring for improved operational safety of offshore wind energy converters. *Journal of Solar Energy Engineering*, 127(2), 253–261.

Changzheng, C., Changcheng, S., Yu, Z., and Nan, W. (2005). Fault diagnosis for large-scale wind turbine rolling bearing using stress wave and wavelet analysis. In *IEEE International Conference on Electrical Machines and Systems*, volume 3, 2239–2244. Nanjing, China.

Chase, D., Danai, K., Lackner, M., and Manwell, J. (2013). Detection of damage in operating wind turbines by signature distances. *International Journal of Prognostics and Health Management. Special Issue on Wind Turbine PHM*, 4, 101–114.

Chen, J. and Patton, R.J. (1999). *Robust Model-based Fault Diagnosis for Dynamic Systems*. Kluwer Academic Publishers, Dordrecht.

Chen, W., Ding, S., Sari, A., Naik, A., Khan, A., and Yin, S. (2011). Observer-based FDI schemes for wind turbine benchmark. In *Proceedings of IFAC World Congress*, volume 44, 7073–7078. Milan, Italy.

Chen, Z. (2010). Fault diagnosis of gear box based on information entropy. In *Chinese Control and Decision Conference (CCDC)*, 1239–1242. Guilin, China.

Cheng, J., Yang, Y., and Yu, D. (2010). The envelope order spectrum based on generalized demodulation timefrequency analysis and its application to gear fault diagnosis. *Mechanical Systems and Signal Processing*, 24(2), 508 – 521.

Chilali, M. and Gahinet, P. (1996). H∞ design with pole placement constraints: an LMI approach. *IEEE Transactions on Automatic Control*, 41(3), 358–367.

Chinnam, R. and Baruah, P. (2004). A neuro-fuzzy approach for estimating mean residual life in condition-based maintenance systems. *International Journal of Materials and Product Technology*, 20(1), 166–179.

Coolen, F., Spinato, F., and Venkat, D. (2010). On modelling of grouped reliability data for wind turbines. *IMA Journal of Management Mathematics*, 21(4), 363–372.

Cordier, M., Dague, P., Dumas, M., Levy, F., Montmain, J., Staroswiecki, M., and Travé-Massuyès, L. (2004). Conflicts versus analytical redundancy relations: A comparative analysis of the model based diagnosis approach from the articial intelligence and automatic control perspectives. *IEEE Transactions on Systems, Man, and Cybernetics*, 34(5), 2163–2177.

Dalai, M., Weyer, E., and Campi, M. (2007). Parameter identification for nonlinear systems: Guaranteed confidence regions through LSCR. *Automatica*, 43(8), 1418–1425.

Dang, D., Wang, Y., and Cai, W. (2008). Nonlinear model predictive control (nmpc) of fixed pitch variable speed wind turbine. In *IEEE International Conference on Sustainable Energy Technologies*, 29–33. Singapore, Singapore.

Darling, D. (ONLINE). *The Encyclopedia of Alternative Energy and Sustainable Living. Wind Turbine*. URL `http://www.daviddarling.info/encyclopedia/W/AE_wind_turbine.html`.

Dirlik, T. (1985). Application of computers in fatigue analysis. Phd. thesis, Warwick University.

Dobrila, C. and Stefansen, R. (2007). *Fault tolerant wind turbine control*. Master thesis, Technical University of Denmark, Kgl. Lyngby,.

Donders, S. (2002). *Fault Detection and Identification for Wind Turbine Systems, a closed-loop analysis.* Master's thesis, University of Twente, Faculty of Applied Physics Systems and Control Engineering.

Dong, J. and Verhaegen, M. (2011). Data driven fault detection and isolation of a wind turbine benchmark. In *18th IFAC world congress*, 7086–7091. Milan, Italy.

Dong, Y., Gu, Y., Yang, K., and Zhang, W. (2004). A combining condition prediction model and its application in power plant. In *IEEE International Conference on Machine Learning and Cybernetics*, volume 6, 3474–3478. Shanghai, China.

Dowling, N. (1999). *Mechanical behavior of materials: Engineering methods for deformation, fracture, and fatigue*. Prentice Hall, Upper Saddle River, New Jersey.

Downing, S. and Socie, D. (1982). Simple rainflow counting algorithms. *International Journal of Fatigue*, 4(1), 31–40.

Du, X., Dixon, R., Goodall, R., and Zolotas, A. (2010). Modelling and control of a high redundancy actuator. *Mechatronics*, 20(1), 102–112.

Dunne, F., Schlipf, D., Pao, L., Wright, A., Jonkman, B., Kelley, N., and Simley, E. (2012). Comparison of two independent lidar-based pitch control designs. In *Proc. AIAA Aerospace Sciences Meeting*, 1151. Nashville, TN.

Ebersbach, S., Peng, Z., and Kessissoglou, N. (2006). The investigation of the condition and faults of a spur gearbox using vibration and wear debris analysis techniques. *Wear*, 260(1-2), 16–24.

Eide, R. (2011). *Control Design for Load Reduction of Wind Turbine System*. Master Thesis, Universitet I Agder.

Eliopoulos, E. and Philippidis, T. (2011). A progressive damage simulation algorithm for GFRP composites under cyclic loading. Part I: Material constitutive model. *Composites Science and Technology*, 71(5), 742–749.

Endo, T., Mitsunaga, K., and Nakagawa, H. (1967). Fatigue of metals subjected to varying stress-prediction of fatigue lives. In *Preliminary Proceedings of the Chugoku-Shikoku District Meeting. Japan Society of Mechanical Engineers*, 41–44. Tokyo, Japan.

Ensslin, C., Durstewitz, B., Hahn, B., Lange, B., and Rohrig, K. (2005). *German Wind Energy Report*. ISET, Kassel, Germany.

Entezami, M., Hillmansen, S., Weston, P., and Papaelias, M. (2012). Fault detection and diagnosis within a wind turbine mechanical braking system using condition monitoring. *Renewable Energy*, 47, 175–182.

Esbensen, T. and Sloth, C. (2009). *Fault Diagnosis and Fault-Tolerant Control of Wind Turbines*. Master Thesis, Aalborg University, Denmark.

Esbensen, T., Sloth, C., Odgaard, M., and Thorarins, J. (2008). *Joint Power and Speed Control of Wind Turbines*. Technical report, Department of Electronic Systems, Aaborg University, Denmark.

Escobet, T., Quevedo, J., Puig, V., and Nejjari, F. (2012). Combining health monitoring and control. In S. Kadry (ed.), *Diagnostics and prognostics of engineering systems: methods and techniques*, 230–256. Engineering Science Reference. IGI Global, Hershey.

Evans, M., Cannon, M., and Kouvaritakis, B. (2014). Robust MPC tower damping for variable speed wind turbines. *IEEE Transactions on Control Systems Technology*, 23(1), 290–296.

Farrar, C. and Lieven, N. (2007). Damage prognosis: the future of structural health monitoring. *Phil. Trans. R. Soc. A.*, 365, 623–632.

Freire, N., Estima, J., and Marques Cardoso, A. (2013). Open-circuit fault diagnosis in pmsg drives for wind turbine applications. *IEEE Transactions on Industrial Electronics*, 60(9), 3957–3967.

Frost, S., Goebel, K., and Obrecht, L. (2013). Integrating structural health management with contingency control for wind turbines. *International Journal of Prognostics and Health Management. Special Issue on Wind Turbine PHM*, 4, 11–20.

Fu, C., Ye, L., Liu, Y., Yu, R., Iung, B., Cheng, Y., and Zeng, Y. (2004). Predictive maintenance in intelligent-control-maintenance-management system for hydroelectric generating unit. *IEEE Transactions on Energy Conversion*, 19(1), 179–186.

Futter, D. (1995). Vibration monitoring of industrial gearboxes using time domain averaging. In *IMechE 2nd International conference on gearbox noise, vibration and diagnostics*, volume 5, 35–46. London, United Kingdom.

García, F., Mark, A., Pinar, J., and Papaelias, M. (2012). Condition monitoring of wind turbines: Techniques and methods. *Renewable Energy*, 46, 169–178.

Garcia, M., Sanz-Bobi, M., and del Pico, J. (2006). SIMAP: Intelligent system for predictive maintenance. application to the health condition monitoring of a windturbine gearbox. *Computers in Industry*, 57(6), 552–568.

Gertler, J. and Singer, D. (1990). A new structural framework for parity equation-based failure detection and isolation. *Automatica*, 26(2), 381–388.

Gertler, J. (1998). *Fault Detection and Diagnosis in Engineering Systems*. Marcel Dekker Inc., New York.

Godwin, J. and Matthews, P. (2013). Classification and detection of wind turbine pitch faults through SCADA data analysis. *International Journal of Prognostics and Health Management. Special Issue on Wind Turbine PHM*, 4, 90–100.

Gong, X., Qiao, W., and Zhou, W. (2010). Incipient bearing fault detection via wind generator stator current and wavelet filter. In *IEEE 36th Annual Conference on Industrial Electronics Society IECON*, 2615–2620. Glendale, USA.

Gray, C. and Watson, S. (2010). Physics of failure approach to wind turbine condition based maintenance. *Wind Energy*, 13(5), 395–405.

Griffith, D., Yoder, N., Resor, B., White, J., Paquette, J., Ogilvie, A., and Peters, V. (2012). Prognostic control to enhance offshore wind turbine operations and maintenance strategies. In *European Wind Energy Conference*. Copenhagen, Denmark.

Guo, H., Watson, S., Tavner, P., and Xiang, J. (2009). Reliability analysis for wind turbines with incomplete failure data collected from after the date of initial installation. *Reliability Engineering & System Safety*, 94(6), 1057–1063.

Guo, Y., Yan, W., and Bao, Z. (2010). Gear fault diagnosis of wind turbine based on discrete wavelet transform. In *IEEE 8th World Congress on Intelligent Control and Automation (WCICA)*, 5804–5808. Jinan, China.

Hameedand, Z. and Vatn, J. (2011). State based models applied to offshore wind turbine maintenance and renewal. In *Advances in Safety, Reliability and Risk Management*, 989–996. Troyes, France.

Hammeed, Z., Honga, Y., Choa, Y., Ahnb, S., and Song, C. (2009). Condition monitoring and fault detection of wind turbines and related algorithms: A review. *Renewable and Sustainable Energy Reviews*, 13(1), 1–39.

Hammerum, K., Brath, P., and Poulsen, N. (2007). A fatigue approach to wind turbine control. 75(1), 012081.

Hand, M. and Balas, M. (2007). Blade load mitigation control design for a wind turbine operating in the path of vortices. *Wind Energy*, 10(4), 339–355.

Hatch, C. (2004). Improved wind turbine condition monitoring using acceleration enveloping. *Orbit*, 61, 58–61.

Heng, A., Tan, A., Mathew, J., Montgomery, N., Banjevic, D., and Jardine, A. (2009). Intelligent condition-based prediction of machinery reliability. *Mechanical Systems and Signal Processing*, 23(5), 1600–1614.

Henriksen, L. (2007). *Model Predictive Control of a Wind Turbine*. Phd. Thesis, DTU Technical University of Denmark, Kongens Lyngby, Denmark.

Huang, Q., Jiang, D., Hong, L., and Ding, Y. (2008). Application of wavelet neural networks on vibration fault diagnosis for wind turbine gearbox. In *Advances in Neural Networks - ISNN 2008*, 313–320. Springer-Verlag Berlin Heidelberg.

Hussain, S. and Gabbar, H. (2013). Vibration analysis and time series prediction for wind turbine gearbox prognostics. *International Journal of Prognostics and Health Management. Special Issue on Wind Turbine PHM*, 4, 69–79.

Hyers, R., McGowan, J., Sullivan, K.L., Manwell, J.F., and Syrett, B. (2006). Condition monitoring and prognosis of utility scale wind turbines. *Energy Materials*, 1(3), 187–203.

Isermann, R. (2011). *Fault-Diagnosis Applications, Model-based condition monitoring: actuators, drives, machinery, planst, sensors and fault-tolerant systems*. Springer-Verlag Berlin Heidelberg.

Iung, B., Monnin, M., Voisin, P., and Cocheteux, E. (2008). Degradation state model-based prognosis for proactively maintaining product performance. *CIRP Annals - Manufacturing Technology*, 57(1), 49–52.

Jardine, A., Lin, D., and Banjevic, D. (2006). A review on machinery diagnostics and prognostics implementing condition-based maintenance. *Mechanical Systems and Signal Processing*, 20(7), 1483–1510.

Jelavic, M., Petrovic, V., and Peric, N. (2008). Individual pitch control of wind turbine based on loads estimation. In *IEEE 34th Annual Conference on Industrial Electronics*, 228–234. Orlando, USA.

Johnson, K., Pao, M., Balas, L., and Fingeresh, L. (2006). Control of variable-speed wind turbines - standard and adaptive techniques for maximizing energy capture. *IEEE Control Systems Magazine*, 26(3), 70–81.

Jonkman, B. (2009). *TurbSim User's Guide: Version 1.50*. National Renewable Energy Laboratory, Colorado, USA. Technical Report NREL/TP-500-46198.

Jonkman, J. and Buhl, M. (2005). *FAST user's guide*. National Renewable Energy Laboratory, Colorado, USA. Technical Report NREL/EL-500-38230.

Jonkman, J., Butterfield, S., Musial, W., and Scott, G. (2009). *Definition of a 5-MW reference wind turbine for offshore system development*. National Renewable Energy Laboratory, Colorado, USA. Technical Report NREL/TP-500-38060.

Kamal, E., Aitouche, A., and Bayart, M. (2011). Fault diagnosis based on fuzzy observers for wind energy conversion systems. In *International Conference on Renewable Energy and Eco-Design in Electrical engineering*, 1–8. Lille, France.

Karami, F., Poshtan, J., and Poshtan, M. (2010). Model-based fault detection in induction motors. In *IEEE International Conference on Control Applications*, 1957–1962. Yokohama, Japan.

Karimi, S., Gaillard, A., Poure, P., and Saadate, S. (2008). FPGA-based real-time power converter failure diagnosis for wind energy conversion systems. *IEEE Transactions on Industrial Electronics*, 55(12), 4299 – 4308.

Kendall, M. and Stuart, A. (1961). *The advanced theory of statistics*, volume II-III. Charles Griffin and Co., Ltd., London.

Kensche, C. and Seifert, H. (1990). Wind turbine rotor blades under fatigue loads. In *Developments in the Science and Technology of Composite Materials*, 173–180. Springer, Netherlands.

Kia, S., Henao, H., and Capolino, G. (2009). Torsional vibration effects on induction machine current and torque signatures in gearbox-based electromechanical system. *IEEE Transactions on Industrial Electronics*, 56(11), 4689–4699.

Knudsen, T. and Bak, T. (2013). Simple model for describing and estimating wind turbine dynamic inflow. In *American Control Conference*, 640–646. Washington DC, USA.

Koerber, A. and King, R. (2013). Combined feedback-feedforward control of wind turbines using state-constrained model predictive control. *IEEE Transactions on Control Systems Technology*, 21(4), 1117–1128.

Krysander, M., Aslund, J., and Nyberg, M. (2008). An efficient algorithm for finding minimal overconstrained subsystems for model-based diagnosis systems. *IEEE Transactions on Systems, Man and Cybernetics*, 38(1), 197–206.

Kusiak, A. and Verma, A. (2011). A data-driven approach for monitoring blade pitch faults in wind turbines. *IEEE Transactions on Sustainable Energy*, 2(1), 87–96.

Kusiak, A. and Verma, A. (2012). Analyzing bearing faults in wind turbines: A data-mining approach. *Renewable Energy*, 48, 110–112.

Lampman, S. (2009). *ASM Metals Handbook - Fatigue and Fracture*, volume 19. ASM International, Novelty.

Langeron, Y., Grall, A., and Barros, A. (2013). Actuator health prognosis for designing LQR control in feedback systems. *Chemical Engineering Transactions*, 33, 979–984.

Laouti, N., Sheibat-Othman, N., and Othman, S. (2011). Support vector machines for fault detection in wind turbines. In *Proceedings of 18th IFAC World Congress*, 7067–7072. Milan, Italy.

Layton, J. (2006). *How Stuff Works. Modern Wind-power Techcnology*. URL `http://static.howstuffworks.com/gif/wind-power-horizontal.gif`.

Lee, Y., Pan, J., Hathaway, R., and Barkey, M. (2005). *Fatigue testing and analysis: theory and practice*, volume 13. Elsevier Butterworth-Heinemann, Oxford.

Lei, Y., Zuo, M.J., He, Z., and Zi, Y. (2010). A multidimensional hybrid intelligent method for gear fault diagnosis. *Expert Systems with Applications*, 37(2), 1419–1430.

Li, R. and Frogley, M. (2013). On-line fault detection in wind turbine transmission system using adaptive filter and robust statistical features. *International Journal of Prognostics and Health Management. Special Issue on Wind Turbine PHM*, 4, 115–123.

Lio, W.H., Rossiter, J., and Jones, B. (2014). A review on applications of model predictive control to wind turbines. In *International Conference on Control UKACC*, 673–678. Loughborough, UK.

Liu, W., Zhang, W., Han, J., and Wang, G. (2012). A new wind turbine fault diagnosis method based on the local mean decomposition. *Renewable Energy*, 48, 411–415.

Ljung, L. (1998). System identification. In *Signal Analysis and Prediction*. Springer, New York.

Loucks, D., Van Beek, E., Stedinger, J., Dijkman, J., and Villars, M. (2005). *Water resources systems planning and management: an introduction to methods, models and applications*. Deltares, UNESCO-IHE, Springer.

Loutas, T., Sotiriades, G., Kalaitzoglou, I., and Kostopoulos, V. (2009). Condition monitoring of a single-stage gearbox with artificially induced gear cracks utilizing on-line vibration and acoustic emission measurements. *Applied Acoustics*, 70(9), 1148–1159.

Maciejowski, J. (2002). *Predictive control with constraints*. Prentice Hall, Essex, England.

Manjock, A. (2005). *Evaluation Report: Design Codes FAST and ADAMS for Load Calculations of Onshore Wind Turbines*. Germanischer Lloyd WindEnergie GmbH, Hamburg, Germany. Report No. 72042.

Marín, J., Barroso, A., París, F., and Cañas, J. (2008). Study of damage and repair of blades of a 300kw wind turbine. *Energy*, 33(7), 1068–1083.

Márquez, F.G., Roberts, C., and Tobias, A. (2010). Railway point mechanisms: condition monitoring and fault detection. *Proceedings of the Institution of Mechanical Engineers, Part F: Journal of Rail and Rapid Transit*, 224(1), 35–44.

Martinen, S., Carlén, I., Nilsson, K., Breton, S.P., and Ivanell, S. (2014). Analysis of the effect of curtailment on power and fatigue loads of two aligned wind turbines using an actuator disc approach. *Journal of Physics: Conference Series*, 524(1), 012182.

McMillan, D. and Ault, G. (2007). Quantification of condition monitoring benefit for offshore wind turbines. *Wind Engineering*, 31(4), 267–285.

Meseguer, J., Puig, V., Escobet, T., and Saludes, J. (2010). Observer gain effect in linear interval observer-based fault detection. *Journal of Process Control*, 20(8), 944–956.

Milanese, M., Norton, J., Piet-Lahanier, H., and Walter, E. (eds.) (1996). *Bounding Approaches to System Identification*. Springer, New York.

Miller, A. (1999). *A New wavelet basis for the decomposition of gear motion error signals and its application to gearbox diagnostics*. Master Thesis, Pennsylvania State University, United States of America.

Miner, M. (1945). Cumulative damage in fatigue. *Journal of Applied Mechanics*, 12(3), 159–164.

Musallam, M. and Johnson, C. (2012). An efficient implementation of the rainflow counting algorithm for life consumption estimation. *IEEE Transactions on Reliability*, 61(4), 978–986.

Myrent, N., Kusnick, J., and Adams, D. (2013). Pitch error and shear web disbond detection on wind turbine blades for offshore structural health and prognostics management. In *54th AIAA/ASME/ASCE/AHS/ASC Structures, Structural Dynamics, and Materials Conference*. Boston, USA.

Negre, P. (2010). *Fault Detection and Isolation of Wind Turbines - A Real Field Data Approach*. Master Thesis, Universitat Politècnica de Catalunya.

Nejjari, F., Pérez, R., Escobet, T., and Travé-Massuyès, L. (2007). Fault diagnosability utilizing quasi-static and structural modelling. *Mathematical Computer Modelling*, 45(5–6), 606–616.

Nielsen, J. and Sørensen, J. (2010). Bayesian networks as a decision tool for O&M of offshore wind turbines. In *Integrating Structural Analysis, Risk and Reliability, 5th International ASRANet Conference*. Edinburgh, UK.

Nielsen, J. and Sørensen, J. (2011). On risk-based operation and maintenance of offshore wind turbine components. *Reliability Engineering & System Safety*, 96(1), 218–229.

Niesłony, A. (2009). Determination of fragments of multiaxial service loading strongly influencing the fatigue of machine components. *Mechanical Systems and Signal Processing*, 23(8), 2712–2721.

Nijssen, R. (2006). *Fatigue life prediction and strength degradation of wind turbine rotor blade composites*. PhD. Thesis, Delft University of Technology, Netherlands.

Niknam, S., Thomas, T., Hines, J., and Sawhney, R. (2013). Analysis of acoustic emission data for bearings subject to unbalance. *International Journal of Prognostics and Health Management. Special Issue on Wind Turbine PHM*, 4, 80–89.

Odgaaard, P. and Hovgaard, T. (2015a). On practical tuning of model uncertainty in wind turbine model predictive control. In *9th IFAC Symposium on Control of Power and Energy Systems CPES*, volume 48, 327–332. New Delhi, India.

Odgaaard, P. and Hovgaard, T. (2015b). Selection of references in wind turbine model predictive control design. In *9th IFAC Symposium on Control of Power and Energy Systems CPES*, volume 48, 333–338. New Delhi, India.

Odgaard, P., Stoustrup, J., and Kinnaert, M. (2013). Fault-tolerant control of wind turbines: A benchmark model. *IEEE Transactions on Control Systems Technology*, 21(4), 1168–1182.

Odgaard, P. and Johnson, K. (2013). Wind turbine fault detection and fault tolerant control - an enhanced benchmark challenge. In *Proceedings of the American Control Conference*, 4447–4452. Washington DC, USA.

Odgaard, P., Knudsen, T., Overgaard, A., Steffensen, H., and Jørgensen, M. (2015a). Importance of dynamic inflow in model predictive control of wind turbines. In *9th IFAC Symposium on Control of Power and Energy Systems CPES*, volume 48, 90–95. New Delhi, India.

Odgaard, P., Larsen, L., Wisniewski, R., and Gybel, T. (2016). On using pareto optimality to tune a linear model predictive controller for wind turbines. *Renewable Energy*, 87(2), 884–891.

Odgaard, P., Sanchez, H., Escobet, T., and Puig, V. (2015b). Fault diagnosis and fault tolerant control with application on a wind turbine low speed shaft encoder. In *9th IFAC Symposium on Fault Detection, Supervision and Safety for Technical Processes*, volume 48, 1357–1362. Paris, France.

Odgaard, P. and Stoustrup, J. (2012). Results of a wind turbine FDI competition. In *8th IFAC Symposium on Fault Detection, Supervision and Safety of Technical Processes (SAFEPROCESS)*, 102–107. Mexico City, Mexico.

Odgaard, P., Stoustrup, J., Nielsen, R., and Damgaard, C. (2009). Observer based detection of sensor faults in wind turbines. In *European Wind Energy Conference*, 4421–4430. Marseille, France.

Ofsthun, S. (2002). Integrated vehicle health management for aerospace platforms. *IEEE Instrumentation and Measurement Magazine*, 5(3), 21–24.

Ozdemir, A., Seiler, P., and Balas, G. (2011). Wind turbine fault detection using counter-based residual thresholding. In *Proceedings of 18th IFAC World Congress*, 8289–8294. Milan, Italy.

Parker, G. and Johnson, C. (2009). Improved drive-train and blade fatigue mitigation in flexible wind turbines using disturbance utilization control. In *17th Mediterranean Conference on Control and Automation, MED'09*, 1283–1288. Thessaloniki, Greece.

Parker, M.A., Ran, L., and Finney, S.J. (2013). Distributed control of a fault-tolerant modular multilevel inverter for direct-drive wind turbine grid interfacing. *IEEE Transactions on Industrial Electronics*, 60(2), 509–522.

Pérez, M., Correcher, A., García, E., Morant, F., and Quiles, E. (2011). Self-growing colored petri net for offshore wind turbines maintenance systems. *Renewable energy and power quality journal*, (9), 381–386.

Poure, P., Weber, P., Theilliol, D., and Saadate, S. (2007). Fault-tolerant power electronic converters: Reliability analysis of active power filter. In *IEEE International Symposium on Industrial Electronics*, 3174–3179. Vigo, Spain.

Puig, V., Quevedo, J., Escobet, T., Nejjari, F., and de las Heras, S. (2008). Passive Robust Fault Detection of Dynamic Processes using Interval Models. *IEEE Transactions on Control Systems Technology*, 16(5), 1083–1089.

Puig, V., Saludes, J., and Quevedo, J. (2003). Worst-case simulation of discrete linear time-invariant interval dynamic systems. *Reliable Computing*, 9(4), 251–290.

Puig, V., Stancu, A., Escobet, T., Nejjari, F., Quevedo, J., and Patton, R. (2006). Passive robust fault detection using interval observers: Application to the damadics benchmark problem. *Control Engineering Practice*, 14(6), 621–633.

Puig, V. (2010). Fault diagnosis and fault tolerant control using set-membership approaches: Application to real case studies. *International Journal of Applied Mathematics and Computer Science*, 20(4), 619–635.

Pulido, B. and Alonso, C. (2004). Possible conflicts: a compilation technique for consistency-based diagnosis. *IEEE Transactions on Systems, Man and Cybernetics Part B: Cybernetics. Special section on Diagnosis of Complex Systems: Bridging the methodologies of FDI and DX communities*, 34(5), 2192–2206.

Qu, Y., Bechhoefer, E., He, D., and Zhu, J. (2013). A new acoustic emission sensor based gear fault detection approach. *International Journal of Prognostics and Health Management. Special Issue on Wind Turbine PHM*, 4, 32–45.

Rafiee, J., Arvani, F., Harifi, A., and Sadeghi, M. (2007). Intelligent condition monitoring of a gearbox using artificial neural network. *Mechanical Systems and Signal Processing*, 21(4), 1746–1754.

Ramachandran, K., Fathi, K., and Rao, B. (2010). Recent trends in systems performance monitoring & failure diagnosis. In *IEEE International Conference on Industrial Engineering and Engineering Management (IEEM)*, 2193–2200. Macao, China.

Reinelt, W., Garulli, A., and Ljung, L. (2002). Comparing different approaches to model error modeling in robust identification. *Automatica*, 38(5), 787–803.

Reiter, R. (1987). A theory of diagnosis from first principles. *Artificial Intelligence*, 32(1), 57–95.

Ronold, K., Wedel-Heinen, J., and Christensen, C. (1999). Reliability-based fatigue design of wind-turbine rotor blades. *Engineering Structures*, 21(12), 1101–1114.

Rose, J. and Hiskens, I. (2008). Estimating wind turbine parameters and quantifying their effects on dynamic behavior. In *IEEE Power and Energy Society General Meeting-Conversion and Delivery of Electrical Energy in the 21st Century*, 1–7. Pittsburgh, USA.

Rosich, A., Sarrate, R., Puig, V., and T., E. (2007). Efficient optimal sensor placement for model-based FDI using an incremental algorithm. In *IEEE Decision and Control Conference (CDC)*, 2590–2595. New Orleans, USA.

Rychlik, I. (1987). A new definition of the rainflow cycle counting method. *International journal of fatigue*, 9(2), 119–121.

Samanta, B. and Nataraj, C. (2008). Prognostics of machine condition using soft computing. *Robotics and Computer-Integrated Manufacturing*, 24(6), 816–823.

Sanchez, H., Sankararaman, S., Escobet, T., Puig, V., Frost, S., and Goebel, K. (2016). Analysis of two modeling approaches for fatigue estimation and remaining useful life predictions of wind turbine blades. In *Third European Conference of the PHM Society - PHME16*, 451–461. Bilbao, Spain.

Sanchez, H., Escobet, T., Puig, V., and Odgaard, P. (2015a). Fault diagnosis of advanced wind turbine benchmark using interval-based ARRs and observers. *IEEE Transactions on Industrial Electronics*, 62(6), 3783–3793.

Sanchez, H., Escobet, T., Puig, V., and Odgaard, P. (2015b). Health-aware model predictive control of wind turbines using fatigue prognosis. In *9th IFAC Safeprocess*, 1363–1368. Paris, France.

Sanchez, H., Escobet, T., Puig, V., and Odgaard, P. (2017). Health-aware model predictive control of wind turbines using fatigue prognosis. *Int J Adapt Control Signal Process.* URL `https://doi.org/10.1002/acs.2784`.

Saranga, H. (2002). Relevant condition-parameter strategy for an effective condition-based maintenance. *Journal of Quality in Maintenance Engineering*, 8(1), 92–105.

Sarrate, R., Puig, V., Escobet, T., and Rosich, A. (2007). Optimal sensor placement for model-based fault detection and isolation. In *IEEE Decision and Control Conference (CDC)*, 2584–2589. New Orleans, USA.

Saxena, A., Celaya, J., Saha, B., and Goebel, K. (2010). Metrics for offline evaluation of prognostic performance. *International Journal of Prognostics and Health Management*, 1(1).

Schlechtingen, M., Santos, I., and Achiche, S. (2013). Wind turbine condition monitoring based on scada data using normal behavior models. part 1: system description. *Applied Soft Computing*, 13(1), 259–270.

Schlipf, D., Schlipf, D., and Kühn, M. (2013). Nonlinear model predictive control of wind turbines using LIDAR. *Wind Energy*, 16(7), 1107–1129.

Schulte, H., Zajac, M., and Gerland, P. (2012). Takagi-sugeno sliding mode observer design for fault diagnosis in pitch control systems of wind turbines. In *8th IFAC Symposium on Fault Detection, Supervision and Safety of Technical Processes*, 546–551. Mexico City, Mexico.

Schulte, K. (1984). Stiffness reduction and development of longitudinal cracks during fatigue loading of composite laminates. In *Proceedings of the European Mechanics Colloquium*, 36–54. Brussels, Belgium.

Sheibat-Othman, N., Othman, S., Benlahrache, M., and Odgaard, P. (2013). Fault detection and isolation in wind turbines using support vector machines and observers. In *American Control Conference (ACC)*, 4459–4464. Washington DC, USA.

Sheng, S., Oyague, F., and S., B. (2009). Investigation of various wind turbine drivetrain condition monitoring techniques. In *7th International Workshop on Structural Health Monitoring*. Stanford, USA.

Shuting, W., Yonggang, L., Herming, L., and Guiji, T. (2006). A compositive diagnosis method on turbine-generator rotor winding inter-turn short circuit fault. In *IEEE International Symposium on Industrial Electronics (ISIE)*, 1662–1666. Montreal, Canada.

Sikorska, J., Hodkiewicz, M., and Ma, L. (2011). Prognostic modelling options for remaining useful life estimation by industry. *Mechanical Systems and Signal Processing*, 25(5), 1803–1836.

Simani, S., Castaldi, P., and Tilli, A. (2011). Data-driven approach for wind turbine actuator and sensor fault detection and isolation. In *18th IFAC World Congress*, 8301–8306. Milan, Italy.

Singh, G. and Ahmed, S. (2003). Induction machine drive condition monitoring and diagnostic research-a survey. *Electronic Power Systems Research*, 64(2), 145–158.

Soleimanzadeh, M. and Wisniewski, R. (2011). Controller design for a wind farm, considering both power and load aspects. *Mechatronics*, 21(4), 720–727.

Soltani, M., Wisniewski, R., Brath, P., and Boyd, S. (2011). Load reduction of wind turbines using receding horizon control. In *IEEE International Conference on Control Applications (CCA)*, 852–857. Denver, USA.

Spinato, F., Tavner, P., Van Bussel, G., and Koutoulakos, E. (2009). Reliability of wind turbine subassemblies. *IET Renewable Power Generation*, 3(4), 387–401.

Spudic, V., Jelavic, M., and Baotic, M. (2012). Explicit model predictive control for reduction of wind turbine structural loads. In *51st Annual Conference on Decision and Control (CDC)*, 1721–1726. Maui, USA.

Staroswiecki, M., Cassar, J., and Declerk, P. (2000). A structural framework for the design of FDI system in large scale industrial plants. In *Issues of Fault Diagnosis for Dynamic Systems*, 245–283. Springer, London.

Sutherland, H. (1999). *On the fatigue analysis of wind turbines*. Sandia National Laboratories, Albuquerque, New Mexico, USA. Report SAND99-0089.

Sutherland, H. and Mandell, J. (1996). Application of the US high cycle fatigue data base to wind turbine blade lifetime predictions. *Energy Week*, 85–92.

Svetozarevic, B., Esfahani, M., Kamgarpour, M., and Lygeros, J. (2013). Fault detection and isolation filter for a horizontal axis variable speed wind turbine. In *American Control Conference*, 4453–4458. Washington DC, USA.

Tamilselvan, P., Wang, P., Sheng, S., and Twomey, J. (2013). A two-stage diagnosis framework for wind turbine gearbox condition monitoring. *International Journal of Prognostics and Health Management. Special Issue on Wind Turbine PHM*, 4, 21–31.

Tang, B., Song, T., Li, F., and Deng, L. (2014). Fault diagnosis for a wind turbine transmission system based on manifold learning and shannon wavelet support vector machine. *Renewable Energy*, 62, 1–9.

Tang, L., Kacprzynski, G., Goebel, K., Saxena, A., Saha, B., and Vachtsevanos, G. (2008). Prognostics-enhanced automated contingency management for advanced autonomous systems. In *IEEE International Conference on Prognostics and Health Management*. Denver, USA.

Tavner, P., Xiang, J., and Spinato, F. (2005). Improving the reliability of wind turbine generation and its impact on overall distribution network reliability. In *18th International Conference on Electricity Distribution (CIRED)*, 1–4. IET, Turin, Italy.

Tavner, P., Xiang, J., and Spinato, F. (2007). Reliability analysis for wind turbines. *Wind Energy*, 10(1), 1–18.

Tsai, C., Hsieh, C., and Huang, S. (2006). Enhancement of damage-detection of wind turbine blades via CWT-based approaches. *IEEE Transactions on Energy Conversion*, 21(3), 776–781.

Van Engelen, T., Marlkou, H., Buhl, T., and Marrant, B. (2007). *Morphological study of aerolastic control concepts for wind turbines*. STABCON project, Task 7 Report, ENK5-CT-2002-000627, Netherlands.

Van Paepegem, W. and Degrieck, J. (2002). A new coupled approach of residual stiffness and strength for fatigue of fibre-reinforced composites. *International Journal of Fatigue*, 24(7), 747–762.

Vassilopoulos, A. (2013). Fatigue life prediction of wind turbine blade composite materials. In P. Brøndsted and R. Nijssen (eds.), *Advances in Wind Turbine Blade Design and Materials*, 251–297. Woodhead Publishing Limited, Cambridge.

Vassilopoulos, A. and Nijssen, R. (2010). Fatigue life prediction of composite materials under realistic loading conditions (variable amplitude loading). In A. Vassilopoulos (ed.), *Fatigue life prediction of composites and composite structures*, 293–333. Woodhead Publishing Limited, Cambridge.

Vedreño Santos, F., Riera-Guasp, M., Henao, H., and Pineda-Sanchez, M. (2014). Diagnosis of rotor and stator asymmetries in wound-rotor induction machines under nonstationary operation through the instantaneous frequency. *IEEE Transactions on Industrial Electronics*, 61(9), 4947–4959.

Verheyleweghen, A. and Jäschke, J. (2016). Health-aware operation of a subsea gas compression station under uncertain operating conditions. In *AIChE Annual Meeting*. San Francisco, CA, USA.

Vichare, N. (2006). *Prognostics and Health Management of Electronics by utilizing environmental and usage loads*. PhD. Thesis, University of Maryland, United States of America.

Walford, C. (2006). *Wind turbine reliability: understanding and minimizing wind turbine operation and maintenance costs*. Sandia National Laboratories, New Mexico, USA. Technical Report SAND2006-1100.

Wang, P. and Vachtsevanos, G. (2001). Fault prognostics using dynamic wavelet neural networks. *Artificial Intelligence for Engineering Design, Analysis and Manufacturing*, 15(4), 349–365.

Wang, W., Golnaraghi, M., and Ismail, F. (2004). Prognosis of machine health condition using neuro-fuzzy systems. *Mechanical Systems and Signal Processing*, 18(4), 813–831.

Wei, X. and Verhaegen, M. (2008). Fault detection of large scale wind turbine systems: A mixed h_∞/h_- index observer approach. In *IEEE 16th Mediterranean Conference on Control and Automation*, 1675–1680. Ajaccio, France.

Wei, X., Verhaegen, M., and Van den Engelen, T. (2008). Sensor fault diagnosis of wind turbines for fault tolerant. In *17th World Congress The International Federation of Automatic Control*, 3222–3227. Seoul, Korea.

Welte, T. and Wang, K. (2013). Models for lifetime estimation - an overview with focus on applications to wind turbines. In *International Workshop of Advanced Manufacturing and Automation (IWAMA)*, 337–350. Trondheim, Norway.

Wilkinson, M., Spianto, F., and Knowles, M. (2006). Towards the zero maintenance wind turbine. In *41st International Universities Power Engineering Conference*, 74–78. Newcastle upon Tyne, UK.

Wilkinson, M., Spinato, F., and Tavner, P. (2007). Condition monitoring of generators and other subassemblies in wind turbine drive trains. In *IEEE International Symposium on Diagnostics for Electric Machines, Power Electronics and Drives (SDEMPED)*, 388–392. Cracow, Poland.

Yam, R.C.M., Tse, P., Li, L., and Tu, P. (2001). Intelligent predictive decision support system for condition-based maintenance. *The International Journal of Advanced Manufacturing Technology*, 17(5), 383–391.

Yang, S., Li, W., and Wang, C. (2008a). The intelligent fault diagnosis of wind turbine gearbox based on artificial neural network. In *IEEE International Conference on Condition Monitoring and Diagnosis (CMD)*, 1327–1330. Beijing, China.

Yang, W., Tavner, P., Crabtree, C., and Wilkinson, M. (2008b). Research on a simple, cheap but globally effective condition monitoring technique for wind turbines. In *18th International Conference on Electrical Machines (ICEM)*, 1–5. Vilamoura, Portugal.

Yang, W., Tavner, P., Crabtree, C., and Wilkinson, M. (2010). Cost-effective condition monitoring for wind turbines. *IEEE Transactions on Industrial Electronics*, 57(1), 263–271.

Yang, W., Tavner, P., and Wilkinson, M. (2009). Condition monitoring and fault diagnosis of a wind turbine synchronous generator drive train. *IET Renewable Power Generation*, 3(1), 1–11.

Zeng, J., Lu, D., Zhao, Y., Zhang, Z., Qiao, W., and Gong, X. (2013). Wind turbine fault detection and isolation using support vector machine and a residual-based method. In *American Control Conference*, 3661–3666. Washington DC, USA.

Zhang, S. and Ganesan, R. (1997). Multivariable trend analysis using neural networks for intelligent diagnostics of rotating machinery. *Journal of Engineering for Gas Turbines and Power*, 119(2), 378–384.

Zhang, X., Shenggang, Y., and Xiaoli, L. (2011). Wind turbine bearing condition monitoring based on high frequency resonance method. In *International Conference on Electronics, Communications and Control (ICECC)*, 1792–1795. Ningbo, China.

Zhang, Y., A.P., V., and Keller, T. (2008). Stiffness degradation and fatigue life prediction of adhesively-bonded joints for fiber-reinforced polymer composites. *International Journal of Fatigue*, 30(10), 1813–1820.

Zhe, W. and Qingding, G. (2007). The diagnosis method for converter fault of the variable speed wind turbine based on the neural networks. In *Second International Conference on Innovative Computing, Information and Control*, 615–619. Kumamoto, Japan.

Zhi-Ling, Y., Bin, W., D., X.H., and Hao, L. (2012). Expert system of fault diagnosis for gear box in wind turbine. *Systems Engineering Procedia*, 4, 189–195.

Zhu, J., Yoon, J., He, D., Qu, Y., and Bechhoefer, E. (2013). Lubrication oil condition monitoring and remaining useful life prediction with particle filtering. *International Journal of Prognostics and Health Management. Special Issue on Wind Turbine PHM*, 4, 124–138.

Zimroz, R., Bartelmus, W., Barszcz, T., and Urbanek, J. (2012). *Statistical Data Processing for Wind Turbine Generator Bearing Diagnostics*, 509–518. Springer Berlin Heidelberg.

Appendix A

Linearization of Wind Turbine Model

The nonlinear model can be described as

$$\dot{x} = f(x, u), \tag{A.1}$$

$$y = h(x, u), \tag{A.2}$$

where the derivatives are as follows

$$f_1(x, u) = \dot{\omega}_r = \frac{T_a - NT_g}{J}, T_a = \frac{1}{2\omega_r}\rho v_w^3 A C_p(\lambda, \beta) \tag{A.3}$$

$$\frac{\partial T_a}{\partial \omega_r} = -\frac{1}{2\bar{\omega}_r^2}\rho \bar{v}_w^3 A C_p(\bar{\lambda}, \bar{\beta}) + \frac{1}{2\bar{\omega}_r}\rho v_w^3 A \frac{\partial C_p(\lambda, \bar{\beta})}{\partial \lambda}\frac{\partial \lambda}{\partial \omega_r} \tag{A.4}$$

$$\frac{\partial T_a}{\partial \beta} = \frac{1}{2\bar{\omega}_r}\rho \bar{v}_w^3 A \frac{\partial C_p(\bar{\lambda}, \beta)}{\partial \beta} \tag{A.5}$$

$$\frac{\partial T_a}{\partial v_w} = \frac{1}{2\bar{\omega}_r}\rho \bar{v}_w^2 A C_p(\lambda, \beta) - \frac{1}{2\bar{\omega}_r}\rho \bar{v}_w^3 A \frac{\partial C_p(\lambda, \bar{\beta})}{\partial \lambda}\frac{\partial \lambda}{\partial v_w} \tag{A.6}$$

$$f_2(x, u) = \dot{d}_t = v_t \tag{A.7}$$

$$f_3(x, u) = \dot{v}_t = \frac{F_t - K_t d_t - B_t v_t}{M_t}, F_t = \frac{1}{2}\rho v_w^2 A C_t(\lambda, \beta) \tag{A.8}$$

$$\frac{\partial F_t}{\partial \omega_r} = \frac{1}{2}\rho v_w^2 A \frac{\partial C_t(\lambda, \bar{\beta})}{\partial \lambda}\frac{\partial \lambda}{\partial \omega_r} \tag{A.9}$$

$$\frac{\partial F_t}{\partial \beta} = \frac{1}{2}\rho \bar{v}_w^2 A \frac{\partial C_t(\bar{\lambda}, \beta)}{\partial \beta} \tag{A.10}$$

$$f_4(x,u) = \dot{\beta} = \frac{1}{\tau_p}\beta_{ref} - \frac{1}{\tau_p}\beta \tag{A.11}$$

$$\frac{\partial \dot{\beta}}{\partial \beta_{ref}} = \frac{1}{\tau_p} \tag{A.12}$$

$$\frac{\partial \dot{\beta}}{\partial \beta} = -\frac{1}{\tau_p} \tag{A.13}$$

$$f_5(x,u) = \dot{T}_g = \frac{1}{\tau_g}T_{g,ref} - \frac{1}{\tau_g}T_g \tag{A.14}$$

$$\frac{\partial \dot{T}_g}{\partial T_{g,ref}} = \frac{1}{\tau_g} \tag{A.15}$$

$$\frac{\partial \dot{T}_g}{\partial T_g} = -\frac{1}{\tau_g} \tag{A.16}$$

$$h_1(x,u) = P_g = \eta_g N_g \omega_r T_g \tag{A.17}$$

$$\frac{\partial P_g}{\partial \omega_r} = \eta_g N_g \bar{T}_g \tag{A.18}$$

$$\frac{\partial P_g}{\partial T_g} = \eta_g N_g \bar{\omega}_r \tag{A.19}$$

$$h_2(x,u) = v_t \tag{A.20}$$

$$h_3(x,u) = \omega_r \tag{A.21}$$